TRITA-FKT 2001:25
ISSN 1103-470X
ISRN KTH/FKT/D--01/25--SE

KTH

Energy Consumption and Running Time for Trains

Modelling of running resistance and driver behaviour based on full scale testing

Doctoral Thesis

by

Piotr Lukaszewicz

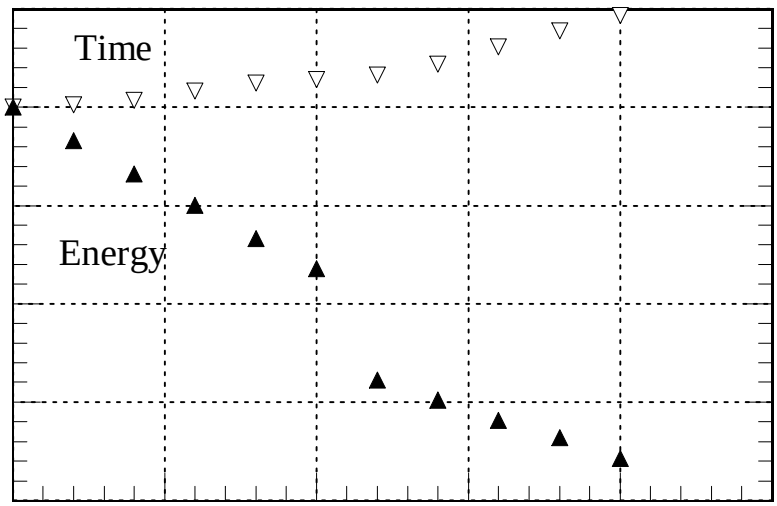

Stockholm
2001

Railway Technology
Department of Vehicle Engineering
Royal Institute of Technology

KTH

Energy Consumption and Running Time for Trains

Modelling of running resistance and
driver behaviour based on full scale testing

Doctoral Thesis

by

Piotr Lukaszewicz

Department of Vehicle Engineering
Royal Institute of Technology

TRITA-FKT 2001:25
ISSN 1103-470X
ISRN KTH/FKT/D--01/25--SE

Akademisk avhandling

som med tillstånd av Kungliga Tekniska Högskolan i Stockholm framlägges till offentlig granskning för avläggande av teknisk doktorsexamen fredagen den 8 juni 2001, kl 10.15 i Sal D1, Lindstedtsvägen 17, KTH, Stockholm.

Abstract

The accuracy in determined energy consumption and running time of trains, by means of computer simulation, is dependent upon the various models used. This thesis aims at developing validated models of running resistance, train and of a general driver, all based on full scale testing.

A partly new simple methodology for determining *running resistance*, called by energy coasting method is developed and demonstrated. An error analysis for this method is performed. Running resistance of high speed train *SJ X2000*, conventional loco hauled passenger trains and freight trains is systematically parameterised. Influence of speed, number of axles, axle load, track type, train length, and train configuration is studied. A model taking into account the ground boundary layer for determining the influence of measured head and tail wind is developed.

Different factors and parameters of a train, that are vital for the accuracy in computed energy consumption and running time are identified, analysed and finally synthesized into a *train model*. Empirical models of the braking and the traction system, including the energy efficiency, are developed for the electrical locomotive of type *SJ Rc4*, without energy regeneration.

Driver behaviour is studied for freight trains and a couple of *driving describing parameters* are proposed. An empirical model of freight train driver behaviour is developed from full scale testing and observations.

A computer program, a simulator, is developed in *Matlab* code, making use of the determined running resistance and the developed models of train and driver. The simulator calculates the energy consumption and running time of a single train. Comparisons between simulations and corresponding measurements are made. Finally, the influence of driving on energy consumption and running time is studied and demonstrated in some examples.

The main conclusions are that:

- The method developed for determining running resistance is quite simple and accurate. It can be used on any train and on any track.
- The running resistance of tested trains includes some interesting knowledge which is partly believed to be new. Mechanical running resistance is less than proportional to the actual axle load. Air drag increases approximately linearly with train length and the effect of measured head and tail wind on the air drag can be calculated if the ground boundary layer is considered.
- The developed train model, including running resistance, traction, braking etc. is quite accurate, as verified for the investigated trains.
- The driver model together with the train model in simulations, is verified against measurements and shows good agreement for energy consumption and running time.
- It is recommended to use a driver model, when calculating energy consumption and running times for trains. Otherwise, the energy consumption will most likely be over-estimated. This has been demonstrated for Swedish ordinary freight trains.

Key words: Aerodynamic drag, Braking ratio, Driver model, Driver behaviour, Degree of coasting, Energy consumption, Energy Coasting Method, Energy saving, Freight trains, Full scale testing, Ore trains, Passenger trains, Powering ratio Mechanical resistance Running time, Running resistance, Slippage, Traction, Train model, Train resistance, Wind.

Acknowledgements

Working on this thesis I have made an effort to study and model important aspects for determination of energy consumption and running time for trains.

This work is to a large extent supported by the former Swedish Transport and Communications Research Board (KFB, now part of VINNOVA), The former Swedish State Railways (SJ) and former ABB Traction (now part of Bombardier Transportation), I owe a great Thank to these organisations. Personally I wish to direct my gratitude to the following staff members:

Firstly, to Mr. Nils Edström at KFB, who always supported this project. The former Director General Stig Larsson, former head of SJ Research and Development. Mrs. Jolanta Drott, former director of SJ Freight Transport Division. Mr. Christer Beijbom, and former head of SJ Quality Department Mr. Bengt Wenning. All of these supported the project by providing and financing operation of test trains.

To the staff of the former SJ Rolling Stock Laboratory, for providing the measuring car and for appropriate measurements during the tests. In particular, Mr. Lars Andersson, Mr Bo Andersson, Mr. Bo Strömberg, Mr. Martin Bäverfeldt, Mr. Dag Andersson and former staff member Mr. Lennart Kloow (former head of staff).

Also to Mr. Kenneth Stjerndorff , former SJ Freight Transport Division, for his effort and personal engagement in scheduling the freight train tests.

At former ABB Traction, a special thank to Mr. Henrik Tengstrand, at the Vehicle Technology Department, who encouraged and supported the tests on the high speed train X2000. Also, a warm thank to Mr. Alf Berg.

To the Swedish National Rail Administration (Banverket), for providing track data and wind measurements during high speed and freight train tests. In particular to the head of the Market Department Mr. Peder Wadman, and his colleges Mr. Magnus Wahlborg and Mrs. Magdalena Grimm.

To the Head of the Division of Railway Technology at KTH, Prof. Evert Andersson for his personal support and advice during this work.

Finally, I also wish to express my gratitude to my whole family for their patience and for supporting me in my decision to write this thesis.

Table of Contents

1 Introduction

1.1 Background and scope of this work

Energy demand and running times of trains in railway networks are of a growing concern for operators, railway administrators, time table designers and train suppliers. This is due to present and future energy cost and demands of the infrastructure, and also due to the aspect of use of limited resources and pollution, which is associated with the production of the energy needed for train operation.

Energy utilised in Sweden for railway electric propulsion, including losses in catenary and feeding system was approximately 1570 GWh in 1993, or about 80% of the total energy utilised, which was 1953 GWh for the same year [1]. In Figure 1-1 it is shown how energy was utilised in 1993. From an international point of view, energy demand constitutes 5 - 10% of the total operational costs of a railway company [2] .

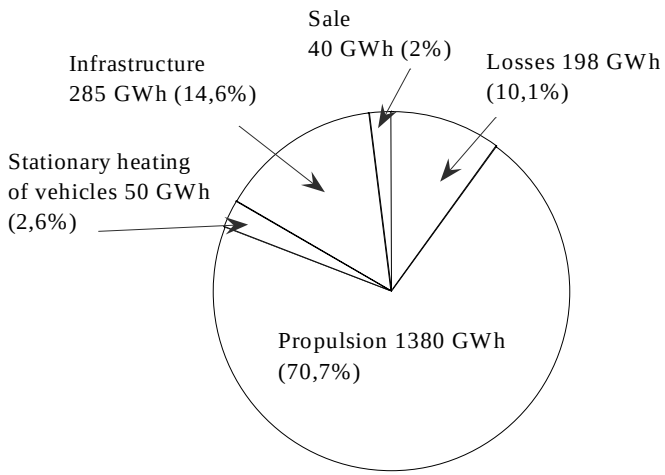

Figure 1-1 Percentage of electric energy utilised for different purposes in the Swedish main line rail network in 1993 [1].

The only efficient way to perform studies on future energy demand and running time of trains is by means of simulations. It is therefore of great importance to have adequate tools for calculating energy demand and running time. To calculate the energy utilised and consumed in train operation and to perform time scheduling, it is necessary to use a computer based simulator due to the complexity of train model and railway network. The accuracy of the simulator depends heavily upon the accuracy of the train model and of the input data, such as track and signalling data, and train data, in particular running resistance data. It is also most important to be able to describe driver behaviour and driving strategy in a systematic and realistic way.

This study addresses the issue of modelling train and driver for simulation purposes. Physical factors which are important for the accuracy in simulations, such as running resistance, characteristics of traction and braking, mechanical and electrical efficiency of the locomotive and driver behaviour are examined. Driver behaviour is in this study investigated only for freight train

operation, where the trains are hauled by the locomotive of type *SJ Rc4* which is not equipped with regenerative brakes.

A method for determining running resistance is proposed. Validated models for prediction of energy consumption and running time simulations are developed, and used to study some basic driver behaviour by means of simulations.

1.2 Earlier work and related fields

1.2.1 Running resistance

For determining power requirements, energy consumption and running times of trains, it is important to know the forces acting on trains against their direction of travel. These forces are known as *running resistance* and also affects the trains top speed and ability to accelerate. In the following, throughout this work, total running resistance, F_{RT}, means the sum of mechanical rolling resistance including curve resistance, aerodynamic drag and resistance due to grades. In many cases running resistance is defined in a more limited sense, F_R, namely the sum of mechanical resistance and aerodynamic drag on straight track.

As described in Muhlenberg [3], Schmidt published already in 1910 a series of formulas for train resistance, based on empirical data. Similar formulas were also developed by Strahl in 1913 and by Davis in 1926 [4]. The formulas for determining running resistance are second degree polynomials with respect to speed, *v,* and are generally written as:

$$F_R = A + Bv + Cv^2 \tag{1-1}$$

According to Davis [4], term *A* contains resistances which are considered independent of speed, but variable with axle load. Coefficient *B* comprises resistances which are proportional to the first power of the speed. Coefficient *C* contains resistances which are proportional to the square of the speed and originates from losses caused by air resistance.

However, original coefficients of these early formulas are not reliable when applied to faster and other types of trains than tested at that time. For instance, Davi's formula was modified [3] by Canadian National Railroads and Eire-Lackawanna Railroad. The development of rolling stock, in particular high speed trains, has made it necessary to modify the coefficients in the formula. This is done mainly by full-scale testing on track, sometimes complemented by testing down-scaled models in wind tunnels, in order to determine principal components of the aerodynamic resistance. Examples are given below.

Aerodynamic drag of Shinkansen trains was reported in 1967 by Hara et al. [5]. Running resistance of TGV-PSE train sets was reported by Guiheau [6] in 1978. Aerodynamic drag reduction due to design changes was reported in 1982 by Peters [7] and in 1983 by Gawthorpe [8]. Aerodynamics of high speed trains is reported by Peters in [9]. A brief summary of research on running resistance performed by SNCF is reported by Chambadal in [10]. In 1991, Peters [11] reported results from full scale tests with the German experimental ICE/V high speed train in tunnels of different lengths and in the open air.

Running resistance of freight trains is for example reported by *ERRI* in [14]. The running resistance is determined for one trainset having six motorrail wagons of the open type, and for one trainset having six modified wagons with smooth and flat side walls. The purpose of this investigation was to verify results from wind tunnel testing, which shows that significant reduction in aerodynamic drag can be achieved by appropriate modifications to the aerodynamics of certain vehicles.

Influence of the number of passenger coaches on aerodynamic drag for conventional loco-hauled trains is reported by ORE [19]. Full scale tests were run with three test trains, having different number of passenger coaches: 6, 10 and 14 respectively. Different test methods were used for determining running resistance. The results show a considerable scatter in the resistance coefficients *A*, *B* and *C*.

1.2.2 Methods used for determining running resistance

In order to investigate running resistance, an appropriate experimental method must be chosen. The method should contain as few error sources as possible and the cost of the tests should be held at a minimum. There are a number of methods which purpose is to determine mechanical rolling resistance and aerodynamic drag. They can be divided into three main groups:

1. Tractive effort methods.
2. Dynamometer or drawbar methods.
3. Coasting methods.

In the *first method* the measurements are taken with the train under traction. The running resistance can be estimated by measuring the *power* or *tractive forces* produced by the traction system. With this method it is necessary to know the resistance of the train due to acceleration or deceleration which can be measured or calculated. It is also important to have high accuracy in the track altitude data, grades. The measurements should preferably be undertaken at almost constant speed, as any speed changes lead to accelerations which would have to be corrected for [18]. The energy efficiency of the tractive vehicle(s) must be known for various conditions. It is also possible to measure the force applied on the wheel rims by means of strain gauges mounted on the wheels, or with approximation, on wheel axles or in the mechanical transmission.

The *second method* makes use of a *dynamometer* or *drawbar*. For measuring mechanical rolling resistance due to rotation of wheels, transmission and motors a dynamometer can be used, which is placed between a winch and a cable connected to the train or vehicle, this is for example reported in [18]. The winch must pull the train smoothly and the track must be straight and of constant gradient. Another method is covered by [14] which makes use of a drawbar for measuring the resistance. The drawbar itself may contribute to precision and bias errors, and the running resistance is determined only for the vehicles following the drawbar, so that running resistance cannot be obtained for a whole train. Also in this case, acceleration and retardation must be measured and compensated for.

In the *third method*, *coasting*, the normal procedure is firstly to bring the train to a certain speed on a track with a known gradient. Before the test train's point of reference arrives at a measuring section, the powering and braking are reduced to zero. From that moment on speed, time and position along the measuring section are determined and recorded. A coasting train on a level track experiences a decrease in speed and kinetic energy due to running resistance, thus making it possible to estimate the running resistance indirectly by calculating the deceleration or direct-

ly by measuring the deceleration [19]. Some methods use inertia pendulum accelerometers to measure deceleration, thus avoiding the effects of track vertical profile. The pendulum system is sensitive to track irregularities and inclination of the test vehicle.

Coasting methods include the idling resistance originating from losses in transmission and motors. However, they don't have the drawbacks of the other methods which have more error sources in the different measuring systems. Coasting methods just require the measurement of speed changes and knowledge of the gradients.

Independent of which method is used, precise track data of track altitude and grades, as well as accurate determination of speed and position of the train along the track are essential.

1.2.3 Simulators and train models

There are numerous computer programs around the world for determining energy consumption and running time of trains by means of simulation, for example [20],[21],[22],[23], [24],[25],[26] and [32]. This list is by no means complete. Most of the programs are developed by traffic operators and train suppliers. In general, it is difficult to obtain a detailed description of the train models used and of the programs themselves.

Four major programs that are developed and used in Sweden are SIMON [20], SIMTRAC [21] and RailPlan [23]. SIMON is owned by the Swedish National Rail Administration and used for capacity and running time studies. SIMTRAC is developed by former ABB and Adtranz, today Bombardier, and is used for analysis and design of electric traction power supply systems. RailPlan is developed by Comreco and used by *SJ* [23].

Some programs are also developed by universities, such as for example DYNAMIS developed at the University of Hannover.

1.2.4 Influence of driver behaviour

A few published reports describe the influence of driver behaviour. They are dealing with a specific train type.

Yasukawa et al. [30] have studied energy saving train operation methods for Shinkansen electric motor coach trains. Simulation tests have been carried out to compare the energy consumption between actual driver's train handling and a proposed method for energy saving. Four driving strategies are studied in [30], namely

1. After constant speed running at v_0 the train is decelerated by repetition of ATC braking and constant speed running and finally train stopping brake is applied. Coasting is not used.
2. The train is decelerated by coasting from a certain point, and after the first application of ATC braking the method becomes the same as method 1.
3. After constant speed running at v_0 and the first ATC braking, coasting and another braking are used for train deceleration.
4. After coasting at a certain point before the first ATC braking, the train is decelerated according to method 3.

The four driving modes are simulated on a particular section (Ohmiya - Oyama on the Tohoku Shinkansen line) and the value of the running time is taken between 1090 and 1200 s with about

4 to 15% of margin to the minimum running time. By finding an optimal speed, $v_0^m(t)$, it is reported that method 4 is the most favourable from the point of energy consumption [30]. Method 4 reduces the energy consumption by about 10 % more than method 1 or 3. The difference between method 2 and 4 is small [30].

The authors of [30] proposes the following driving method for energy saving:

1. An optimal running speed in *method 4* is chosen, according to a residual running time to the next train stop.
2. After the acceleration to $v_0^m(t)$ by *maximum powering*, the constant speed control is applied at this speed.
3. The coasting mode is started at a point where it is possible to make the train arrive at the next station on-schedule by iteration of the coasting and ATC braking.
4. Finally, the train is stopped by the train stopping brake.

Running tests were performed for comparing energy consumption between actual driver's train operation and the suggested driving method. A special on-board system for assisting the driver was constructed and implemented in the test. The system indicated to the driver the optimum running speed, $v_0^m(t)$ and when to enter the coasting mode. The driver was asked to operate in the following way:

- To accelerate the train to the indicated optimum running speed, $v_0^m(t)$, by maximum powering.
- Not to use the brake when, due to slopes, the train speed exceeds the indicated optimum speed, $v_0^m(t)$, even in coasting mode, unless the speed was approaching the ATC signal speed.
- To enter the coasting mode when the on-board assisting system told the driver to do so and not to use the powering.

The results from the tests indicates firstly that on-schedule accuracy is improved because of the on-board system that assists the driver. Secondly, energy consumption is lowered by 13% including the energy consumed by the auxiliary system. In Figure 1-2, percentage of the train running time in each driving mode is compared between the actual average driver's manual train operation and when the driver is assisted by the on-board assisting system. It is seen that powering and braking are reduced while coasting time is increased.

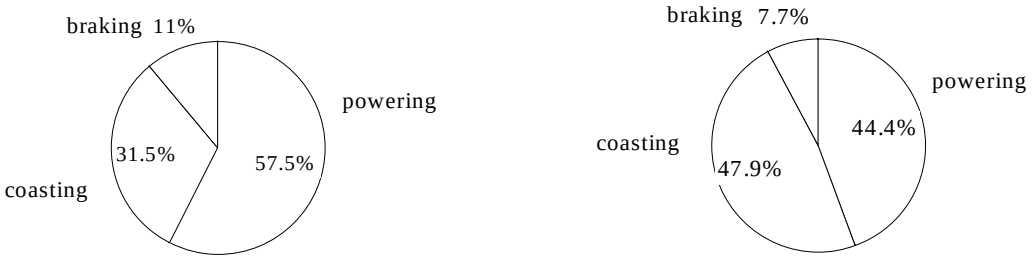

Figure 1-2 Percentage of train running time in each driving mode.

Another example is reported by Schuler-Hainsch [31] who investigated by means of a simulation programme how different driving methods affects energy consumption in comparison to a driving method where the running time is as short as possible for a specific track section:

Method 1, reduction of top speed, resulted in energy savings of about 15% for an additional running time of 5%.

Method 2, coasting down before braking, resulted in energy savings of 23% for an increase in running time of 5%.

Method 3, coasting down before a down gradient followed by gravity acceleration, resulted in energy savings of up to 26% for an extended running time of 5%.

Method 4, coasting down before a down gradient followed by engine and gravity acceleration, allows an energy save of about 12%. The running time is extended by 5%.

The investigation showed that methods 2 and 3 are superior to the other two.

Development of an enhanced train-handling (driving technique) module for the AAR (Association of American Railroads) *Train Energy Model* [25] is reported by Young et al. in [32]. The report outlines a method of integrating a realistic train-handling simulation module into an existing computer program. The train-handling module provides locomotive control settings and is designed to obey speed restrictions with respect to type of train and type of terrain.

1.2.5 Conclusions

It is difficult to find reliable train data and train models which are validated through full scale tests, in particular train driving data. At present, there are only a few published reports which deals with driver behaviour.

Since driver behaviour has a significant impact on energy consumption [1], [31], [33], it is desirable to make simulations with different driving modes. To be able to do this, a train model which resembles a real train as much as possible must be used in the simulations. Even a relatively small discrepancy between a model and a real train may cause misleading results. Therefore, realistic models of running resistance, characteristics of the brake and traction system as well as adhesion utilisation, including wheel slippage, must be included. This is in particular believed to be true in freight train operations, where adhesion is often limiting the tractive force and where considerable brake system time lags are present.

It is also important that the theoretical models of trains and drivers are validated against measurements during real train operations.

1.3 This thesis

1.3.1 Objective and approach

The aim with this work is to develop a verified empirical *model of a freight train* and a verified empirical *driver model* which, combined in simulations, results in a high accuracy for the predicted energy consumption and running time.

The train- and driver models are synthesised from empirical data. Relations and conclusions are made from results achieved by means of full-scale observations and testing. Although the approach in this work is mainly empirical, some theoretical modelling is made to support and explain some of the empirical findings.

This work focuses on five areas and has the following approach:

1. Development of a methodology for experimental determination of running resistance, with an error estimation, still applying the form as defined in Eq. (1-1).
2. Empirical investigation, by means of full-scale testing, and parameterisation of running resistance for different types of passenger and freight trains.
3. Investigation of, by means of full-scale testing, parameters needed for modelling a locomotive and different types of freight trains as well as development of a verified model for simulation purposes in *Matlab* code.
4. Analysis of driver behaviour from observations made during real freight train operations and development of parameters which describe the behaviour.
5. Development of a verified driver model in *Matlab* code for simulation purposes using a few parameters which describe the driver behaviour.

In [34] Andersson & Lukaszewicz, it is suggested to define the purpose of energy consumption and where in the energy conversion and transmission chain the energy is measured. Otherwise comparison of energy consumption for railways, different train types and driving strategies may be useless. In this study, the following approach is used:

- The energy measured at the pantograph is considered as total intake energy. This means that losses in electric power plants, transmission lines as well as the railway's catenary and feeding systems are not considered.

- The energy fed into the train is divided into three areas of usage:
  1. Propulsion, including internal losses of the locomotive.
  2. Auxiliary systems, such as pumps, compressors, motor ventilation, external illumination etc.
  3. Comfort systems, such as air conditioning, heating, internal illumination etc. For an ordinary freight train this can be neglected and is therefore not studied in this thesis.

1.3.2 Thesis contribution

This work is believed to contribute to the understanding of the different parameters which are important for determining energy consumption and running time of trains, especially freight trains.

This thesis is believed to make significant contributions to the following areas:

- A new alternative method is described and suggested for determining running resistance, aiming at minimising measuring complexity and measuring errors.

- Running resistance is systematically determined due to parameters such as speed, number of cars, number of axles, train length, configuration, type of vehicles, axle load and type of track. This is making the running resistance formulas up to date, especially for the Swedish case.

- The small influence of axle load upon the linear resistance term, with respect to speed is a new finding and contradicting previous studies.

- The influence of measured head and tail wind on air drag is investigated. It is also shown that the conventional method for calculating the contribution of measured head- and tail wind on air drag is not adequate.

- The uncertainties and possible errors in determined running resistance are shown.

- Parameters, variables and train data, which are believed to have an important influence on energy consumption calculations are investigated empirically, thus giving reliable train data for the development of a train model and for future usage. Relative slippage of the locomotives axles is measured and included in energy consumption determinations.

- A verified empirical model of an ordinary freight train is developed, having a high accuracy for determining energy consumption and running time, giving the possibility to achieve reliable results.

- Driver behaviour is investigated empirically.

- Parameters describing driver behaviour and driving strategy are introduced and suggested.

- Modelling of a verified average driver.

- A study on the influence of driver behaviour and driving strategy on running time and energy consumption for a freight train is shown, by some examples.

1.3.3 Outline of doctoral thesis

Chapter 2 describes the used methodology used for determining running resistance.

Chapter 3 presents results from full-scale testing of running resistance for high speed trains, conventional passenger trains and different types of freight trains.

Chapter 4 deals with the analysis of the results from Chapter 3. An error analysis is performed. The resistance is investigated due to train type, speed, axle load, number of axles, train length and track type.

Chapter 5 describes a method for calculating the influence of measured head and tail wind on air drag.

Chapter 2 - 5 is a summary of the Licentiate thesis [15].

Chapter 6 gives an introduction and describes the freight train testing with aims to provide test data for the development of train model and driver model.

Chapter 7 deals with the analysis of the locomotive SJ Rc4 and the train modelling.

Chapter 8 gives a general description if the simulation model used.

Chapter 9 shows results from tests and observations of driver behaviour, made during normal driving and normal operation. An analysis is performed and parameters, which are describing the driver behaviour, are defined and introduced.

Chapter 10 describes the driver model, as used in the simulation program.

Chapter 11 deals with the validation of the simulation program. A comparison is shown between measurements and simulations with the train and driver model developed

Chapter 12 performs a parametric study on influence of driver behaviour.

Chapter 13 concludes and outlines further research.

2 Methodology used for experimental determination of running resistance

2.1 General description of running resistance

The total forces acting on a train against its direction of travel are known as total running resistance, F_{RT}. They can be divided into four main categories:

- *Mechanical resistance*, F_M, due to mechanical energy dissipation in vehicle, track and the contact areas between wheels and track. In addition there is an increment in mechanical resistance as a train is negotiating a curve, *curve resistance* F_C.

- *Aerodynamic resistance* or *aerodynamic drag*, F_D.

- *Grade resistance*, F_G; as ascending a grade a train will experience a resistive force due to gravity.

Additional tractive force which is required for acceleration due to inertia [35], [54], can be expressed as:

- *Inertia resistance*, F_I.

Energy is dissipated due only to mechanical resistance and aerodynamic drag. Energy for overcoming grades and inertia can be recovered while descending grades or coasting.

Experimental findings show that the sum of mechanical resistance (on straight track) and aerodynamic drag can be quantified, [4], [14], [15], [19], [37], [38], [54], with adequate accuracy by:

$$F_R = F_M + F_D = A + Bv + Cv^2 \tag{2-1}$$

The coefficients A, B and C are however not constants; they vary with type of train, track, wheel-rail friction etc.

Mechanical resistance is generally accepted [4], [38], as covered by the terms A and Bv in Eq. (2-1). However, there is little theoretical justification in limiting this part of running resistance to a constant and linear term, [35], [43]. Term Bv includes also air momentum drag, [8], but may also include other aerodynamic phenomena not covered by the next term.

Term Cv^2 is considered to cover aerodynamic drag, [8], [35],[37], [42], [64], except air momentum drag, believed to depend linearly upon speed, [8]. Also in this case, there is no theoretical justification that aerodynamic drag is described *only* by this term.

The terms A, Bv and Cv^2 cover various complex and interrelated physical phenomena. The magnitudes of the coefficients determined from experiments, are affected by resistive forces that may vary with other powers of speed than those in Eq. (2-1), [43], [37], [66].

Eq. (2-1) is *generally accepted and wide spread* and is therefore applied here as the development of a new algebraic model for running resistance is not the aim of this work.

2.2 Methodology

Only mechanical, curve resistance not included, and aerodynamic resistance is experimentally determined in this thesis. Curve resistance and grade resistance are however included in the model developed for computational purposes in Section 7.6.

The method chosen for determining running resistance should be as simple as possible and have as few error sources as possible. Also, the possible error sources should be possible to estimate.

With this objective in mind, the Energy Coasting Method is developed in this chapter.

2.2.1 The Energy Coasting Method

Running resistance, F_R, is associated with energy dissipation. This dissipation equals the work, W_R, done by F_R. For a track section of length ΔX, this relation can be written as

$$W_R = \int F_R dx = \bar{F}_R \cdot \Delta X = (\bar{F}_M + \bar{F}_D)\Delta X \qquad (2\text{-}2)$$

If a coasting train's *total energy*, kinetic, E_{kin} and potential, E_{pot}, is determined at successive measuring positions separated by a distance $\Delta x = x_{a+1} - x_a$ from each other along the track, the difference in the train's total energy between these positions can be calculated. The difference in total energy between the measuring positions is due to energy dissipation. The train's position at each measuring position must be determined with respect to some point of reference on the train.

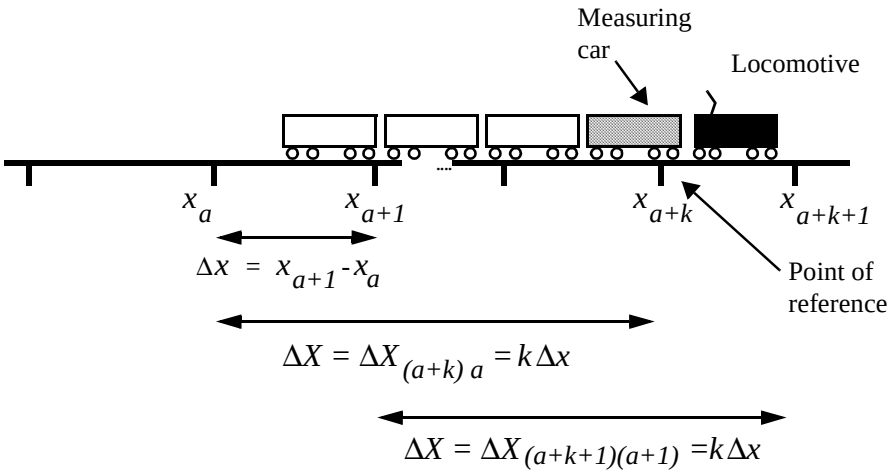

Figure 2-1 Track with equidistantly spaced measuring positions.

The energy dissipation, thus the mean running resistance, between two arbitrary measuring positions, x_a and x_{a+k}, separated by the evaluation distance $\Delta X_{(a+k)a} = k\,\Delta x$ can be estimated from the balance equation:

$$E_{kin_a} + E_{pot_a} = E_{kin_{a+k}} + E_{pot_{a+k}} + \bar{F}_{R_{(a+k)a}}\,\Delta X_{(a+k)a} \tag{2-3}$$

This is provided that no energy is supplied from any external source and all vehicles of the train have the same speed.

In order to estimate a train's potential energy at the measuring positions, with respect to the train's point of reference, the train mass, m_T, has to be distributed as individual vehicle masses over the length of the train. The total mean running resistance, $\bar{F}_R$, for a coasting train and the corresponding mean speed, $\bar{v}$, are calculated by:

$$\bar{F}_{R_{(a+k)a}} = \frac{1}{\Delta X_{(a+k)a}}\left(\sum_{i=1}^{n_v} m_i\left(\frac{1}{2}(1+H_i)(v_a^2 - v_{a+k}^2) + g(h_{i_a} - h_{i_{a+k}})\right)\right) \tag{2-4}$$

$$\bar{v}_{(a+k)a} = \frac{\Delta X_{(a+k)a}}{\Delta t_{(a+k)a}} = \frac{x_{(a+k)} - x_a}{t_{(a+k)} - t_a} \tag{2-5}$$

H_i is a factor taking rotational inertia into account, i is the vehicle number, n_v is the number of vehicles in the train set, h_i is the altitude of a vehicle and g is the gravitational acceleration and t is time.

The evaluation distance ΔX, can be several measuring intervals, $k\,\Delta x$, long, $k \geq 1$. This is advantageous for reducing output data scatter, which reduces as ΔX increases, see Section 4.1.

By shifting $\Delta X_{(a+k)a}$ forward, $a = 1....j$, along the measuring section by Δx the mean running resistance with its corresponding mean speed can be estimated successively for each ΔX until the end of the measuring section is reached, or the train stops by itself. In this way j number of data pairs of $(\bar{v}, \bar{F}_R)$ are formed. The data pairs can now be used for fitting a polynomial having the form:

$$\bar{F}_R = A + B\bar{v} + C\bar{v}^2 \tag{2-6}$$

for each test run by means of the method of least squares.

A step-by-step description of the Energy Coasting Method can be found in APPENDIX C.

2.3 Minimising ambient wind influence

While measuring the wind direction and wind speed in the ambience of the test section, tests are run in both directions along the measuring section, thus forming pairs of fitted polynomials. Test runs in such a pair shall have about the same wind conditions with respect to the measuring section.

From each pair of fitted polynomials, a mean polynomial, thus mean running resistance, is determined for the two wind conditions.

The mean polynomials determined from each test run pair of the same train consist are then averaged. This results in *wind averaged values* of the coefficients *A*, *B* and *C*; thus the *wind minimised running resistance* is estimated. However, this is not exactly the same as running resistance for no wind conditions, mainly due to the following reasons:

- The magnitude of the increase in aerodynamic drag of a train due to ambient wind, when running in one direction, is not necessarily the same as the decrease in aerodynamic drag when running in the opposite direction, even though the wind conditions are exactly the same, [35].

- The average of aerodynamic drag in side wind is not the same as at zero wind conditions, as the aerodynamic drag may increase considerably at large side wind angles.

It should be pointed out that only coefficient C, and to some extent B, are expected to show significant influence from ambient wind. Coefficient A is considered to originate from mechanical resistance.

2.4 Errors in estimated running resistance

A result based on experiments, such as field tests, is always associated with errors due to faulty data. These errors can be divided [36] into two main groups:

1. Precision errors which are random and can have different signs and values for each successive measurement. They can be treated using statistical techniques.
2. Bias errors which are systematical and occur in the same way each time, often resulting in an offset from the true value.

2.4.1 Precision errors

Precision errors, ε_p, are due to the determination of:

- *Speed, v,* from which also the *evaluation distance* can be calculated.
- Each vehicles *altitude,* h_i, given by track data.

An estimation of the maximal error due to precision errors can be made by analytical means. By differentiating successively Eq. (2-4) as shown in Eq. (2-7), with respect to *v, h* and ΔX, it is possible to approximately estimate the *maximal error* $\Delta\bar{F}_{Rp}$, due to precision errors in *v, h* and ΔX for the determined mean running resistance:

$$\Delta\bar{F}_{Rp} \approx \left|\frac{\partial\bar{F}_R}{\partial v}\Delta v\right| + \left|\frac{\partial\bar{F}_R}{\partial h}\sum_{i=1}^{n_v}\Delta h_i\right| + \left|\frac{\partial\bar{F}_R}{\partial(\Delta X)}\Delta(\Delta X)\right| \tag{2-7}$$

where $|\Delta v| \ll |v|$ and $|\Delta(\Delta X)| \ll |\Delta X|$.

The relative maximal error, ε_p, due to precision errors can be calculated by:

$$\varepsilon_p = \frac{\Delta\bar{F}_{Rp}}{\bar{F}_R} \tag{2-8}$$

The precision error in speed, Δv, is estimated from:

- Error in measuring precision.

- Variation in wheel radii due to wheel conciliate and variation in track gauge
- Longitudinal oscillatory motions of the measuring car.

A numerical estimation of precision errors, with examples from actual test runs is presented in Section 4.1.

2.4.2 Bias errors

According to equations Eq. (2-4) and Eq. (2-5), the bias errors in the evaluated running resistance are due to determination of:

- Running resistance as a function of mean speed.
- Train mass.
- Rotating inertia.

The determination of running resistance as a function of mean speed for a given evaluation distance ΔX, gives a bias error. This is exemplified in the following. For simplicity, we assume no grades.

The work done by $\bar{F}_{R_{(a+k)a}}$ as a function of speed, along $\Delta X_{(a+k)a}$, must equal the decrease in total energy of a coasting train, which speed is in the range of v_a - v_{a+k}.

Hence, the calculated mean speed $\bar{v}$ is:

$$\bar{v} = \frac{x_{a+k} - x_a}{t_{a+k} - t_a} \tag{2-9}$$

However, assume the running resistance of the coasting train is given exactly by:

$$F_R(v) = A + Bv + Cv^2 \tag{2-10}$$

then, for the calculated constant mean speed, the work done by $F_R(v=\bar{v})$ does not generally equal the dissipation according to the decrease in energy.

Instead by assuming a constant train speed, $v = \bar{v}_{corr}$, which satisfies (2-11) along $\Delta X_{(a+k)a}$, the work done by $F_R(v = \bar{v}_{corr})$ can be written as:

$$(A + B\bar{v}_{corr} + C\bar{v}_{corr}^2)\Delta X_{(a+k)a} = \frac{M_T(1+H)}{2}(v_a^2 - v_{a+k}^2) \tag{2-11}$$

From (2-11) we resolve the constant speed $\bar{v}_{corr}$, corresponding to the running resistance:

$$\bar{v}_{corr} = \frac{B}{2C} \pm \sqrt{\left(\frac{B}{2C}\right)^2 - \frac{A}{C} + \frac{M_T(1+H)}{2C\Delta X_{(a+k)a}}(v_a^2 - v_{a+k}^2)} \tag{2-12}$$

The error in determined running resistance due to the difference between the determined mean speed and the corresponding speed, varies with evaluation distance ΔX and speed interval.

Maximal error in determined running resistance due to estimated train mass, m_T, and the term, $m_T H$, due to rotating masses, can be calculated in the same way as the precision errors:

$$\Delta\bar{F}_{Rb} \approx \left|\frac{\partial\bar{F}_R}{\partial M_T}\sum_{i=1}^{n_v}\Delta M_i\right| + \left|\frac{\partial\bar{F}_R}{\partial M_T H}\sum_{i=1}^{n_v}\Delta(M_i H_i)\right| \tag{2-13}$$

where: $M_T = \sum_{i=1}^{n} M_i$

The relative maximal error, ε_b, due to bias errors is calculated by:

$$\varepsilon_b = \frac{\Delta\bar{F}_{Rb}}{\bar{F}_R} \tag{2-14}$$

A numerical evaluation of bias errors, with examples from actual test runs is presented in Section 4.1.

2.5 Conclusions

The *Energy Coasting Method* is a useful tool for estimating train running resistance. Running resistance of any train can be determined on *any track* regardless of grades. Precision and bias errors can be estimated. In comparison with other methods, tractive forces, drawbar forces or similar are not measured, thus simplifying the testing procedures. Also, it is not necessary to compensate in real time for acceleration due to grades, thus eliminating error sources due to accelerometers and their possible inclinations. On the other hand as with drawbar and tractive force methods, track altitude data must be correct and available.

Influence of ambient wind upon the determined running resistance can be minimised by averaging polynomials from test runs which are run in each direction along the same measuring section during similar wind conditions.

3 Results from running resistance tests

This Chapter deals only with mechanical resistance and aerodynamic drag. Throughout the following, running resistance, F_R, means the sum of mechanical resistance and aerodynamic drag at non zero speed:

$$F_R = F_M + F_D \tag{3-1}$$

Resistance due to curves, curve resistance, which is a part of the mechanical resistance, and additional resistance encountered at starting, starting resistance [9], which decreases rapidly as the speed increases, is not studied separately.

3.1 General conditions

Tests are run with four train types:

1. Conventional loco hauled passenger trains.
2. High speed trains.
3. Ordinary freight trains, (from now on just called freight trains).
4. Ore train.

Train data and corresponding running resistance coefficients for the train types are summarised in Table 3-3 - Table 3-6.

Ambient temperature, wind speed and direction, plus atmospheric pressure are recorded locally at the measuring section during the tests; see Table 3-1. The anemometer is calibrated in a wind tunnel.

Table 3-1 Atmospheric conditions during tests

Train	Temp. (°C) mean, (min./max.)	Wind speed (m/s) mean, (min./max.)	Atm. pressure (hPa) mean, (min./max.)
Conv. passenger	2.5, (-7/ 7)	3.4, (1.2/10.0)	994, (983/1025)
High speed	15.0	1.9	1007
Freight	2.4, (-8/8)	3.3, (0.0/13.3)	1021, (1008 /1033)
Ore train	15.0	--, (0.0/5.0)	--.

Different measuring sections having different track types are used for tests with different types of trains. The track types are summarised in Table 3-2 for comparison.

Track altitude data for each test section was measured before the tests started [48].

Table 3-2 Track type properties

	Track 1	Track 2	Track 3	Track 4
Mass of rail (kg/m	50	43	50	60
Rail type	welded, CWR	jointed	welded, CWR	welded, CWR
Rail pad	hard rubber	steel	hard rubber	soft rubber
Sleeper	concrete, SJ 101	wood spacing 65 cm	wood spacing 55 cm	concrete
Ballast	macadam	gravel	macadam	macadam
Curves	Straight	straight	straight	$R \geq 7000$ m

CWR = Continuous Welded Rail

3.1.1 Conventional loco hauled passenger trains

Four conventional passenger trains, *P1 - P4*, of different lengths are used as shown in Table 3-3. Each train consists of 1 locomotive + trailing cars (empty. An ordinary passenger car, *SJ AB3RT*, is used as a measuring car. The influence of the measuring car, *SJ AB3RT*, upon the running resistance is assumed to be of about the same magnitude as an *SJ B7* car. The measuring car is thus treated as an *SJ B7* car in the evaluation.

The speed profile is recorded and measured by means of tacheometer. Bogies of the passenger cars are of type Minden Deutz with relatively stiff wheelset guidance.

The total projected frontal area for each passenger train is approx. 12.5 m^2. The ventilation of the passenger cars is shut down during tests. The locomotive uses about 15.2 m^3/s of cooling and ventilation air in all tests [47].

Tests for *P3* are run on Track type 1 and 2. No rail lubrication is present. The wind averaged result of the test runs on each track, could thus be compared for the same train.

No curves occurs for the measuring section on Track 1 and 2.

An evaluation distance of ΔX = 1000 m and ΔX = 100 m is used for speeds above 10 m/s and below 10 m/s, respectively.

3.1.2 High Speed trains

Three configurations are used, as shown in Table 3-4. Two of the trains consists of 1 power unit (pu.) + cars + 1 power unit (pu. Train X2, usually known as SJ X2000, consists of 1 pu + 4 cars + 1 driving trailer (dt). No special measuring car is used. The speed profile is measured on board the train by means of tacheometer. None of the trains is carrying passengers during tests. The weight of the train is determined by means of a scale. Bogies of the cars are of the radial self-steering type.

The ventilation of the passenger cars is shut down during tests. The power unit uses about 14 m^3/s of cooling and ventilation air in all tests, [13]. The total frontal area for each train is approximately 10.5 m^2.

Tests with X2-5 and X2-7 are performed on a CWR Track type 4 where the measuring section contains grades and curves having large radii of 7000 m. These curves are judged to have no significant influence on running resistance, in particular as the bogies are of the radial self-steering type. Tests with X2 are performed on track type 1 on a measuring section with no curves. An evaluation distance of ΔX = 2000 - 7000 m and ΔX = 10 - 100 m is used for speeds above 10 m/s and below 10 m/s, respectively.

3.1.3 Freight trains

A total of seven freight trains, *F1 - F7*, are tested, as described in Table 3-5. Two different freight wagons, the covered type *Hbis* and the open type *Oms* are used to form homogeneous and mixed train configurations, consisting of alternated *Hbis* and *Oms* wagons. In the tests where the influence of axle load upon running resistance is determined, only *Hbis* wagons are used. The weight of each wagon is estimated by means of a scale. The same *Hbis* wagons are used in the axle load tests.

The measuring car is an SJ Qib 022 equipped with one axle with non-conical measuring wheels.

The locomotive used for these tests is an *SJ Rc4*, which uses about 15.4 m^3/s of cooling and ventilation air in all tests.

All tests are run on the same measuring section on Track type 1, as the passenger trains *P1 - P4*. No rail lubrication is present. An evaluation distance of ΔX = 2000 m and ΔX = 100 m is used for speeds above 10 m/s and below 10 m/s, respectively.

3.1.4 Ore trains

Separate tests are run with one four axle ore wagon, OreW, having 3 different axle loads. Tests are also run with a short ore train, *Ore-T*. Consisting of one *SJ Rm* locomotive + 10 *Uad* ore wagons. *OreW* differs from *Uad* in length and bogie type, where its axles are guided more softly than in *Uad*, which is equipped with so-called “three-piece bogies”. The weight of each wagon is determined by means of a scale. The locomotive is of type *SJ Rm* which resembles *SJ Rc4* aerodynamically.

For *OreW* and *Ore-T*, speed is recorded aboard an ore wagon and measured by means of tacheometer. The measurements are triggered by reflexes as the wagon enters a measuring section.

Tests are run on Track type 3 on a tangent measuring section. No rail lubrication is present. The sleeper spacing on Track 3 is 55 cm.

An evaluation distance of ΔX = 2000 m and ΔX = 10 m is used for speeds above 10 m/s and below 10 m/s, respectively.

3.2 Test results

The results of the full scale tests for passenger, high speed, freight and ore trains are shown in Table 3-3 - Table 3-6, respectively.

The results are wind averaged in accordance with Section 2.3, and are considered to be an approximate mean value of running resistance during the prevailing wind conditions. Comparison of results achieved at no wind conditions with wind averaged, for the same freight train set, shows a difference of 1.0 - 2.5% in running resistance at 25 m/s.

Table 3-3 Loco hauled passenger trains. Train data and resistance coefficients.

Train	Config	Trailing axles	*Tot. mass (tonnes)	Tot. length (m)	Track type	*A* (N)	*B* (Ns/m)	*C* (Ns^2/m^2)
P1	loco + 1	4	124	40	1	2150	8	6.9
P2	loco + 5	20	300	145	1	3300	28	10.8
P3	loco + 9	36	476	251	1	4400	48	14.7
P3	loco + 9	36	476	251	2	5050	113	14.9
P4	loco + 13	52	562	356	1	5500	68	18.6

* Mass of loco SJ Rc6 included 74 tonnes.

Table 3-4 High speed trains. Train data and resistance coefficients.

Train	Config	Axles	Tot. mass (tonnes)	Length (m)	Track type	*A* (N)	*B* (Ns/m)	*C* (Ns^2/m^2)
X2-5	pu + 3 cars + pu	20	300	109	4	1600	51.6	6.22
X2-7	pu + 5 cars + pu	28	398	159	4	2300	57.8	7.74
X2	pu + 4 cars + dt	24	318	139	1	2000	40.0	6.90

Table 3-5 Freight trains. Train data and resistance coefficients

Train	Config	Wagons*	Axles*	Total mass (tonnes)	Axle* load (kN)	Tot. train length (m)	*A* (N)	*B* (Ns/m)	*C* (Ns^2/m^2)
F1-mixed		36	72	1470	183	514	15400	279	49.2
F2-mixed		24	48	1041	187	355	11500	258	37.0
F3-mixed		12	24	579	185	195	7000	92	21.6
F4-Hbis		18	36	797	183	294	8000	148	20.9
F5-Hbis		18	36	581	124	294	6750	142	20.2
F6-Hbis		18	36	395	73	294	5600	160	20.7
F7-Oms		18	36	798	183	256	8050	73	30.2

* Loco SJ R4 and measuring car not included.

Table 3-6 Ore wagon and ore train. Train data and resistance coefficients.

Train	Config	Axles	Tot. mass (tonnes)	Axle load (kN)	Length (m)	*A* (N)	*B* (Ns/m)	*C* (Ns^2/m^2)
OreW-1	1 *Uad*	4	21.2	52	9.8	450	-2	4.7
OreW-2	1 *Uad*	4	100.0	245	9.8	1100	-2	4.7
OreW-3	1 *Uad*	4	118.8	291	9.8	1300	-3	4.4
Ore-T	*SJ Rm* + 10 *Uad*	40	1090.0	245	100	12000	20	16.75

4 Analysis and discussion of evaluated running resistance

In this chapter, the error in the evaluated running resistance is estimated. The resistance coefficients *A*, *B* and *C* are analysed as well.

4.1 Discussion and comparison of errors with test runs

In this section, a numerical estimation of errors according to Section 2.4 is made and compared to errors of actual test runs.

According to the *precision error* in speed, Δv, is estimated from:

- Error in measuring precision of about ±0.002 m/s [39].
- Variation in wheel radii due to wheel conicity and variation in track gauge, if an ordinary passenger car with conical wheels is used as measuring car.
- Longitudinal oscillatory motions of the measuring car.

If a measuring wheelset, of an ordinary passenger car, with an equivalent conicity of 0.2 - 0.4, [54] is used; a variation in track gauge of ±5 mm gives a variation in wheel radius of ±0.5 - 1.0 mm. This results in an additional error in speed of approx. ±0.1 - 0.2%.

Longitudinal oscillatory motions of the measuring car, with respect to the train's mean speed superimpose an error in determined running resistance. By assuming for a short speed interval, a linear decrease in the train's mean speed, the magnitude of the speed variations can be approximately determined. An average speed variation of the measuring car of approx. ±0.05 m/s with respect to the train's mean speed is observed in some test results [13].

The estimated precision error, Δh_i, in the altitude of each vehicle with respect to track data is approximately +10 mm and -80 mm [45]. However, for an evaluation distance of ΔX = 100 m, an error of -80 mm with respect to track data is judged to be unusual [46]. Therefore it is assumed that for ΔX = 100 m, the error in the altitude of each vehicle's centre of gravity is +10 mm and -40 mm.

The precision error, $\Delta(\Delta X)$, in determined *evaluation distance***,** is estimated from:

- Error in measuring precision, as measured by the measuring car, which is about ±0.1%, [39], for a cylindrical measuring wheel.
- Variation in wheel radii. For a wheelset, with an equivalent conicity of 0.2 - 0.4, the difference in wheel radius is due to variation in track gauge, superimposing an error in determined evaluation distance ΔX of about ±0.2%.

Since ΔX is measured by the measuring car and taken as a mean value for the whole train, the rest of the vehicles have an additional error in their individual ΔX due to their oscillatory motions. This error is however comparatively small.

The estimated values of maximal precision errors are:

$$\Delta h_i \approx \begin{cases} +\ 10 \text{ mm, for all } \Delta X \\ -\ 40 \text{ mm, } \Delta X = 100 \text{ m} \\ -80 \text{ mm, } \Delta X \geq 1000 \text{ m} \end{cases}$$

$$\Delta v \approx \begin{cases} \pm 0.052 \text{ m/s for cylindrical measuring wheel.} \\ \pm 0.05 + 0.002\text{v m/s for conical worn type measuring wheel.} \end{cases}$$

$$\frac{\Delta(\Delta X)}{\Delta X} \approx \begin{cases} \pm 0.001 \text{ for cylindrical measuring wheel.} \\ \pm 0.003 \text{ for conical worn type mesuring wheel.} \end{cases}$$

According to Section 2.4.2, *bias errors* are due to determination of:

- Running resistance as a function of mean speed.
- Train mass.
- Rotating inertia.

The error in determined running resistance due to the difference between the determined mean speed and the corresponding speed, varies with evaluation distance ΔX and speed interval. For train *F1*, the evaluation distance ΔX = 100 m is used for lower speeds, v < 10 m/s, and ΔX = 2000 m is used for higher speeds, v > 10 m/s. This effect of the discrepancy in speed upon the results of running resistance is small. For train *F1*, at v = 10 m/s and ΔX= 2000 m, the relative difference in running resistance is about 0.8 % [15] at a calculated speed difference of $\bar{v}_{corr} - \bar{v}$ = 0.16 m/s.

The error in determined train mass, M_T, is approximately ±500 kg/vehicle. The estimated error in the term, $M_T H$, accounting for the rotating inertia is approximately ±120 kg/wheelset [12], caused by different wheel radii due to wear.

In the following, the error analysis from Section 2.4 is applied and exemplified on a freight train consisting of a *SJ Rc4* electric locomotive + 36 wagons. The wagons are of the closed *SJ Hbis* and open type *SJ Oms*, alternated to form a mixed consist. This mixed freight train is referred to as *F1*. Tests with this train configuration represent a relatively difficult case, due to scatter in output data caused mainly by ambient wind, in comparison with a smooth high speed train.

The estimated relative *maximal* precision, ε_p, and bias errors, ε_b, according to section 2.4.1 and 2.4.2, are shown for comparison in Figure 4-1 and Figure 4-2. The total relative maximal, ε_T, error is

$$\varepsilon_T = \varepsilon_p + \varepsilon_b \tag{4-1}$$

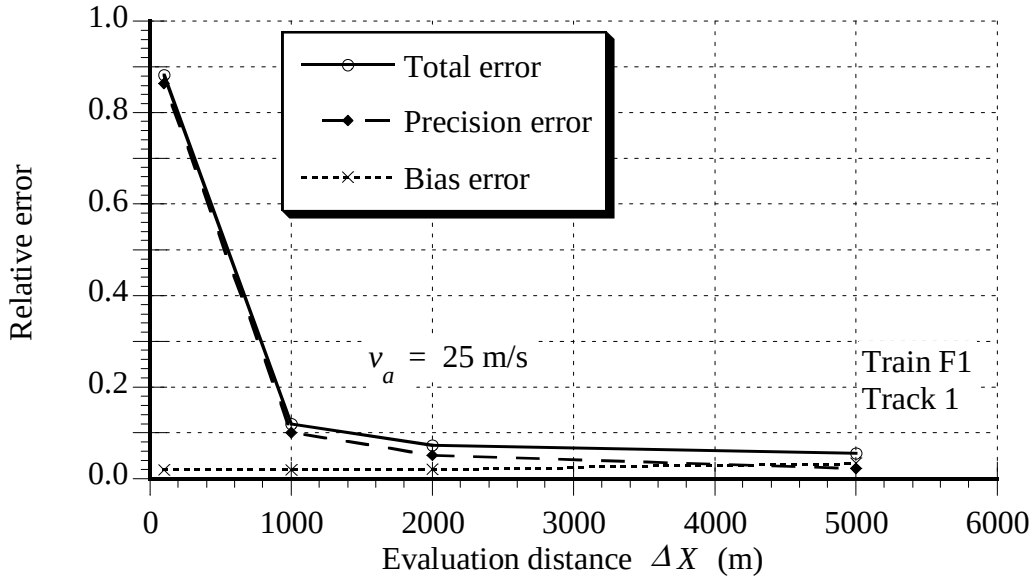

Figure 4-1 Estimated relative maximal errors for train F1 for different ΔX at 25 m/s.

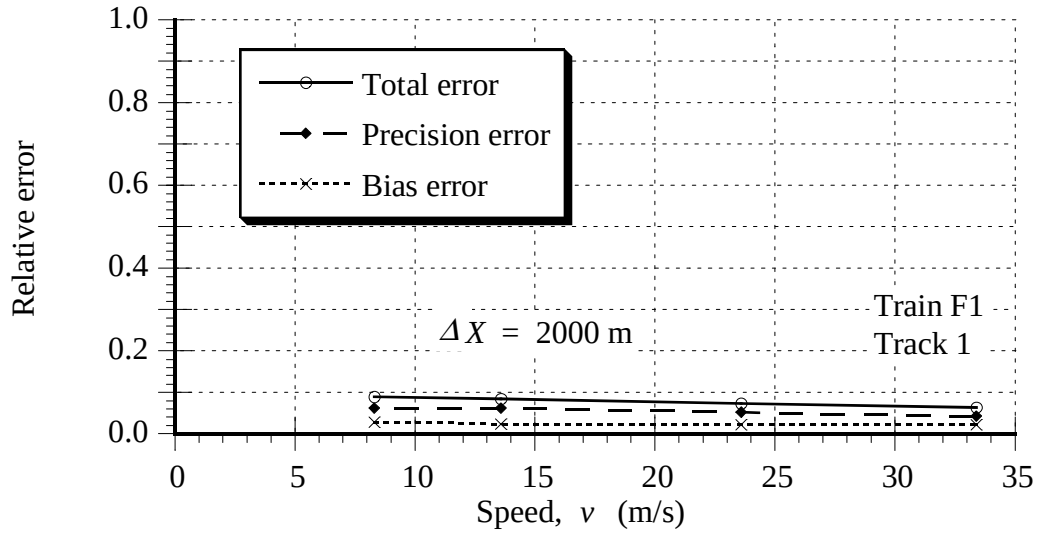

Figure 4-2 Estimated relative maximal errors for train F1 at ΔX = 2000 for different speed.

An important effect of the evaluation distance ΔX, is that precision errors, and thus the scatter, around the fitted polynomial, decrease considerably for increasing values of ΔX, as shown in Figure 4-1.

These estimated maximal errors are shown in Figure 4-3, as error bars around fitted polynomials from a single test run. The coefficient of determination, denoted by R^2, is a measure of how well the data is explained by the fitted polynomial. The higher value of R^2, the better the fit.

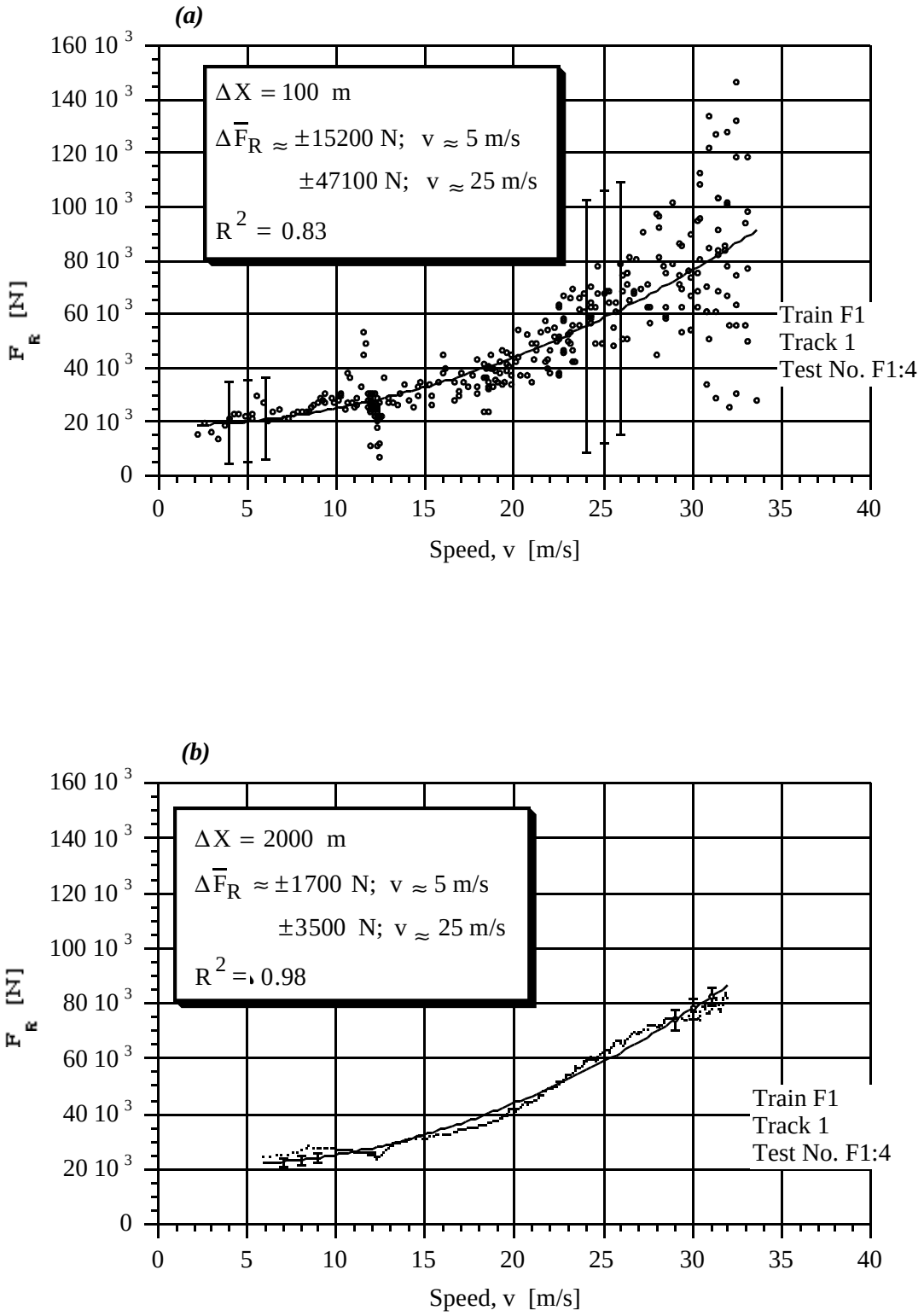

Figure 4-3 Example of scatter and maximal error bars for estimated mean running resistance. Single test run with train F1, for a) ΔX = 100 m and b) ΔX = 2000 m.

A source of error difficult to control, are the longitudinal motions of the vehicles in a train. This affects the estimation of the train speed, since the measured speed is in fact the speed of the measuring car; thus the determined running resistance is also affected. The big scatter in Figure 4-3 a, in the speed interval of 30 - 34 m/s at the beginning of the test run, is most likely originating from the measuring car's longitudinal oscillatory motions as the locomotive's drive is cut off somewhat too late at the beginning of the test run.

The value of ΔX has an another important influence upon the result of curve fitting with the method of least squares. As the value of ΔX increases, the number of data pairs, and the speed interval over which the running resistance polynomial is fitted, decreases. This is exemplified by a test run in Figure 4-4 evaluated with three different ΔX, ΔX = 5000 m, ΔX = 2000 m and ΔX = 100 m. A large value for parameter k, thus a large ΔX, may cause problems in attaining a correct curve fit for the running resistance, with respect to low and high speeds. The effect of the bias error due to determination of running resistance as a function of mean speed, is also clearly shown in Figure 4-4.

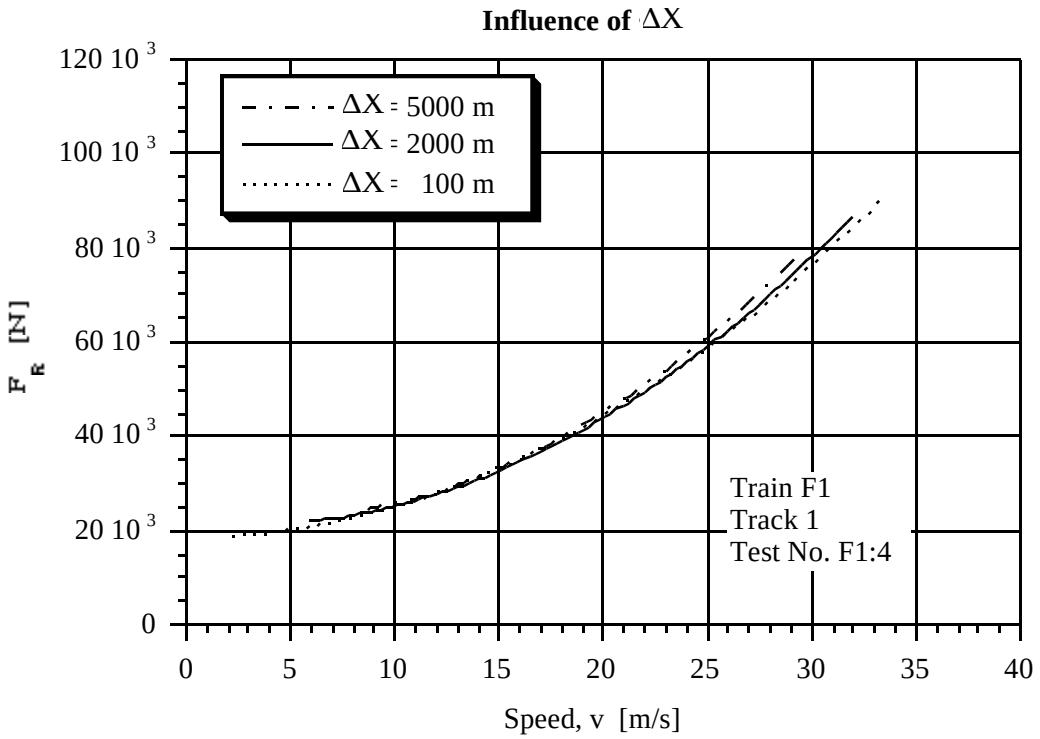

Figure 4-4 Comparison between polynomials of estimated running resistance for the same test run with different ΔX.

From full-scale tests with conventional loco-hauled passenger trains and various freight trains it is determined [15] by means of Student's t-distribution that for a confidence interval of 95 % the uncertainty in wind-averaged running resistance is about ± 8 %, taken as an average for all speeds. However, from tests performed with passenger trains a standard deviation of less than ± 3 % is achieved from individual test run pairs at 25 m/s (90 km/h).

4.2 Speed independent resistance - term *A*

4.2.1 Influence of axle load

Influence of axle load can be investigated by taking the difference in term *A* between train *F4*, *F5*, and *F6* and expressing it as a function of corresponding difference in axle load per axle, see Figure 4-5. In this way the influence of the loco + measuring car is approximately subtracted from the results for the freight trains

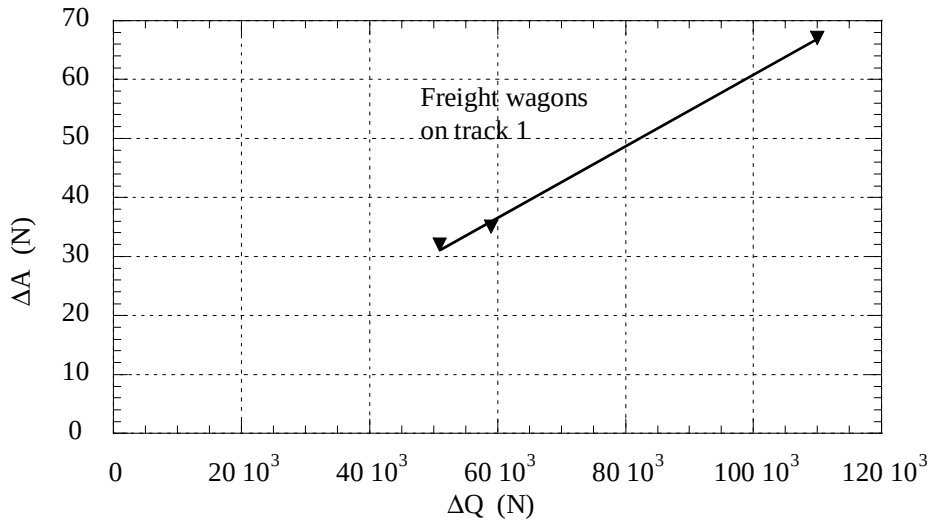

Figure 4-5 Change in term A per axle due to change in axle load.

By means of linear regression, the change in *A* per axle due to change in axle load is

$$\text{Freight: } \Delta A \approx 0.60 \cdot 10^{-3} \Delta Q \text{ (N)} \tag{4-2}$$

The variation of term *A* per axle for a single ore wagon due to axle load is shown in Figure 4-6.

It is clearly seen that running resistance increases approximately linearly and just slightly with increasing axle load. An increase of about 150% in axle load, for the freight trains tested, rises the running resistance by about 2.5 kN.

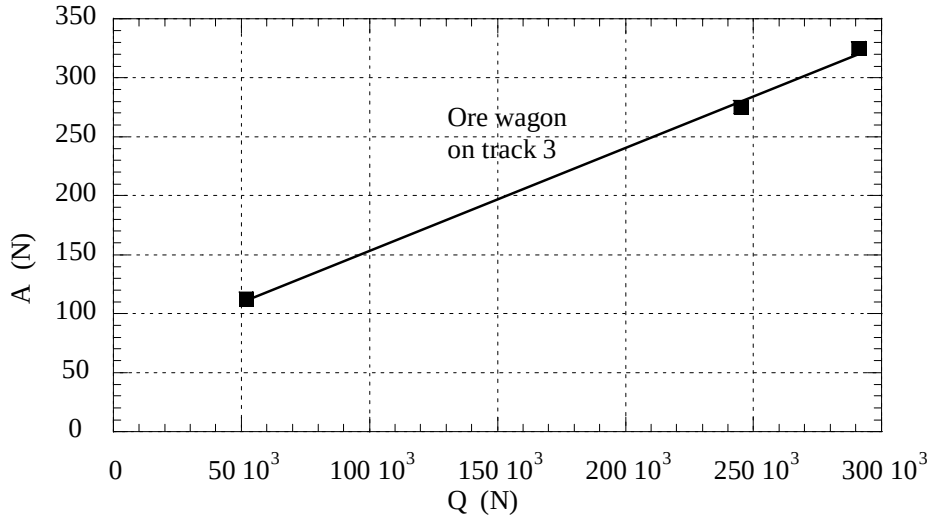

Figure 4-6 Variation of term A per axle due to axle load for an ore wagon.

$$\text{Ore: } A \approx 66 + 0.9 \cdot 10^{-3} Q \text{ (N)} \tag{4-3}$$

4.2.2 Influence of number of trailing axles

Results for term *A*, as a function of *number of trailing axles* for freight wagons, passenger cars and high speed trains, are shown in Figure 4-7. Term *A* is approximately linear with respect to the number of axles, at constant axle load for each train. The locomotive and propulsion units are included in order to distinguish their contribution.

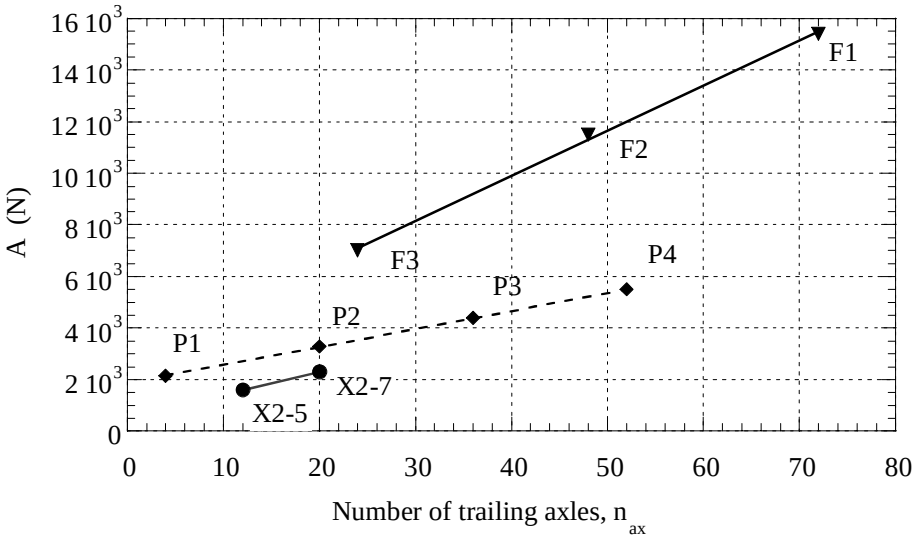

Figure 4-7 ***Term A as a function of number of trailing axles.***
The axle load of the freight wagons is adjusted to 183 kN by using Eq. (4-2). Loco or power units are included.

Term *A* for the test trains run on *track 1*, is described by the equations:

$$\text{loco + four axle passenger cars: } A \approx 1880 + 70n_{ax} \text{ (N)} \qquad (4\text{-}4)$$

$$\text{loco + two axle freight wagons: } A \approx 2540 + 175n_{ax} \text{ (N)}, \quad \text{for } Q \approx 183\ kN \qquad (4\text{-}5)$$

The first term in Eq. (4-4) - (4-5) is believed to originate from the mechanical resistance caused by the locomotive *SJ Rc6* and *SJ Rc4*, respectively. The estimated contribution of the measuring car *SJ Qib 022*, of approx. 300 N, is subtracted in (4-5). The contribution in (4-5) to the *A* term from the locomotive *SJ Rc4*, is in this case about 2540 N. This can be compared with the 1880 N for the loco *SJ Rc6*, in (4-4). However, it is not possible to estimate the constants in (4-4) and (4-5) with such accuracy. Instead, for practical reasons, the contribution from the locomotives to the constant terms is assumed to be the same; approx. 2000 N. The second term in (4-4) and (4-5) is the speed independent part of the mechanical resistance for the passenger cars and the freight wagons, respectively. For the *high speed train*, the term *A* is calculated by:

$$\text{pu + 4 axle cars + pu: } A \approx 550 + 88n_{ax} \text{ (N)} \qquad (4\text{-}6)$$

The first term in (4-6) which represents the resistance of two propulsion units is remarkably low and thus probably unreliable. Fitting a straight line through only two data points is risky for the analysis, since a small error in one of them can cause a large error in (4-6).

Combining Eq. (4-2) with (4-5), the total *A* term for trailing *two axle freight wagon axles* can be written as a function of axles and axle load:

$$A \approx \sum_{i=1}^{n_{ax}} (65 + 0.6 \cdot Q_i) \text{ (N)} \tag{4-7}$$

valid for at least $73 \text{ kN} \leq Q \leq 183 \text{ kN}$.

Term *A* for the ore wagons as a function of number of axles and axle load is determined from (4-3) which results in:

$$A \approx \sum_{i=1}^{n_{ax}} (66 + 0.9 \cdot Q_i) \text{ (N)} \tag{4-8}$$

valid for at least $52 \text{ kN} \leq Q \leq 291 \text{ kN}$.

The first term in Eq. (4-7) and (4-8) is believed to originate mainly from the part of roller bearing resistance which is independent of axle load, [51], [52]. The second term is believed to originate mainly from the portion of mechanical resistance, due to the deflection in the Track and in the wheel - rail contact area, as well as frictional forces in the wheel - rail interface. Dissipations due to these phenomena are dependent upon the axle load. Eq. (4-7) is only valid on *Track 1* for freight wagons with two axles and conical roller bearings, while Eq. (4-8) is only valid on *Track 3* for ore wagons.

4.2.3 Influence of track type

It is clearly seen in Table 3-3, that running resistance on *Track 2*, jointed tails on wooden sleepers in gravel, is higher than on *Track 1*, for the same train *P3*. The estimated wind averaged *C* coefficients resulting from test runs on *Track 1* and *Track 2*, are almost the same. The difference between the two *C* coefficients is about 2%. This consistency in the *C* coefficient, which originates mainly from the aerodynamic drag, shows that the increase in running resistance on *Track 2* is probably due to *increased mechanical resistance*. This conclusion is also plausible because it is hard to find reasons that aerodynamic drag should be dependent upon track construction and maintenance standards.

4.3 Resistance linearly dependent upon speed - term *Bv*

4.3.1 Influence of axle load, train mass and train length

Coefficient *B* is normally expressed as function of train mass, [8]. However, from tests with freight trains on *Track 1* and ore wagons on *Track 3*, see Figure 4-8, where the axle load is varied for the same train configuration, *F4*, *F5* and *F6*, and the ore wagon *OreW*, no systematic variation of coefficient *B*, due to axle load, can be distinguished.

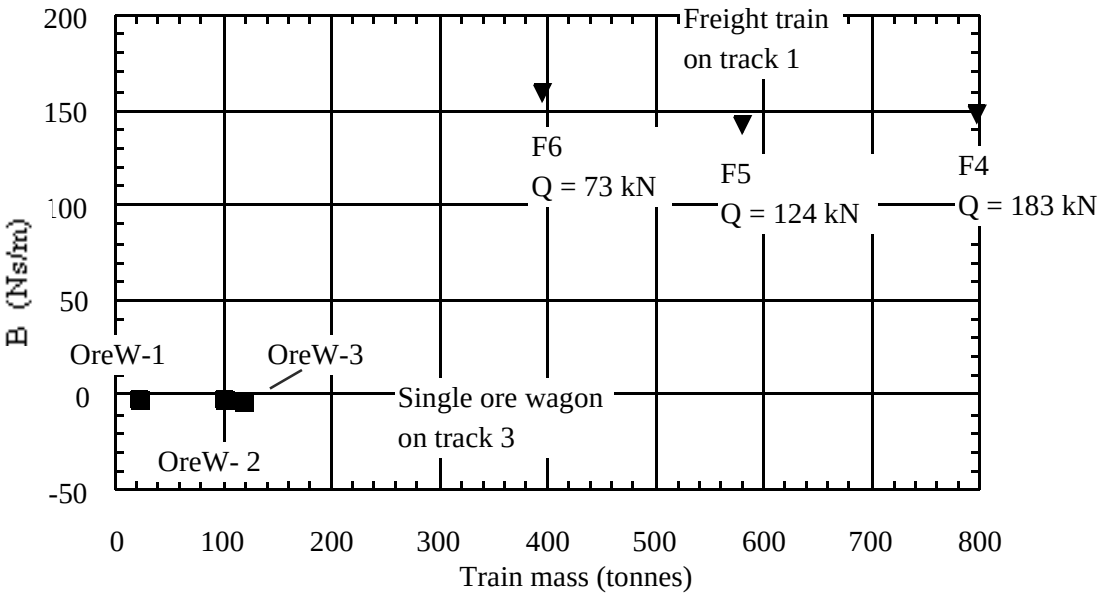

Figure 4-8 ***Variation of coefficient B as a function of train mass, due to change in mean axle load Q.*** *Train length is constant for each type of train. Locomotive and measuring car are not included in the mean axle load of F4 - F6.*

Although there are statistical uncertainties in the determined *B*-coefficients it may indicate that the main part of this coefficient is not due to mechanical resistance but rather originates from portions of air drag not covered by Cv^2. Therefore, coefficient *B* may be expressed as a function of total train length rather than train mass. This is shown in Figure 4-9. It clearly indicates that the B-term is almost linearly dependent on the train length, although train F2 is outside this tendency.

During the evaluation of the test runs, a positive correlation was observed between ambient wind and the scatter of the magnitude of coefficient *B*. This supports the hypothesis that the major part of the B-term originates from the air drag.

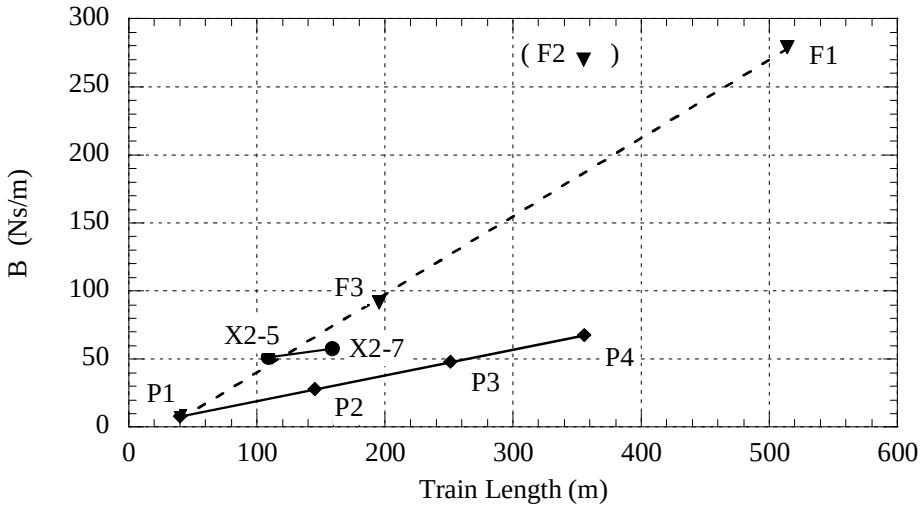

Figure 4-9 ***Coefficient B as a function of train length.*** *The dotted line for the freight trains coincides with P1, if F2 is omitted.*

From Figure 4-9 it is observed that in the freight train case test results for coefficient *B, F1 - F3*, are not linear with respect to train length as for the passenger trains. However, if the results for coefficient *B* for passenger as well as freight trains are depicted together, it is seen that by omitting the *B* coefficient for train *F2*, almost a straight line, dashed, can be drawn through the resulting B terms of trains *F1*, *F3* and *P1*. Train *P1* consists of a measuring car and a locomotive. It should therefore be possible to extrapolate the *B* coefficient for train *P1* from the *B* coefficients of the freight trains, since the locomotive and the measuring car in the freight trains are much alike train *P1*. This can be done only if the *B* coefficient for train *F2* is omitted. Therefore, it is most likely that the result of the *B* coefficient for train *F2* is somewhat erroneous.

Coefficient *B* for a passenger and freight train of mixed consist on *Track 1* is described by:

$$\text{Passenger train: } B \approx 1 + 0.19L_T \text{ (Ns/m)} \tag{4-9}$$

$$\text{High speed train: } B \approx 38 + 0.12L_T \text{ (Ns/m)} \tag{4-10}$$

$$\text{Freight train: } B \approx -22 + 0.58L_T \text{ (Ns/m)} \tag{4-11}$$

where L_T is train length.

The negative constant in (4-11), cannot be explained by simple means. It is important to remember that (2-6) is only an algebraic approximation of the running resistance. The parts of the running resistance that depend upon powers of speed other than those in (2-6), affect the values of

the fitted *A*, *B* and *C* coefficients. The statistical uncertainty in the *B* coefficient is significant, therefore a thorough explanation of coefficient *B* is not meaningful. Also, the negative constant does not produce any significant contribution to the total running resistance.

4.3.2 Influence of Track type

Tests with train *P3* result in higher values for the *B* coefficient on Track type 2 than on Track type 1. Due to statistical uncertainty it is not possible to conclude if this originates from the difference in Track types or not. However according to [4] dynamic motions of the vehicles contributes to the *B* coefficient. Track type 2 has more track irregularities which cause the vehicles to sway more on Track type 2 than on Track type 1.

4.3.3 Influence of air momentum drag

A trainset ingests air for cooling and ventilation. This causes additional air momentum drag [53].

Tests are run with the ventilation of the locomotive, on at its maximum as well as shut off. The ventilation of the passenger cars in *P1* - *P4* during the tests is shut off. No effect from the air momentum drag due to ventilation is distinguished in the test results. However, this result does not prove that such an influence does not exist.

A locomotive, *SJ Rc4*, as used in the freight train tests, ingests at most about 15.2 m^3 of air for cooling and ventilation. According to [8] the contribution to the resistance from the air momentum drag of the locomotive is calculated by

$$F_{Dint} \approx \rho \frac{dV_{int}}{dt} v \approx 20v \tag{4-12}$$

where V_{int} is the air intake volume per second and the air density, ρ, is 1.3 kg/m^3 at 0° C and 1013 hPa.

For *P3*, the drag due to ventilation at 30 m/s (108 km/h) is about 600 N. This is about 3% of the total running resistance, thus making it difficult to distinguish in the test results.

Air momentum drag was not investigated for the high speed, freight or ore trains.

4.4 Resistance dependent upon speed squared - term Cv^2

Aerodynamic drag, the part which is dependent upon speed squared, is usually written for no wind conditions as

$$F_D = \frac{1}{2}\rho A_f C_D v^2 = Cv^2 \tag{4-13}$$

where A_f is the projected cross section area.

Coefficient C is considered to originate mainly from the part of aerodynamic drag, that depends upon the speed squared. It is convenient [35] to express coefficient C as air drag area $C_D A_f$:

$$C_D A_f = \frac{2}{\rho} C \tag{4-14}$$

In Figure 4-10, the wind averaged $C_D A_f$ is shown as a function of total train length.

The results reveal that aerodynamic drag for passenger, *P1 - P4*, and freight trains, *F1 - F3*, increases approximately linearly with train length. This is also supported by [35].

According to the test results the aerodynamic drag can be written:

$$F_D = \frac{1}{2}\rho A_f C_D v^2 = \frac{1}{2}\rho A_f (C_p + C_l L_T) v^2 = C v^2 \tag{4-15}$$

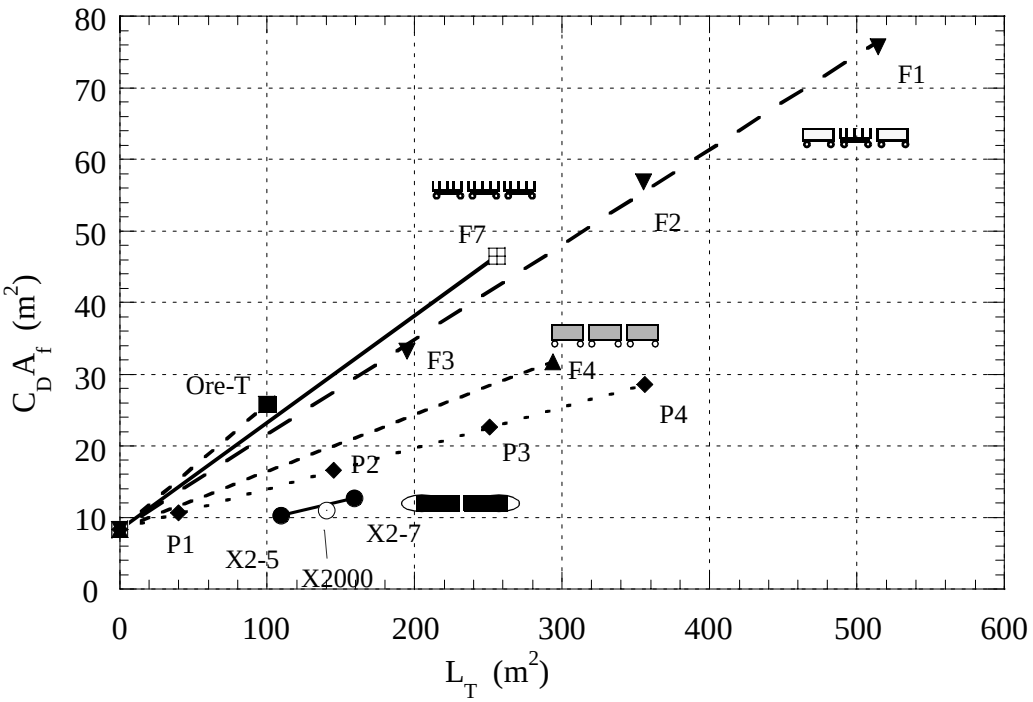

Figure 4-10 Comparison of linearised drag areas, $C_D A_f$.

By means of the method of least squares, a line is fitted to the wind averaged results of $C_D A_f$, giving:

$$\text{Conventional passenger trains: } C_D A_f \approx 8.3 + 0.057 L_T \ (\text{m}^2) \tag{4-16}$$

$$\text{High speed train } X2 \text{ with 2 pu: } C_D A_f \approx 4.7 + 0.050 L_T \ (\text{m}^2) \tag{4-17}$$

$$\text{Freight trains of mixed consist: } C_D A_f \approx 8.2 + 0.133 L_T \ (\text{m}^2) \tag{4-18}$$

The first term in $C_D A_f$ expresses the contribution to the pressure and suction drag acting on the front and rear of a train, [35]. In these terms the drag contribution from pantograph and roof equipment of the loco is also included. The second term, linearly dependent on train length, is assumed to originate from skin friction and pressure effects along the train.

The pressure and suction drag area constant of 8.3 m^2 in (4-16) for the passenger trains is considered to be a more accurate value than that of the freight trains, because of less scatter in the input data used for the evaluation of running resistance.

Setting the value of the pressure drag to 8.3 m^2 for trains *F4* and *F7*, and assuming a linear dependency upon train length, it is possible to express their wind averaged air drag area as a linear function of train length as well. This can be done since locomotive *SJ Rc6* and *SJ Rc4* are aerodynamically almost identical, hence should the air drags of the locomotives be the same.

Freight trains consisting of

$$\text{covered } Hbis \text{ wagons: } C_D A_f \approx 8.3 + 0.079 L_T \ (\text{m}^2) \tag{4-19}$$

$$\text{open type } Oms \text{ wagons: } C_D A_f \approx 8.3 + 0.149 L_T \ (\text{m}^2) \tag{4-20}$$

$$Ore \text{ trains: } C_D A_f \approx 8.3 + 0.175 L_T \ (\text{m}^2) \tag{4-21}$$

In Figure 4-10, the wind averaged $C_D A_f$ is expressed as a linear function of total train length.

4.5 Conclusions

Running resistance can now be reliably determined for Swedish conventional passenger trains, high speed trains, ordinary freight trains and ore trains for different axle loads, train lengths and speed.

Theoretically, the *total maximal relative error* in running resistance is approximately ± 8% for the freight trains. From full scale tests a standard error of less than 3% is achieved for the test run pairs. The Energy Coasting Method is sensitive, like all other methods, to precision errors in *speed* and in determined *Track altitude*. This can be coped with by choosing an appropriate *evaluation distance*, since scatter of the data from which a running resistance polynomial is fitted, decreases with increasing evaluation distance. However, for obtaining enough output data for low speeds, a short evaluation distance is necessary.

Term *A* increases linearly with number of axles and can be divided into two parts. One part is constant for a given type of running gear, while the other part increases approximately linearly with the axle load. This term is also affected by track standard; for a passenger train it is higher on a jointed track having wooden sleepers and gravel ballast, *Track type 2*, than on a CWR having concrete sleepers on macadam, *Track type 1*.

Term *Bv* can be divided into two parts and increases approximately linearly with number of axles or train length but does not show any systematic variation with axle load. This implies that term *Bv* is probably affected by the part of aerodynamic drag not covered by the quadratic term. Air momentum drag due to ventilation can not be distinguished from the test results, likely due to its small contribution to total running resistance. Term *Bv* is also probably affected by track standard and is higher on *Track type 2* than on *Track type 1* for a passenger train. Small negative test results for coefficient *B* are not uncommon.

Term Cv^2 can be divided into two parts. The first part is constant and depends mainly upon the front and rear of the train. The second part increases approximately linearly with train length. The drag area as a function of train length for train *F7*, which consists of open type *Oms* wagons, is higher than that of a train where the *Oms* and covered *Hbis* cars are alternated, trains *F1*, *F2*, *F3*, despite their quite small cross section area. This is most likely due to the poles along each side of the wagons. Moreover, both of the configurations with open type wagons or alternated covered/open type wagons shows considerably higher drag area than train configurations with covered type wagons only.

5 Influence of measured ambient wind on air drag during full scale tests

It is outside the scope of this study to explain in *detail* the influence of various wind conditions upon aerodynamic drag. However, the influence of head and tail wind in the test results is not consistent with conventional theory based on relative speed between train and wind. Therefore, this issue will be further analysed and discussed. A model for the influence of head and tail wind is suggested in Section 5.2.

5.1 Test results versus conventional theory based on relative speed

In this Chapter the discussion will be focused mainly on the effects on almost pure head and tail wind. Investigations and discussions will, in this context, be limited to the *C* term, i.e. the term depending upon speed squared. This is in most cases the term contributing to at least 80 % of the air drag at the train´s maximum speed (cf. Sections 3.2, 4.3 and 4.4). This is not to state that the *B* term (linearly dependent on speed) is negligible from an air drag point of view (cf. Section 4.3.1), especially not in strong side winds. However, the latter effects will not be studied in detail or discussed here.

Aerodynamic drag, not including the *B*-term, against the direction of travel, is normally proposed, [64], to be determined by:

$$F_D = \frac{1}{2}\rho A_f C_D(\beta) v_{rel}^2 \tag{5-1}$$

where $C_D(\beta)$ is the drag coefficient corresponding to air drag forces in the longitudinal direction, as function of yaw angle β. Yaw angle $_b$, and relative wind speed, v_{rel}, are defined in Eq. (5-2) and (5-3), respectively. The relations can be identified from the vector representation in Figure 5-1.

$$\beta = \operatorname{atan}\left(\frac{v_w \sin\alpha}{v + v_w \cos\alpha}\right) \tag{5-2}$$

$$\left|v_{rel}\right| = \sqrt{(v^2 + {v_w}^2 + 2v \cdot v_w \cos\alpha)} \tag{5-3}$$

v = train speed

v_W = wind speed

α = wind direction relative to measuring section

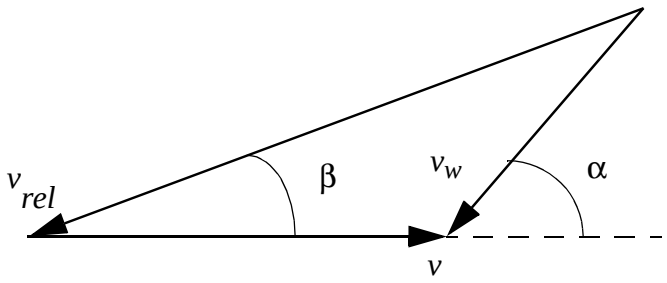

Figure 5-1 Definition of yaw angle β and relative wind speed v_{rel}

From Figure 5-1 it is seen that the yaw angle is $\beta = 0°$ for pure head wind, $\alpha = 0°$, and for pure tail wind, $\alpha = 180°$. The aerodynamic drag for pure head and tail wind, calculated as normally proposed, is thus

$$\text{Pure head wind: } F_D = \frac{1}{2}\rho A_f C_D(0) \cdot (v + v_w)^2 \tag{5-4}$$

$$\text{Pure tail wind: } F_D = \frac{1}{2}\rho A_f C_D(0) \cdot (v - v_w)^2 \tag{5-5}$$

Let us take one example by considering the aerodynamic drag for train *P2*, loco + 5 cars, for almost pure head and tail wind conditions, as shown in Figure 5-2. The influence of wind calculated by Eq. (5-4) and Eq. (5-5), upon aerodynamic drag for head and tail wind does not agree with test results, as determined in this study.

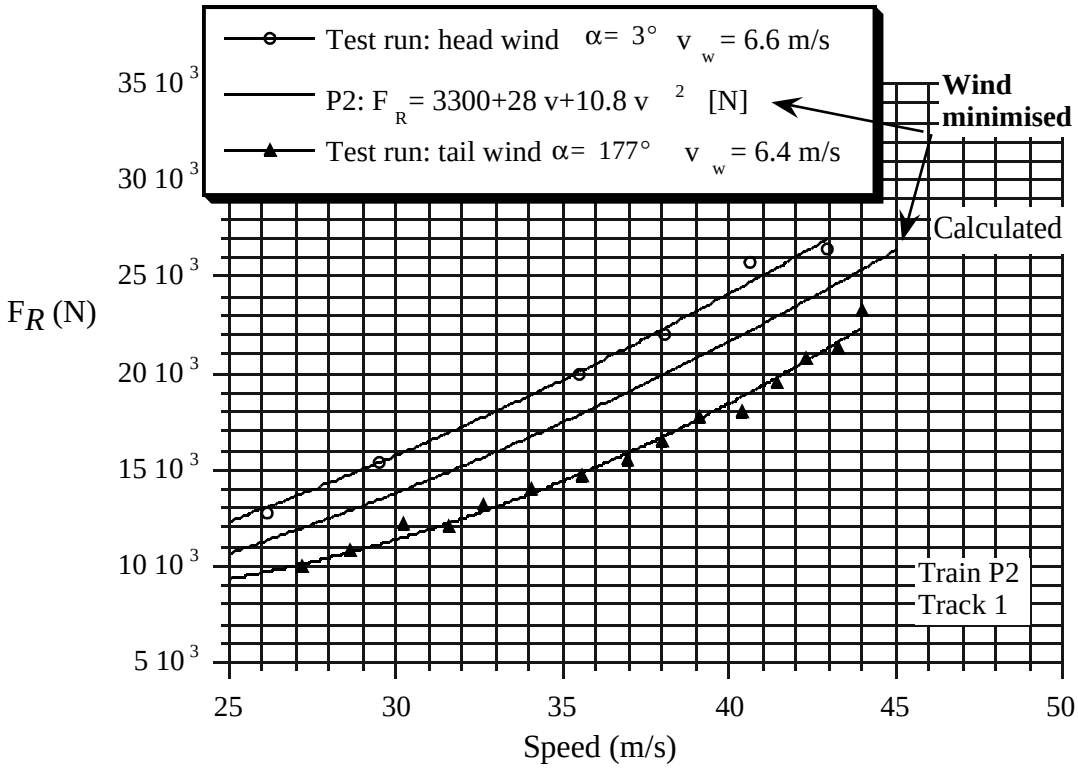

Figure 5-2 Example of influence of wind upon running resistance for train P2, loco + 5 cars.

From Figure 5-2 it is seen that the change in aerodynamic drag for train *P2*, loco + 5 cars, at a train speed of v = 35 m/s, is about 2 - 3 kN for a head wind of v_w = 6.6 m/s.

Calculating the influence of head wind by using Eq. (5-4) and (5-5) for the same train *P2*, by setting $\beta = 0°$, gives for the same conditions as in Figure 5-2:

$$\Delta F_D = \frac{1}{2}\rho A_f C_D(0) \cdot (v_{rel}^2 - v^2) \approx C(v_{rel}^2 - v^2) = \left\{ \begin{array}{l} v = 35 \text{ m/s} \\ v_w = 6.6 \text{ m/s} \end{array} \right\} \approx 5.5 \text{ kN} \qquad (5\text{-}6)$$

This calculated increase in air drag of *5.5 kN* is not in agreement with the increase of approx. *2 - 3 kN* as found from the test results, shown in Figure 5-2. The evaluated increase in air drag due to wind is about 50 % of the calculated by Eq. (5-1).

This phenomenon appeared for all the test runs performed with passenger trains. Similar results for the increase in air drag due to wind, were obtained by [62]; however, no thorough explanation for this phenomenon is given.

5.2 Model for influence of head and tail wind

A possible explanation to this phenomenon may be the actual variation of wind speed with height above ground, [64], [65], as schematically shown in Figure 5-3.

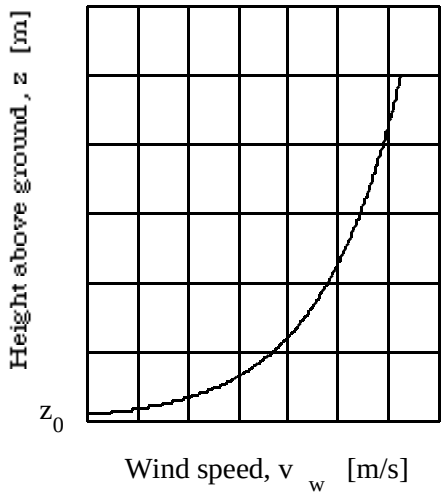

Figure 5-3 Schematic wind speed profile.

The wind speed as a function of height above ground can be calculated from, [65]:

$$v_w = \frac{u_y}{k}\ln\left(\frac{z}{z_0}\right); \quad z > z_0 \tag{5-7}$$

where:

z = height above ground (m)

z_0 = roughness length (m)

u_y = shear speed (m/s)

k = 0.4, von Karman's constant

The roughness length, z_0, which is a measure of the roughness of the terrain, surrounding the track, is purely empirical, [65]. z_0 is typically about 0.01 - 0.04 m for low grass and 0.9 - 1.0 m for pine forest.

If the wind speed is measured at a specific height, $z_m > z_0$, then the local wind speed profile, according to [65], is:

$$v_w(z) = v_m \frac{\ln\left(\frac{z}{z_0}\right)}{\ln\left(\frac{z_m}{z_0}\right)}; \quad z_m > z_0 \tag{5-8}$$

v_m = measured mean wind speed (m/s)

z_m = measuring station's height above ground (m)

Influence of head wind, $\cos\beta \approx 1$, upon aerodynamic drag, can now be approximately calculated, from the basic Equation (5-4), if the aerodynamic drag is, for simplicity, divided into *front and rear pressure drag*, *car body drag* and *undercarriage drag*.

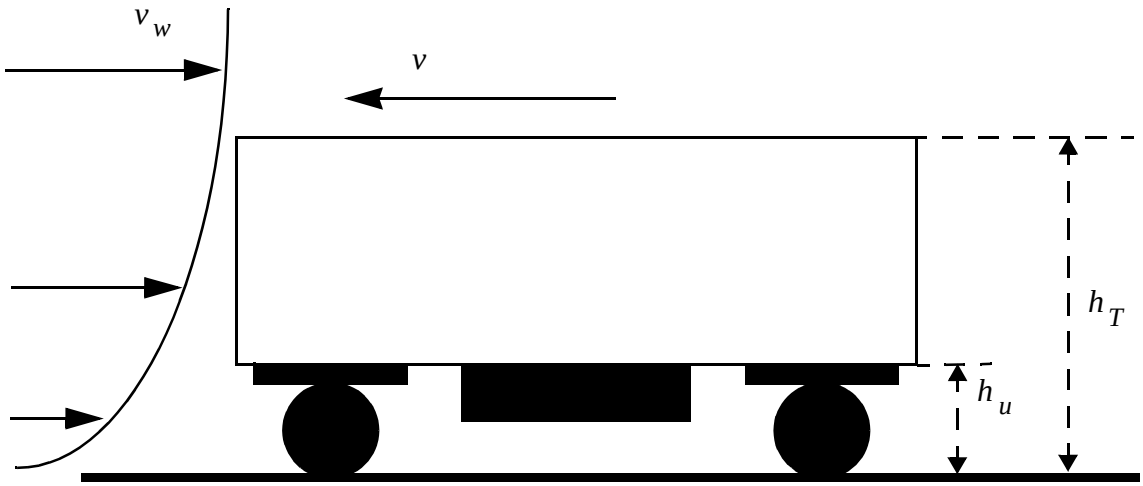

Figure 5-4 Schematic variation of wind speed as a function of height above ground.

Front and rear pressure drag:

$$F_{Dp} \approx \frac{1}{2}\rho C_p A_f \left(v^2 + \frac{1}{h_T - z_0} \int_{z_0}^{h_T} (2v \cdot v_w(z) + v_w^2(z)) dz \right) \quad (5\text{-}9)$$

where:

C_p = mean front pressure and rear suction drag coefficient

h_T = height of vehicle (m)

v_w = wind speed (m/s)

Car body friction drag is divided into drag from side walls and roof:

$$F_{Db} = F_{Dwall} + F_{Droof} \quad (5\text{-}10)$$

where:

drag from side walls:

$$F_{Dwall} \approx \frac{1}{2}\rho \bar{c}_f A_{wall} \left(v^2 + \frac{1}{h_T - h_u} \int_{h_u}^{h_T} (2v \cdot v_w(z) + v_w^2(z)) dz \right) \quad (5\text{-}11)$$

$\bar{c}_f$ = mean skin friction coefficient of the side walls or roof

h_u = height of undercarriage, see Figure 5-4.

A_{wall} = 2 L_T (h_T - h_u), total side wall area of the train

drag from roof:

$$F_{Droof} \approx \frac{1}{2}\rho \bar{c}_f A_{roof} \left(v + v_m \frac{\ln\left(\frac{h_T}{z_0}\right)}{\ln\left(\frac{z_m}{z_0}\right)} \right)^2 \tag{5-12}$$

A_{roof} = $b_T L_T$, total roof area (m^2)

b_T = train width (m)

Undercarriage drag:

$$F_{Du} \approx \frac{1}{2}\rho C_u L_T A_f \left(v^2 + \frac{1}{h_u - z_0} \int_{z_0}^{h_u} (2v \cdot v_w(z) + v_w^2(z)) dz \right) \tag{5-13}$$

Undercarriage drag coefficient, C_u is calculated from:

$$\frac{1}{2}\rho C_u L_T A_f v^2 = \frac{1}{2}\rho A_f C_l L_T v^2 - \left(\frac{1}{2}\rho \bar{c}_f A_{roof} + \frac{1}{2}\rho \bar{c}_f A_{wall} \right) v^2 \tag{5-14}$$

$$C_u = C_l - \bar{c}_f \frac{2(h_T + h_u) + b_T}{A_f} \tag{5-15}$$

where C_l is the total mean pressure and friction coefficient along the train from Eq. (4-15).

The running resistance including the influence of head or tail wind, can now be calculated from:

$$F_R = A + Bv + F_{Dp} + F_{Db} + F_{Du} \tag{5-16}$$

In Figure 5-5 and Figure 5-6, the aerodynamic drag due to wind is added to the wind minimised running resistance polynomials according to Eq. (5-16). The agreement is good with the results received for windy conditions if the empirical roughness length is assumed to be in the range of

0.2 - 0.4 m. The following values for the constants in Eq. (5-9) - (5-15) are used for calculating the aerodynamic drag, including head or tail wind:

$C_p A_f = 8.3\ \mathrm{m}^2$ — $h_T = 4.1\ \mathrm{m}$, approx height of train

$C_l A_f = 0.057$ — $h_u = 1.0\ \mathrm{m}$, (measured)

$A_f = 12.5\ \mathrm{m}^2$ — $z_0 = 0.2\ \mathrm{m}$, roughness length (empirical)

$\Rightarrow \begin{cases} C_p = 0.66 \\ C_l = 4.56 \cdot 10^{-3} \end{cases}$ — $z_m = 2.3\ \mathrm{m}$, (measured)

$\bar{c}_f = 0.0015$, (approx.) according to [66]. — $b_T = 3.0\ \mathrm{m}$, approx. width of train

$\rho = 1.27\ \mathrm{kg/m}^3$, ($T = 5°$ C, $p = 1013$ hPa)

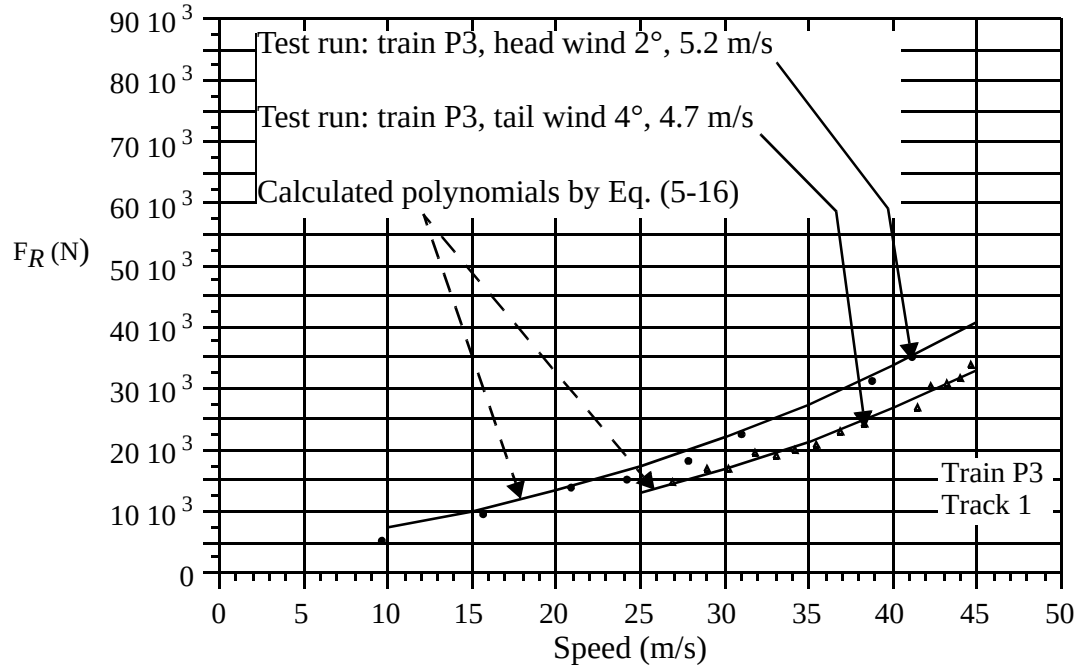

Figure 5-5 Comparison between determined running resistance for windy conditions and wind minimised polynomials where the calculated aerodynamic drag due to wind, F_w, is added. Train P3, loco + 9 cars.

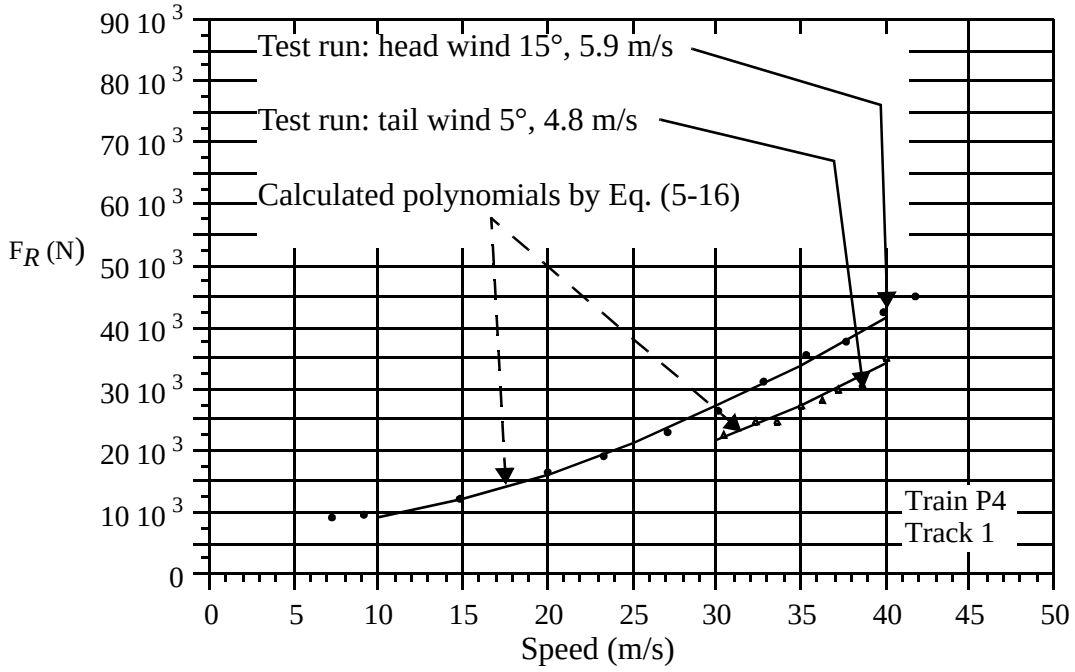

Figure 5-6 Comparison between determined running resistance for windy conditions and wind minimised polynomials where the calculated aerodynamic drag due to wind, F_w, is added. Train P4, loco + 13 cars

5.3 Conclusions

The resulting influence of head and tail wind is considerably lower for the tests, than estimated from the conventional method by considering relative speed between train and wind.

The effect of head and tail wind upon aerodynamic drag for passenger trains can be approximately calculated, if the vertical distribution of the air flow above ground is considered, thus giving good agreement with test results.

6 Freight train testing - energy, running time and driver behaviour

Ordinary Swedish freight train operations were studied in special tests during 1996-97. An electric locomotive was instrumented for measuring and recording variables such as speed, powering and braking levels, power intake, line voltage, motor currents, auxiliary power, ATC signalling data, etc. Also GPS information on positions was recorded. From these data it is possible to estimate tractive forces, accelerations and retardations, wheel slippage, geographical position etc., as well as driver´s actions.

A great number of various freight trains were run with this locomotive all over the Swedish long haul freight rail network.

This Chapter describes the tested locomotive and freight trains, test sections and the automatic train control system (ATC) as well as the experimental setup. Samples of data from the tests are shown in Chapters 7-11.

6.1 Objectives and general information

The objective of the full-scale tests is to provide the necessary data for *making a model of trains and their drivers*, with respect to running time, energy consumption and driver behaviour. At this stage only *freight trains* are tested and modelled.

Tests were performed during the time period June 1996 - August 1997. Testing equipment was installed by former *SJ* Rolling Stock Division´s Laboratory, partly for *SJ:s* own purposes. KTH was allowed to participate in the tests. The test data used in this thesis is recorded and provided by former SJ Rolling Stock Division's Laboratory (SJ/ MTL).

An ordinary freight train locomotive was selected: *SJ Rc4*, No 1197. The locomotive was operated by a great variety of ordinary drivers in ordinary freight trains, who had no special instructions with regard to the tests. Thus it is assumed that the driver´s way of driving is essentially unaffected by the measurements and the recordings. This is in particular important for the development of a *driver model*.

6.2 General description of locomotive *SJ Rc4*

The Rc type of locomotive is shown in Figure 6-1. The locomotive is connected to the catenary by the pantograph, which is connected to the main transformer aboard the locomotive. The nominal voltage at the catenary is 15 kV at $16\ ^{2}/_{3}$ Hz.

There are seven separate secondary transformer windings. One winding is used for the auxiliary 3-phase power which is needed for ventilation, cooling and compressors. A second winding is used for train heat power and a third is used for magnetising the separately excited D.C. motors. Each of the four remaining windings is feeding the four D.C. traction motors with power through two half-controlled bridges connected in series [57].

Each of the locomotive's four traction motors is connected by a transmission gear to its respective wheelset. The locomotive, *SJ Rc4* 1197, used in the tests has a modified electrical control of traction, [58] which compared to the original traction control unit reduces the tractive effort available. The purpose with this modification is to reduce the motor temperature. This modification is implemented on most of the *SJ Rc4* used for hauling freight trains. The modified tractive effort characteristic is shown in Figure 7-1.

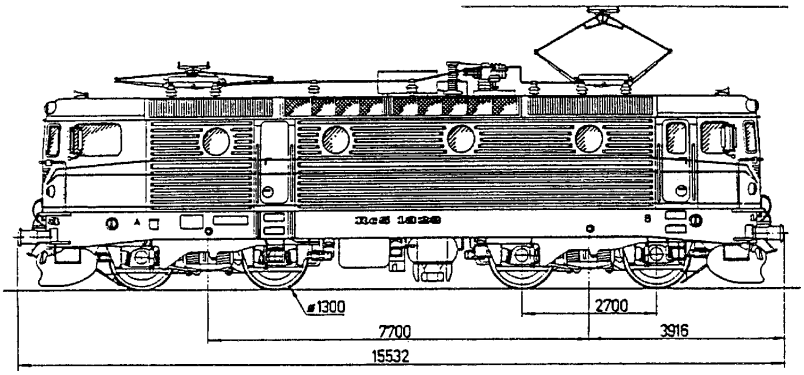

Figure 6-1 Locomotive of type SJ Rc. *Length 15.5 m. Mass 79 tonnes.*

The driver can control the power needed for traction by means of a powering lever. The lever has non-discrete notch levels. By means of automatic speed control, it is possible to overrule the lever setting [39].

Braking is applied by the driver by means of a brake lever which is connected to a valve. As the air pressure is reduced in the main air pipe, the pressure in the brake cylinders increases. In the *nominal braking mode* the pressure in the pipe is reduced by 100 kPa and the braking force is about 2/3 of maximal [55], [68]. To enter the full braking mode the pressure is reduced by 150 kPa. To enter the non-braking mode the main air pipe pressure is restored to and maintained at 500 kPa.

The locomotive is not equipped with a regenerative braking system.

6.3 Automatic Train Control (in Sweden)

Automatic Train Control, ATC, data and signalling data are stored in *beacons* which are set out strategically along almost the entire track in Sweden. The data is recorded by means of ATC antennas aboard the locomotive as the antenna passes over a beacon. The recorded data is briefly [61]:

- Present speed restriction, $v_{ATC(n)}$
- Next speed restriction, $v_{ATC(n+1)}$
- Distance to next speed restriction.

- Grade, *G*.

Also, the driver must enter necessary data manually into the system:

- The braking ability of the train.

- The permissible speed of the train.

- Train length.

If the speed exceeds the speed restriction by 5 km/h (1.4 m/s), the driver is alerted by *short signals* and a *warning lamp*. If the speed restriction is exceeded by 10 km/h (2.8 m/s), the train automatically enters full braking mode. The train enters *emergency braking mode* if the speed exceeds the speed restriction by 15 km/h (4.2 m/s).

The system is also supervising the driver so that he starts braking from a feasible distance before a speed restriction or stop occur. If the driver starts braking too late, the system starts braking the train automatically.

6.4 Tested trains

The present locomotive operates in *ordinary freight traffic* throughout the *whole of Sweden*, thus hauling different freight train configurations, driven by different drivers. Data of the train configurations is provided by *SJ*, through a *train data base*. The train data base contains useful information about the hauled trains during the measurements. More specifically, the data base contains:

- Train identification number.

- Departure station, date and time.

- Arrival station, date and time.

- Total hauled mass (loco not included).

- Length (loco not included)

- Number of axles

- Type of wagons and their positions in the train.

- Number of locomotives hauling the trains.

Data from a total of 54 different train sets, driven by different drivers, is evaluated. Most train sets are running on long hauls. Therefore each longhaul with a specified train set has been divided into a number of shorter test sections, here called tests. Each test has normally a duration of 3000 - 3600 s (50 - 60 min). Figure 6-2 shows the mass of the trains and the number of tests.

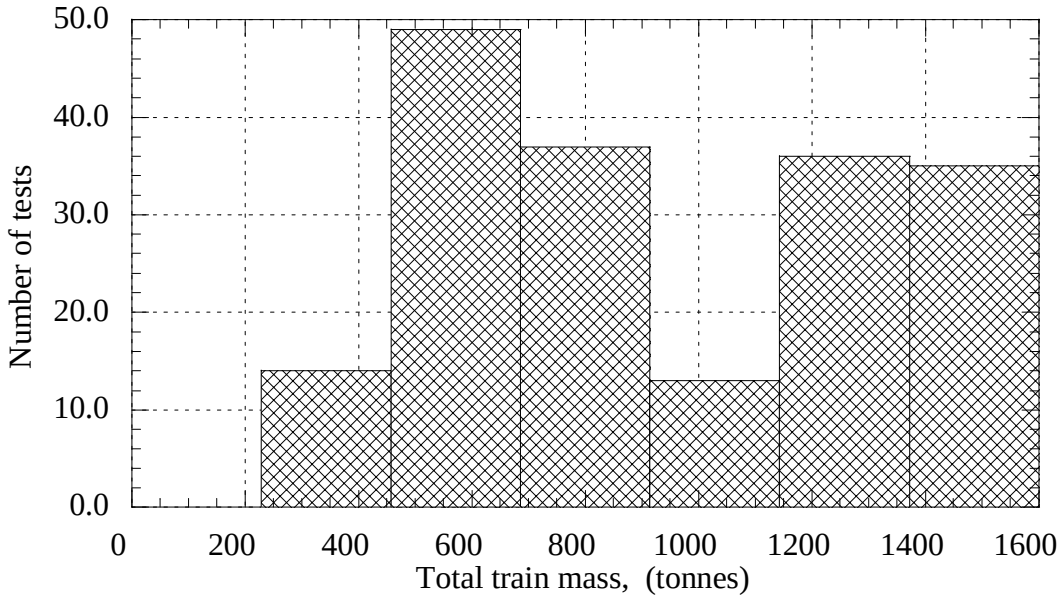

Figure 6-2 Mass of tested train sets and number of tests.

6.5 Experimental setup and recorded variables

In Table 6-1, the recorded test data used for evaluation is shown. The data is recorded every single second except for the data provided by the GPS, geographical positioning system, which is recorded every ten seconds.

It is important to bear in mind that the relative *maximal error* as shown in Table 6-1 contains both bias and precision errors and represents the worst case. Since precision errors are random, it is most likely that the error in fact is substantially less than the maximal error.

Table 6-1 Recorded test data used for evaluation.

Variable	Description	Unit	Approx. max rel. error (± %) [39], [40], [41]
P_{tot}	Total active power intake at pantograph	kW	1
U_L	Rectified mean value of catenary voltage	V	1
I_A	Rotor current of each motor	A	2
I_F	Field current of each motor	A	2
t	Time	s	-
n_{rot}	Number of rotor revolutions/s of each motor	Hz	-
v_w	Train speed measured at wheel rim	m/s	1 m/s
v_r	Train speed measured by radar	m/s	1
v_{ATC}	Signalled speed collected by ATC antenna	m/s	-
γ	Powering level [1)]	0-10	-
Pcv	Braking pilot pressure	0-360 kPa	-
GPS coordinates.	Geographical positions according to WGS-84		±100 m (1996)

1) The actual powering level of the locomotive has 9 notch levels, plus zero. However, powering level is scaled from 0 to 10, where 0 corresponds to zero powering, notch 0, and 10 corresponds to maximal powering, notch 9.

Active power intake at the pantograph was measured by means of a special measuring transducer, Tillquist P200R-14, having an accuracy class of 0.5%. The maximal relative error in measured active power is approximately 1.0 %.

By making use of the rotor current, I_A, and the field current, I_F, the tractive force , F_{mot0}, is determined from the measurements by means of a computer program [60] provided by SJ. The maximal relative error in F_{mot0} is estimated to be approximately ± 2 %.

The recorded powering level is in the range of 0 - 10. However, the real locomotive has 9 non-discrete notch levels for the powering.

If u is the gear ratio and n_{rot} is the number of rotor revolutions/s, the angular velocity, ω_w, of wheelset number j is calculated by

$$\omega_{w(j)} = 2\frac{\pi}{u} n_{rot(j)} \tag{6-1}$$

In this context it is important to make some clarifications regarding to tractive force and how it is related to rotating accelerating masses.

The nominal tractive force from motor *j* is calculated for steady state conditions, zero acceleration, by the provided program [60] from:

$$F_{mot0(j)} = \eta_{gear} \frac{1}{r_{w(j)}} \cdot u \cdot K_m \cdot I_{A(j)} \cdot \psi(I_{F(j)}) \tag{6-2}$$

η_{gear} is the efficiency of the gear, and is for simplicity used as a constant in this context, r_w is the wheel radius, K_m is a motor constant and ψ is the air-gap flux as a function of I_F. The total power, P_{mot0}, of one locomotive having four motors is:

$$P_{mot0} = \sum_{j=1}^{4} r_{w(j)} \omega_{w(j)} F_{mot0(j)} \tag{6-3}$$

Taking *rotational inertia* into account, F_{mot} is calculated at the wheel periphery by

$$F_{mot(j)} = F_{mot0(j)} - K_J \frac{r_{w(j)} d\omega_{w(j)}}{dt} \tag{6-4}$$

$$K_J = \frac{1}{r_{w(j)}^2} (u^2 J_{rot} + J_{gear} + J_w) \tag{6-5}$$

where J_{rot}, J_{gear} and J_w is the rotational inertia of rotor, gear and wheelset, respectively.

The total tractive force, F_{mot}, of the locomotive at the wheel rims determined from the measurements is

$$F_{mot} = \sum_{j=1}^{4} F_{mot(j)} \tag{6-6}$$

and the tractive power P_{mot}, at the wheel periphery is

$$P_{mot} = \sum_{j=1}^{4} r_{w(j)} \omega_{w(j)} F_{mot(j)} \tag{6-7}$$

During the tests, the wheel radii of the locomotive's four wheelsets were measured once every two weeks.

Geographical position of the locomotive is determined by means of GPS and by correlating the ATC antenna recordings with the corresponding positions of the ATC beacons in the track data base which is provided by *Banverket* (Swedish National Rail Administration), see Section 6.6.

The drivers way of driving the trains is assumed to be essentially unaffected by the recordings. This is in particular important for the development of the driver model in Chapter 9 - 10.

6.6 Test sections

The track data base for the evaluation is provided by *Banverket* (Swedish National Rail Administration) and contains:

- The distance along the track from a starting position.
- Position of stations.
- Curves; radii, starting and ending positions.
- Grades; inclination, starting and ending position.
- Signalled speed restrictions; position on the track and speed.

Since the locomotive runs over the whole of Sweden during the recordings, no particular test section is used. Most of the recordings, however, are made on the approximately 1500 km long track section between Sävenäs - Borlänge - Boden, in both directions. The altitudes are calculated by using information on grades with strating/ending positions from the track data base. This method is quite simple and is expected to produce approximative information on relative amplitudes. The calculated vertical profile of this track section is shown in Figure 6-3. The profile is calculated from the provided track data.

It is observed from the calculated vertical profile that the altitude of Boden is 47 m lower than Sävenäs. The difference in altitude is in reality about 1 m. However, this has a negligible practical influence on the further analysis, since this error is comparatively small in relation to the distance of almost 1500 km between Sävenäs and Boden.

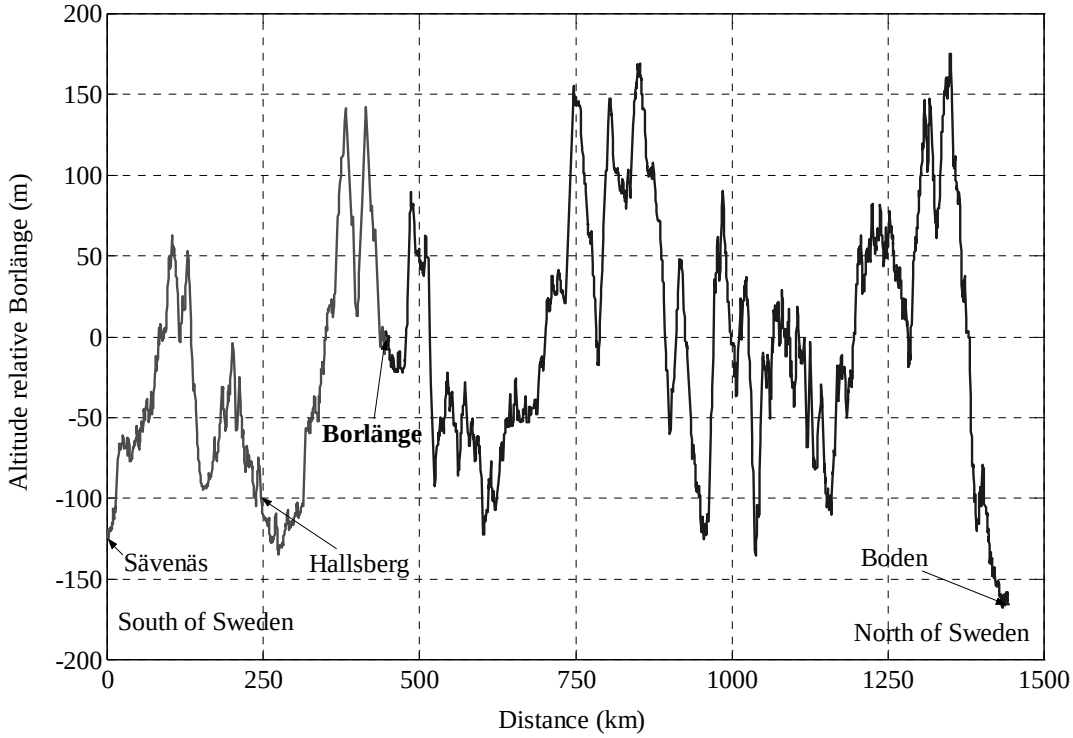

Figure 6-3 Vertical profile of track section between Sävenäs - Borlänge - Boden. The altitude is in relation to Borlänge.

7 Train modelling

In this chapter the locomotive and the freight trains are modelled with respect to traction and braking systems, mechanical and electrical efficiency, running resistance, etc.

7.1 Traction model

The tractive effort characteristics of locomotive *SJ Rc4* is shown in Figure 7-1. The nominal tractive effort, F_{t0}, is determined at the wheel periphery and is valid at steady state, i.e. at zero acceleration, and is not restricted by adhesion.

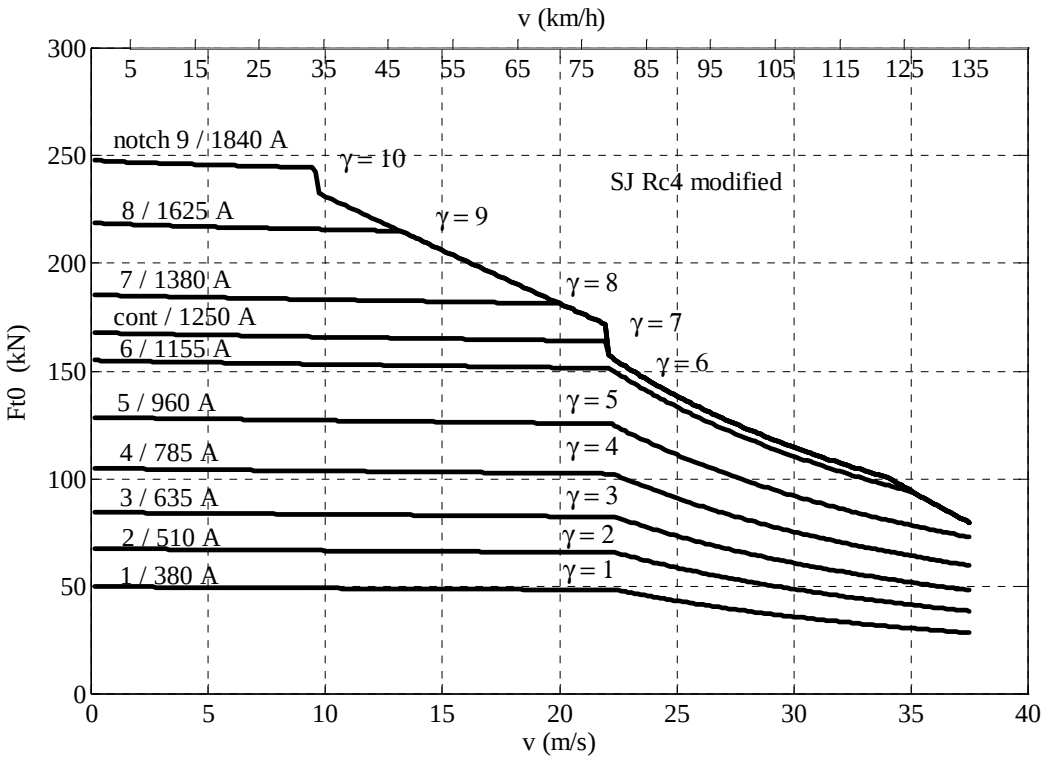

Figure 7-1 ***Tractive effort, F_{t0}, for SJ Rc4 versus speed, nominal at wheel rims, at zero acceleration. At different notch levels, powering levels, γ, and rotor current [59].*** *Wheel radius is 0.635 m (semi-worn wheels) and line voltage is 15 kV.*

The computer program for *calculating tractive effort, F_{t0},* at the *wheel rims*, as delivered by the motors of the locomotive *SJ Rc4,* is provided by *SJ* [59].

Calculated influence of line voltage on tractive effort, F_{t0}, for *SJ Rc4*, is shown in Figure 7-2. It is clearly seen that a line voltage drop significantly reduces the available tractive effort at higher speeds. It is therefore of great importance to implement line voltage variation in the model.

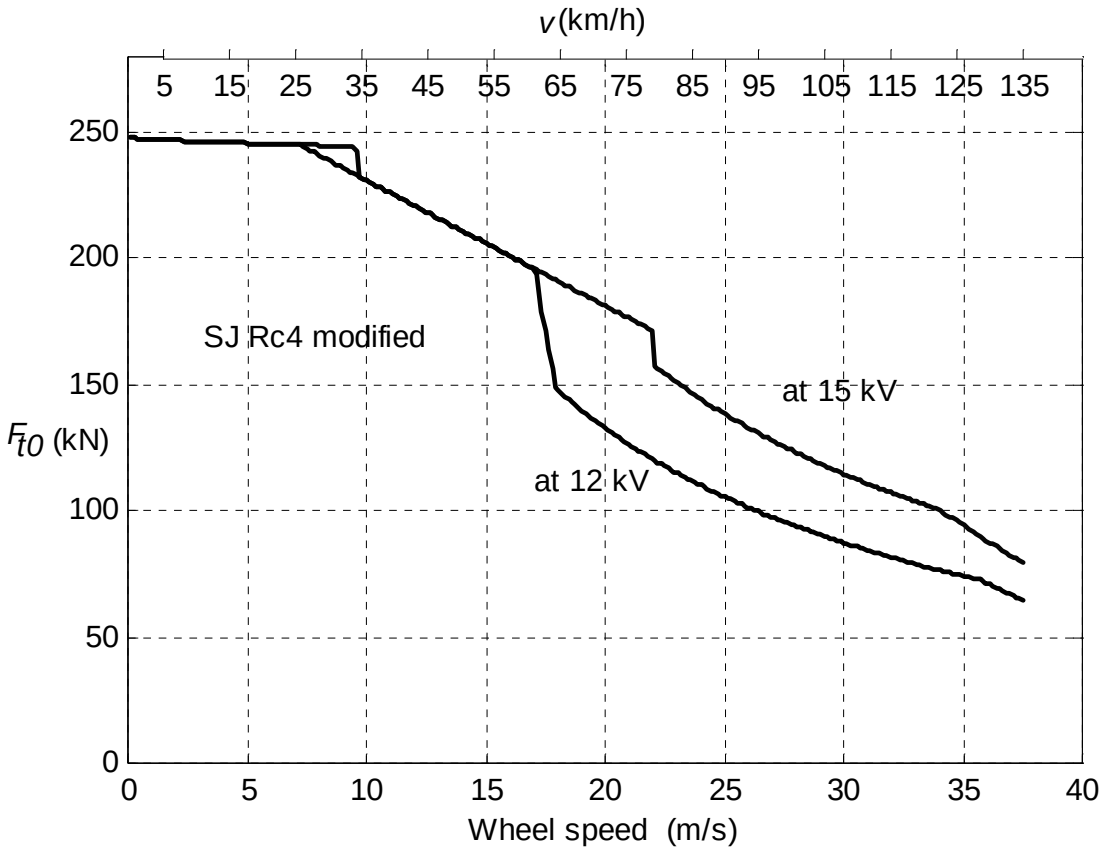

Figure 7-2 Calculated influence of line voltage on nominal tractive effort, F_{t0}, at full powering and at a line voltage of 12 kV and 15 kV respectively [59].

Measured line voltage drop due to increasing total power intake at pantograph level, P_{tot}, is shown in Figure 7-3. The voltage is evaluated for a power intake in steps of 0.25 MW, i.e. 0 - 0.25, 0.25 - 0.5, etc. There are considerable variations in line voltage for different reasons. There is as on average a significant influence from the power intake of the actual tested locomotive. Other trains, on the same electrical power feeding section, may also affect the line voltage.

The line voltage, U_L, as a function of total power intake, P_{tot}, can as on average be expressed empirically as

$$U_L = 14.11 - 0.19P_{tot} \text{ (kV)} \tag{7-1}$$

where P_{tot} is given in MW.

In Figure 7-4, a typical response of the *measured tractive force*, F_{mot}, is shown due to a change in powering level. A typical delay in response is approx. 7-10 s due to a time lag in the locomotives control system and due to the delay in magnetisation of the traction motors.

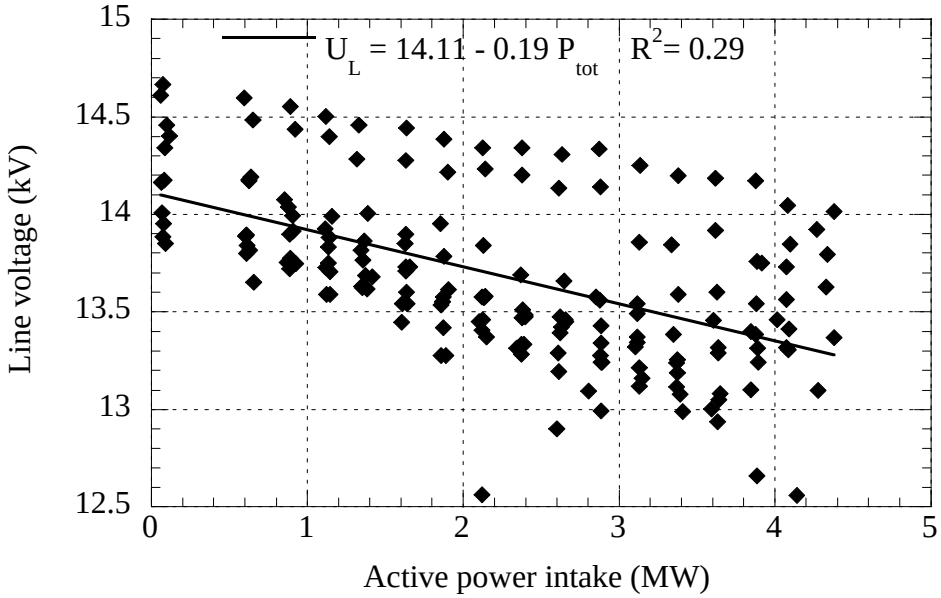

Figure 7-3 ***Line voltage, U_L, as a function of total power intake, P_{tot}, at the pantograph, measured for different track sections and trains.***

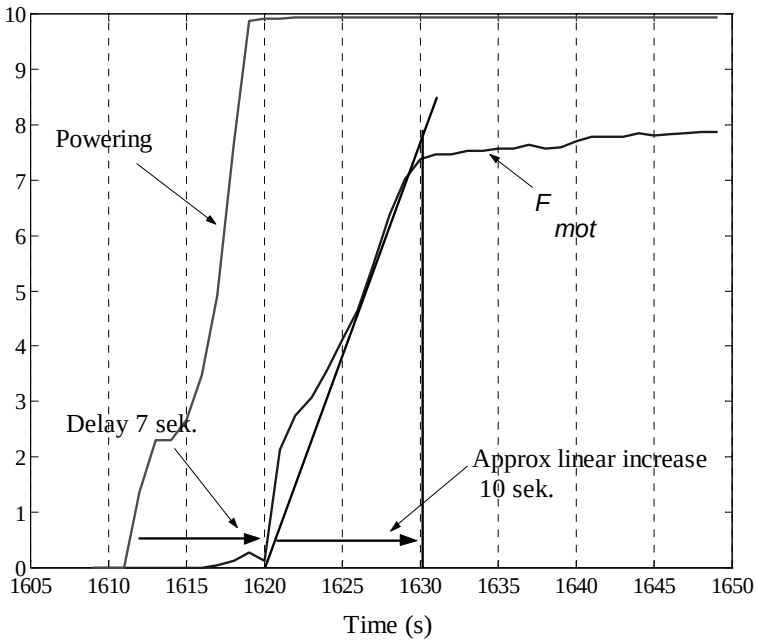

Figure 7-4 ***Example of delay in measured tractive force, F_{mot}, response when powering level increases from zero to maximum.***

It is important to implement this lag in the propulsion model. For a train travelling at 30 m/s a lag of 10 s results in an offset of 300 m on the track, from the point where the driver starts powering.

From the moment when the powering is increased by the driver, the increase in tractive force F_{t0}, in the model is divided into two parts:

1. Delay mode.
2. Increasing mode.

In the delay mode, F_{t0} is empirically delayed by 7 s. Thereafter in the increasing mode, F_{t0} increases linearly until it reaches its final level corresponding to that given by the powering level, γ. It takes about 10 seconds for F_{t0} to reach its maximal level if γ = max.

The flowchart of the powering model is shown in Figure 7-5.

Data for calculation of the tractive force, is precalculated and is for this work stored in a three-dimensional matrix, $\Phi[\gamma, v(1+\zeta), U_L]$, and depends on powering level γ, actual wheel speed $v(1+\zeta)$ which includes slippage ratio, ζ, and line voltage U_L. The slippage ratio is discussed in Section 7.4.1. Thus at time step i:

$$F_{t0(i)} = \Phi[\gamma_i, v_i(1+\zeta_i), U_{Li}] \text{ [N]} \tag{7-2}$$

for *zero acceleration*.

The power is calculated for steady state conditions by:

$$P_{t0} = F_{t0} v(1+\zeta) \tag{7-3}$$

During acceleration, $a > 0$, the tractive force at the wheel rims of the locomotive is in reality somewhat lower than F_{t0} as calculated in Eq. (7-2), due to influence of total rotational inertia, J_{tot}, in rotor, gear, wheels, axles and disc brakes of the locomotive. Taking rotational inertia into account, F_t is calculated for wheelset number, j, by:

$$F_t = F_{t0} - 4K_J \; a(1+\zeta) \tag{7-4}$$

$$F_t = \left\{ \begin{array}{c} u = \frac{87}{26} \\ r = 0.63\text{m} \\ J_{rot} \approx 58\ \text{kgm}^2 \\ J_{gear} \approx 40\ \text{kgm}^2 \\ J_w \approx 394\ \text{kgm}^2 \end{array} \right\} \approx F_{t0} - 10750 \cdot a(1+\zeta) \quad \text{(N)} \tag{7-5}$$

F_{t0} is calculated and stored in Φ for

- γ in steps of 1, from 0 - 10.
- v in steps of 0.14 m/s (0.5 km/h), from 0 to 37.5 m/s (135 km/h).
- U_L in steps of 100 V, from 10.0 to 17.0 kV.

F_{t0} for intermediate, non-integer, values of γ, is achieved by means of linear interpolation. The calculated train speed and line voltage is rounded off to their closest corresponding value stored in Φ.

The force that can be applied at the wheel rims is also limited by *adhesion*, α, [55]. The expression for the adhesion is empirical [55], [56] and can be approximately estimated by Curtius Kniffler's formula for ''dry rail'' conditions. This tractive force, $F_{t\alpha}$, limited by adhesion can be calculated for dry rail conditions as a function of speed by:

$$F_{t\alpha} = M_{t\alpha} \cdot g \cdot \alpha = M_{t\alpha} \cdot g \cdot \left(0.161 + \frac{7.5}{44 + 3.6v}\right) \quad \text{(kN)} \tag{7-6}$$

$M_{t\alpha}$ is the adhesive mass of the locomotive in traction.

For ''wet rail'' conditions:

$$_{t\alpha} = M_{t\alpha} \cdot g \cdot \alpha = M_{t\alpha} \cdot g \cdot \left(\frac{3.78}{23.6 + v}\right) \text{(kN)} \tag{7-7}$$

The final resulting tractive force, F_w, at the wheel rims is obtained by taking the minimum of F_t and $F_{t\alpha}$.

$$F_w = min(F_t, F_{t\alpha}) \tag{7-8}$$

The delay in tractive force, as shown in Figure 7-4, is modelled by a Powering Delay module according to Figure 7-5.

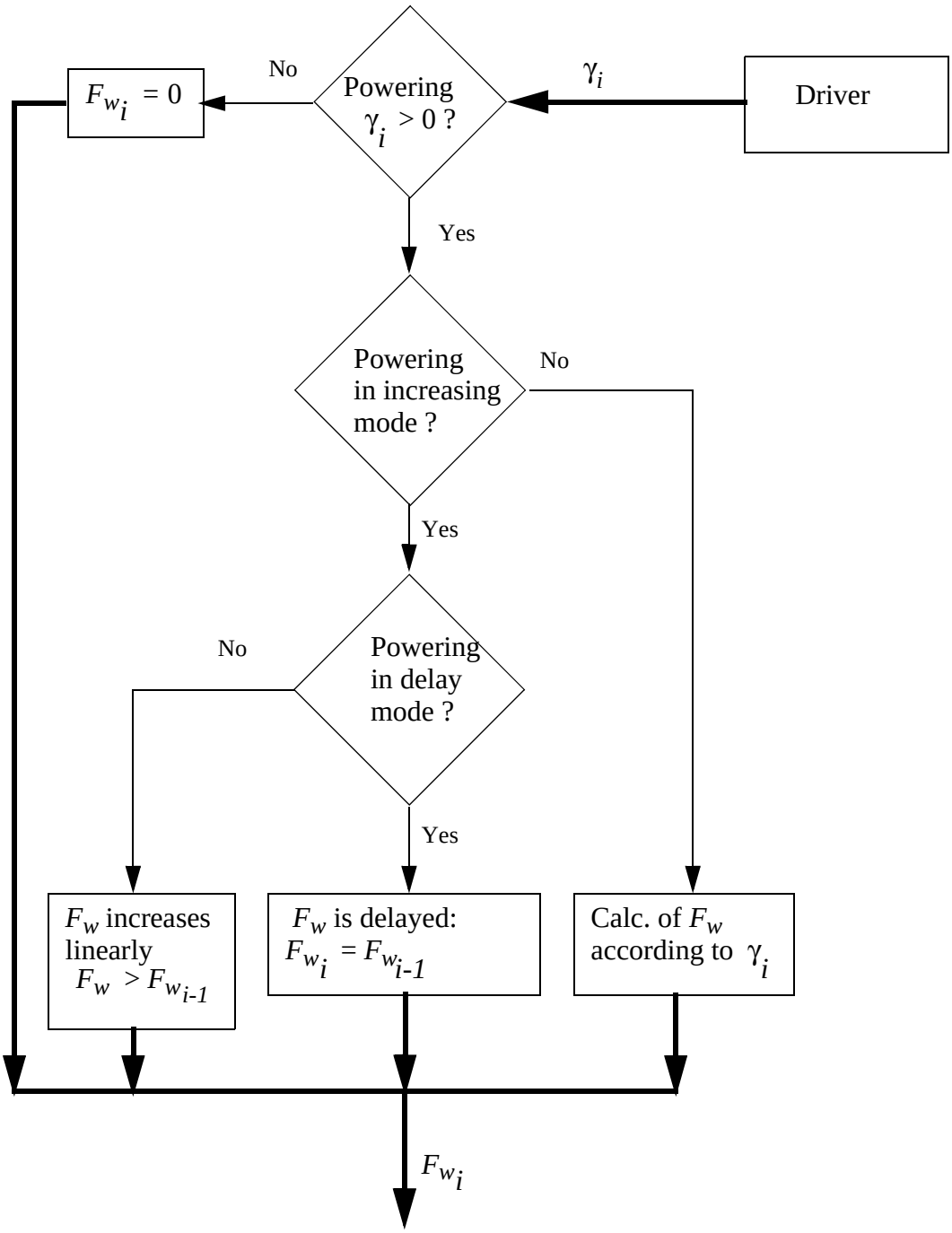

Figure 7-5 Flow chart of Powering Delay Module

A comparison between F_w and F_{mot} is shown in Figure 7-6. It is seen that F_w follows F_{mot} when the driver changes the powering level. F_w is calculated according to the Powering Delay module and Eq. (7-8).

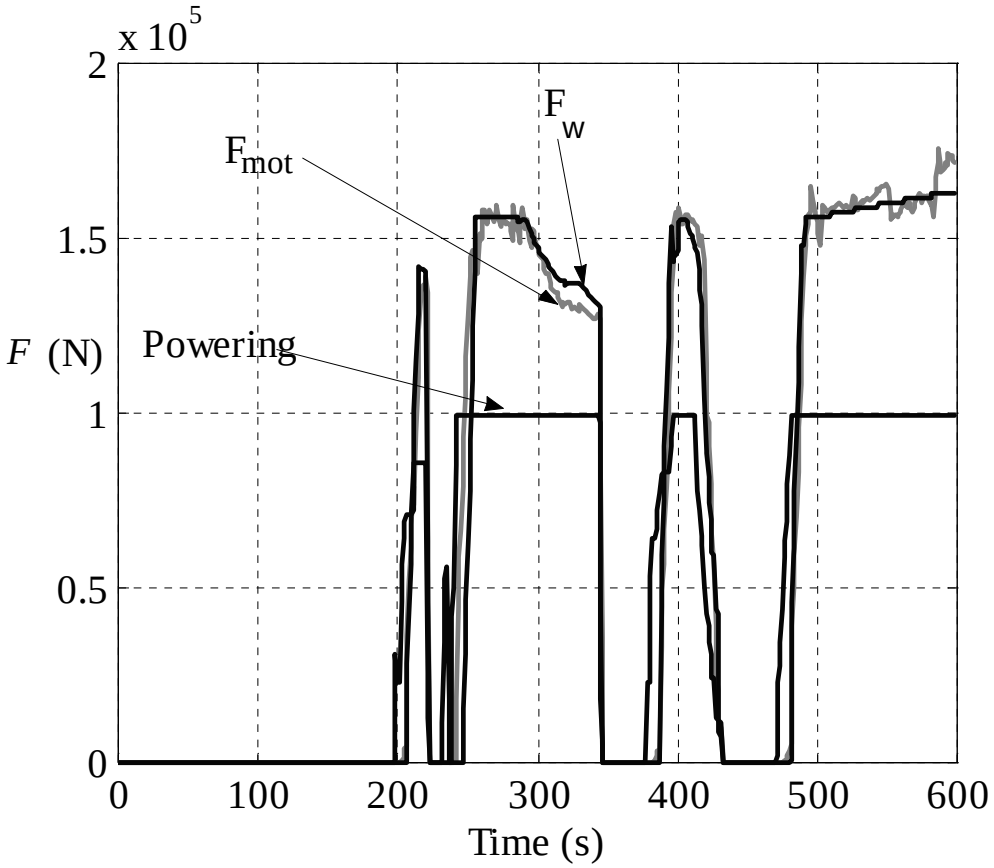

Figure 7-6 Comparison between measured, F_{mot}, and simulated, F_w, tractive force.

7.2 Braking model

The braking force, F_{brk}, at the wheel rims in the model is an empirical expression deduced from the full scale tests and expressed as an approximate function of braking pilot pressure level, applied by the driver, brake gain time, duration and brake release time. An example of how the relative braking pilot pressure of the locomotive varies with time is shown in Figure 7-7.

However, since the braking pilot pressure is a measure of the driver's desired braking level, it is from now on simply called as the *braking level*, β. The actual braking level in relation to maximum is called the *braking ratio*, σ_{brk}:

$$\sigma_{brk} = \frac{\beta}{360} \tag{7-9}$$

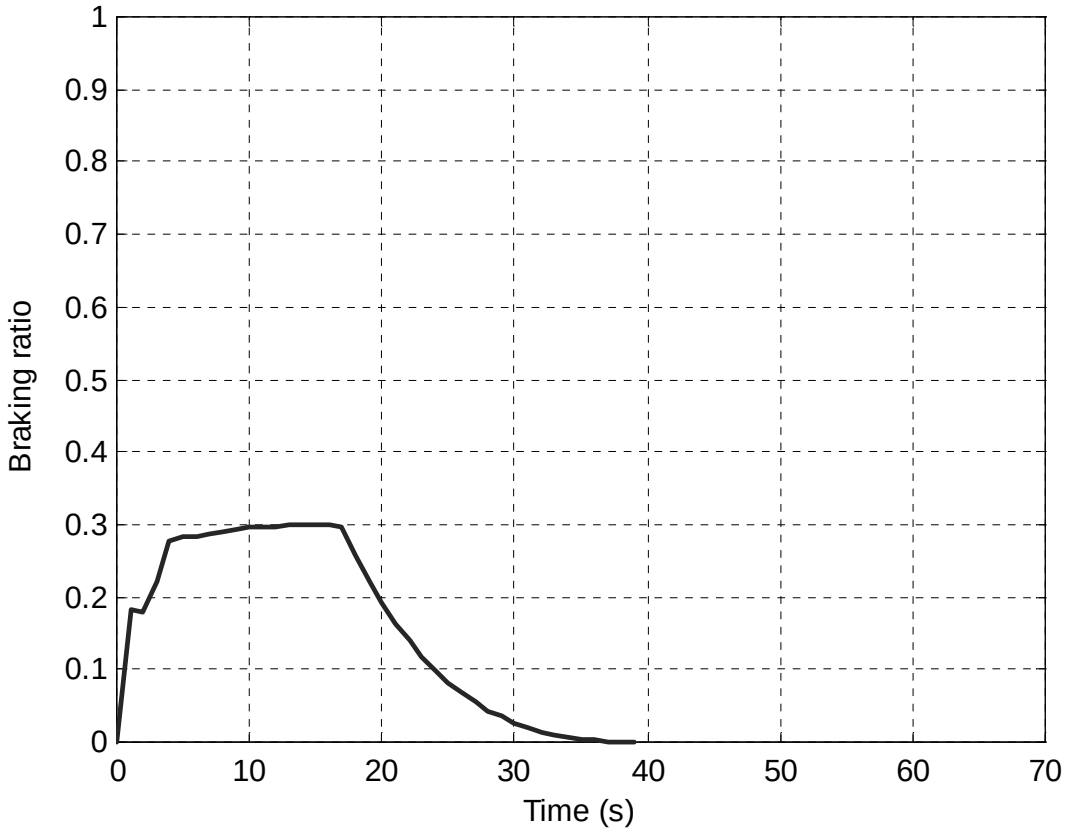

Figure 7-7 Example of how the braking ratio of the locomotive varies with time.

The braking ratio requires about 5 s to increase to 30 % of maximum and approx. 15 s to return to zero. In the simulation, the increasing and decreasing braking force is modelled, for simplicity as a linear function of desired braking level and time for the whole train. This model is approximative and is not complete with respect to the real braking system of a train. However, the model is taking into account important aspects such as braking gain time and braking release time and is verified versus full scale measurements.

If the braking force is starting to increase at time $t_i = t_{b0}$ and reaches its final level at time $t_{gain} = t_{b0} + \lambda_{gain}$ and starts decreasing at time t_{rel}, the approximative empirical equation for the mean braking force of the tested freight trains is:

$$F_{brk(i)} \approx M_{b\alpha} \cdot g \cdot \frac{\beta}{360} \cdot K_{brk} \cdot \frac{t_i - t_{b0}}{\lambda_{gain}} \text{ ; for } t_{b0} \le t_i \le t_{gain} \tag{7-10}$$

$$F_{brk(i)} \approx M_{b\alpha} \cdot g \cdot \frac{\beta}{360} \cdot K_{brk} \text{; for } t_{gain} < t_i \le t_{rel} \tag{7-11}$$

$$F_{brk(i)} \approx M_{b\alpha} \cdot g \cdot \frac{\beta}{360} \cdot K_{brk} \cdot \left(1 - \frac{t_{rel} - t_i}{\lambda_{rel}}\right); \text{ for } t_{rel} < t_i \leq t_{rel} + \lambda_{rel} \qquad (7\text{-}12)$$

where $M_{b\alpha}$ is the total adhesive mass in braking

$0 \leq \beta \leq 360$,

$K_{brk} = 0.092$, empirical value achieved from tuning in the braking retardation of simulated trains compared with measured retardation from full scale measurements, see Section 8.4.

The braking gain and release times are empirical mean values for a whole freight train

$\lambda_{gain} \approx 10$ s for increasing braking force.
$\lambda_{rel} \approx 30$ s for decreasing braking force. ;

A braking module is designed according to the flow chart shown in Figure 7-8.

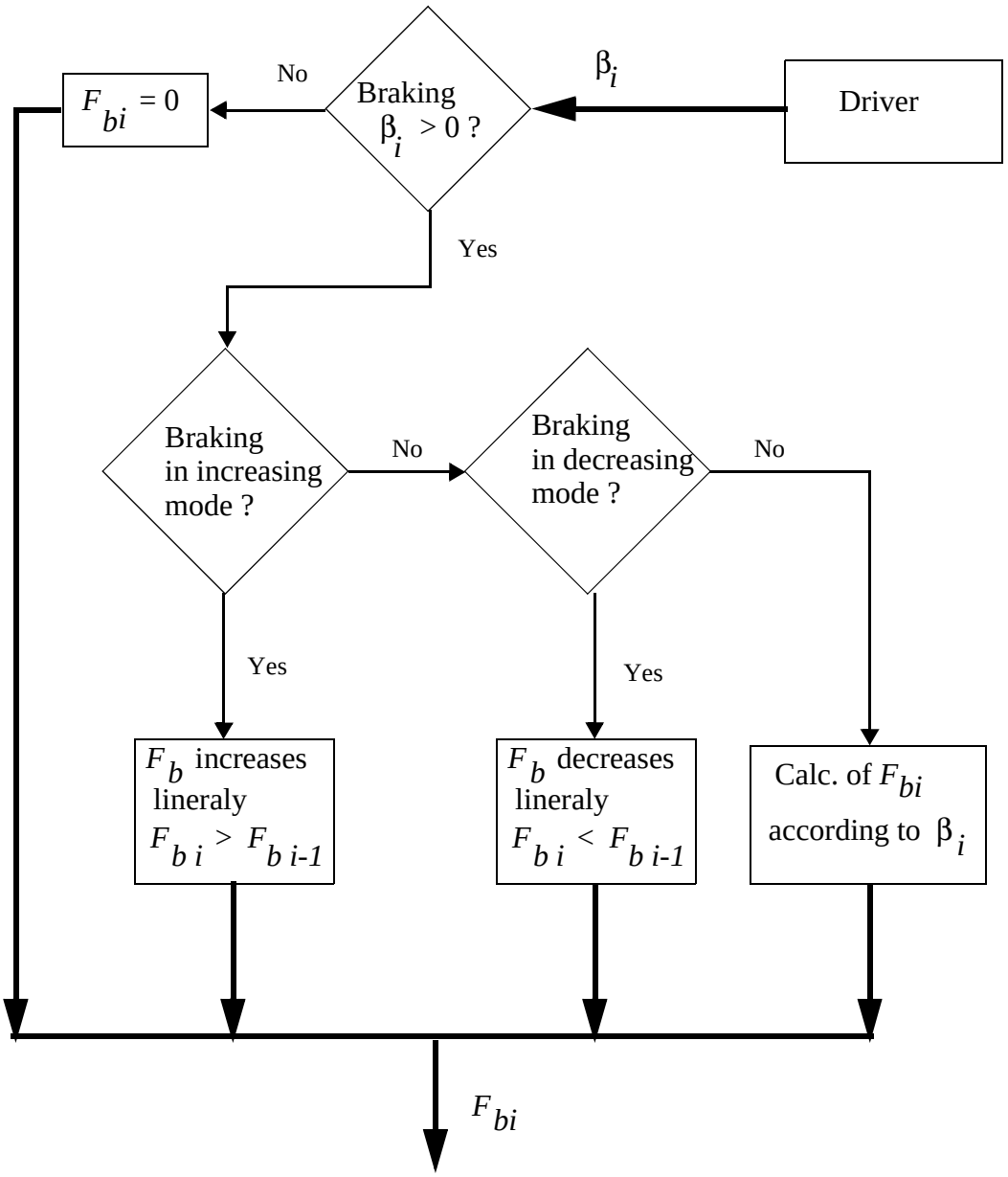

Figure 7-8 Flow chart of braking module.
$F_b = F_{brk}$, from Eq. (7-10) - (7-12).

7.3 Auxiliary power and electrical losses

A quite important factor for determining the total energy efficiency is the need for auciliary power as well as the electrical losses at idling or coasting. An investigation performed by SJ [58] shows that an *SJ Rc4* locomotive uses on average about 56 kW for auxiliary power. An example of measured total power intake and auxiliary power, needed for cooling, ventilation and the loco's illumination during coasting, is shown in Figure 7-9.

The total power intake during idling or coasting is on average approximately 10 kW higher than the auxiliary power, due to electrical losses.

For determining energy consumption, the auxiliary power and electrical losses are included in the efficiency of the locomotive for $\gamma > 0$ and $v > 0$. For $\gamma = 0$, during coasting for instance, the average value of $P_0 = 66$ kW is used in the developed simulation program. The auxiliary power is for simplicity not varying in time.

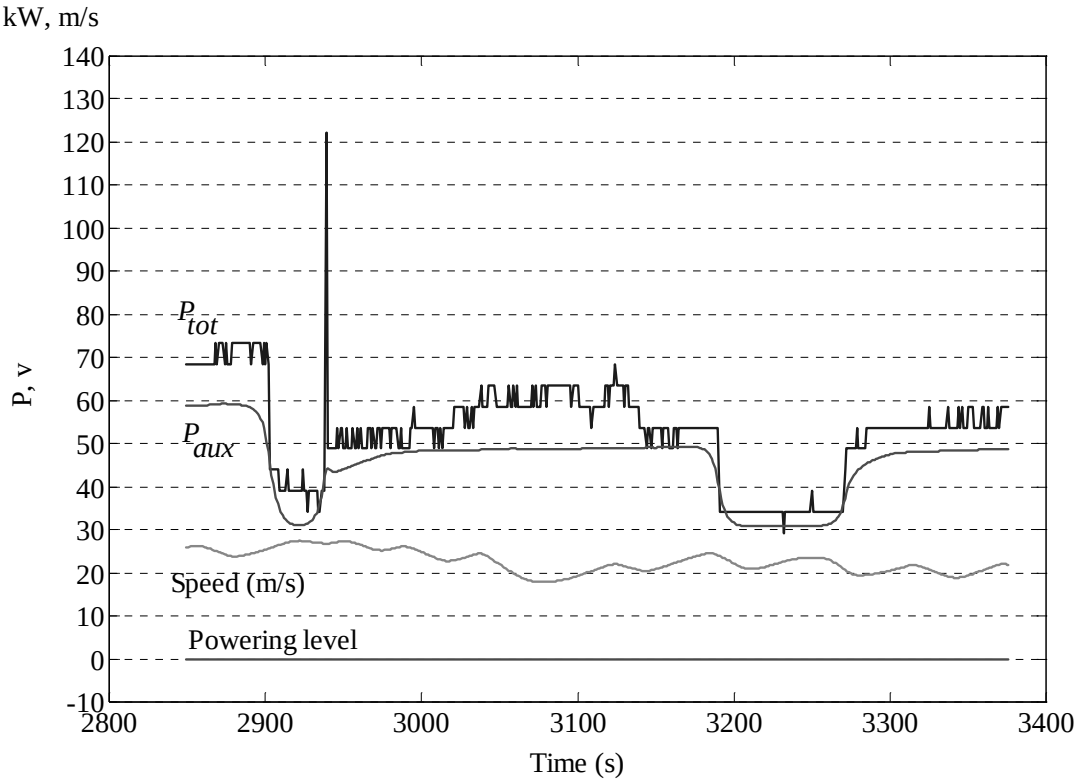

Figure 7-9 Example of recorded total power and auxiliary power when coasting.

7.4 Mechanical efficiency

7.4.1 Slippage

In the model, a special attention is given to wheel slippage. Slippage affects the energy consumption, tractive force and the real speed, in relation to the speed measured from the locos axles.

To be able to make a correct prediction of energy consumption and running time and to compare simulations with full-scale tests it may be important to include the slippage in the model. The *slippage ratio*, ζ, for each axle *j* and sample *i*, is determined from

$$\zeta_{ij}(F_{mot(ij)}) = \frac{\omega_{w(ij)} r_{w(ij)}}{v_{r(ij)}} - 1 \tag{7-13}$$

where ω_w is the angular velocity of the wheel, r_w is the wheel radius and v_r is speed measured by means of a radar mounted on the locomotive, and is assumed to be close to the real speed. The corresponding *wheel speed* v_w is

$$v_{w(i)} = \omega_{w(i)} r_{w(i)} \tag{7-14}$$

The data is scatterous due to precision errors in speed measurements of approx. ± 1% [39] and the stochastic nature of adhesion. Axle No. 1, which is leading, shows clearly a relatively larger slippage than axles 2, 3 and 4 due to impact of axle load distribution and possibly different adhesion levels. This is in agreement with present knowledge.

The determined *mean slippage ratio, f*or the different axles, with its corresponding standard deviation for a tractive force of $F_w > 15.0$ kN are:

Axle 1: $\zeta = 0.046 \pm 0.041$

Axle 2: $\zeta = 0.026 \pm 0.039$

Axle 3: $\zeta = 0.023 \pm 0.033$

Axle 4: $\zeta = 0.017 \pm 0.047$

However, a more detailed analysis of the test results show that the slippage ratio varies with tractive force above approx. 15 kN. This is taken into account in the model.

The slippage ratio in the model is purely empirical and expressed as a function of tractive force per axle. Empirically, the slippage ratio is very low at tractive forces of up to 15 kN per axle. This is clearly exemplified in Figure 7-10. For $F_w \geq 15$ kN, it is shown that slippage increases approximately linearly with the tractive force. Therefore, the following model is used:

$$\zeta \approx 1.1 \cdot 10^{-3} \cdot (F_w - 15)\,, \qquad \text{for } F_w > 15 \text{ kN} \tag{7-15}$$

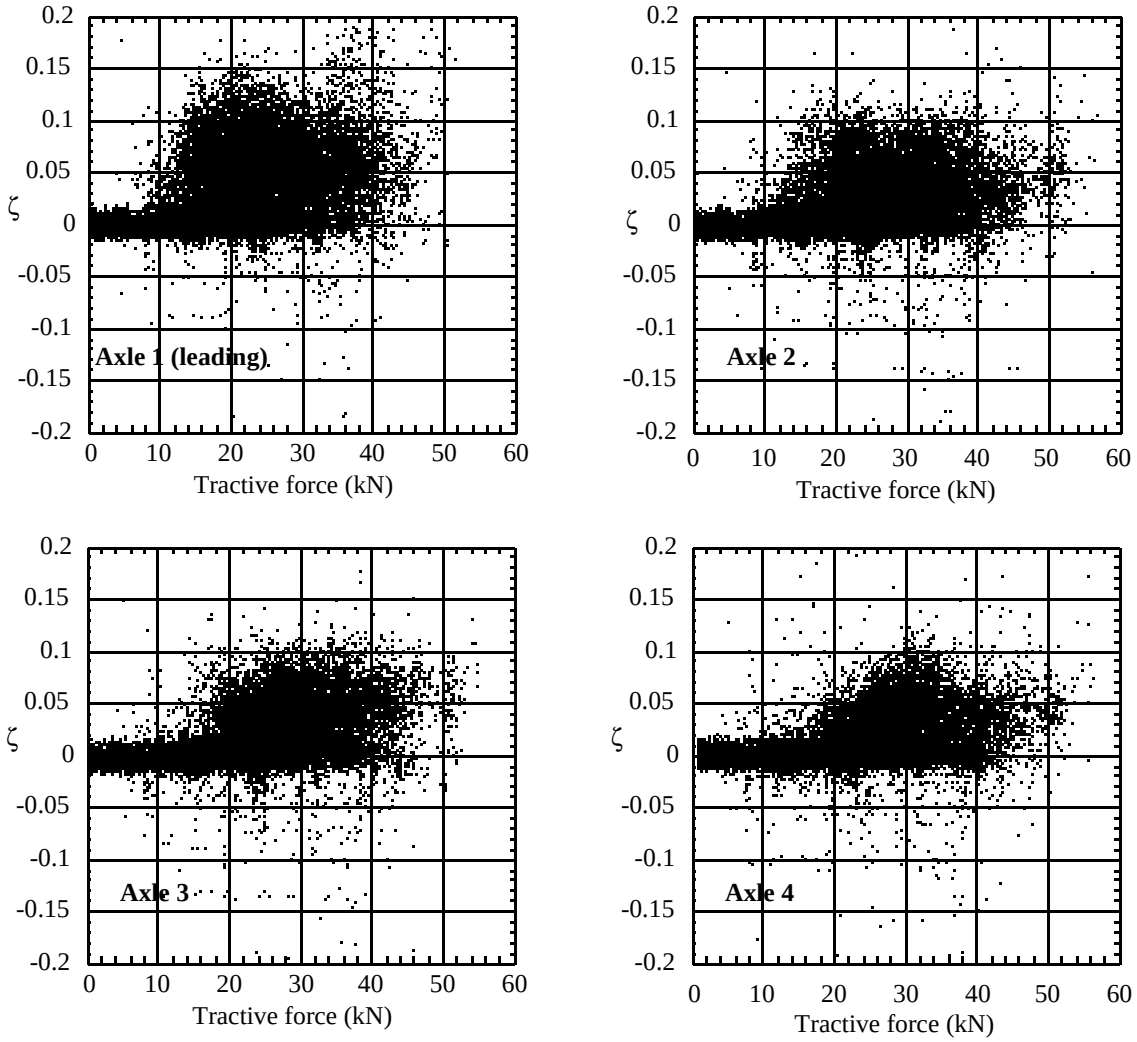

Figure 7-10 Evaluated relative slippage ratio, ζ, of loco axles 1 - 4 during propulsion.

The determined mean value and standard deviations of the slippage ratio in the interval of 0.1 - 2.0 kN are 0.00 ± 0.54 %, -0.09 ± 0.55 %, -0.17 ± 0.56 % and 0.09 ± 0.55 % for each axle respectively. This shows that the bias- and precision errors are small at low tractive forces.

No obvious slippage can be detected during braking, see Figure 7-11, probably because the braking forces are about or less than 15 kN per axle, for the locomotive. An adhesion coefficient of 0.08 is rarely exceeded during normal braking operation for freight trains. All or most axles in the train are braked which limits the need for a high adhesion utilisation during braking.

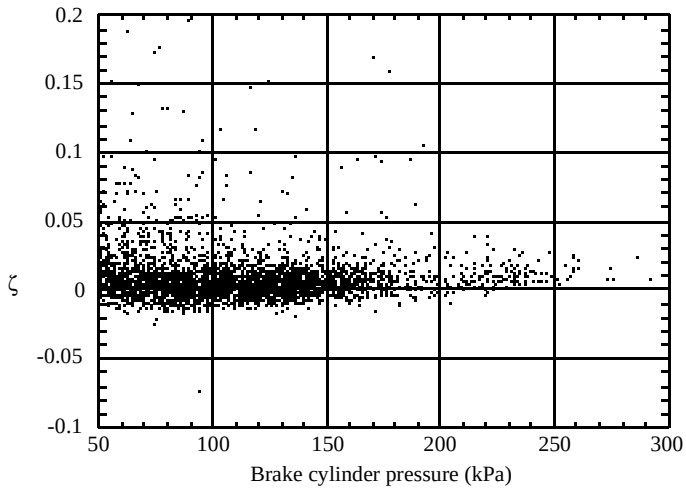

Figure 7-11 Evaluated slippage ratio of loco axle No. 2 during braking.

7.4.2 Transmission losses

Losses originating from mechanical transmissions are normally 1-2% for parallel gears with two gear wheels [55]. They are included in the total efficiency of the locomotive which is described in Section 7.5.

7.5 Energy efficiency

The efficiency of the locomotive is evaluated from the measurements and is used to calculate the energy consumption as described in Section 8.3.

Each measured efficiency sample η_i, is *during powering* and at *non-zero speed* calculated as:

$$\eta_i = \frac{P_{mot0(i)}}{P_{tot(i)}} \tag{7-16}$$

for: $0 < F_{mot0} < 260$ kN
$0.0 < v < 34$ m/s
$(0 < v < 122$ km/h$)$
$\gamma < 0$

P_{tot} is the total input power of the locomotive measured at the pantograph. The auxiliary power, electrical and mechanical losses as well as all other losses, are included in P_{tot}.

P_{mot0} is calculated by Eq. (6-7).

An example of how the evaluated efficiency varies due to speed and tractive force is shown in Figure 7-4.

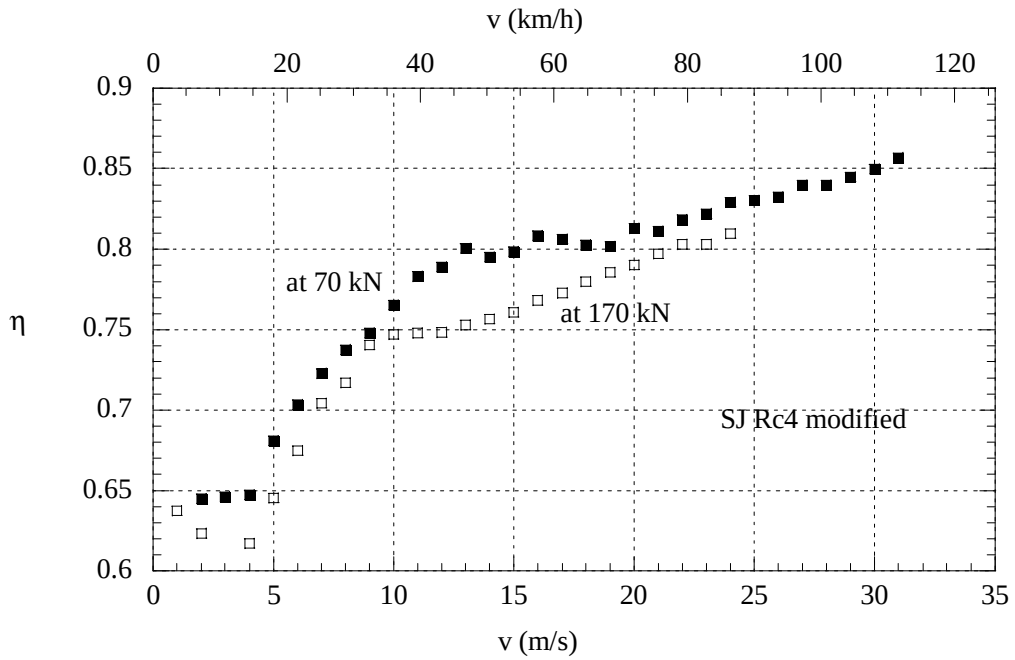

Figure 7-12 Example of determined variation of efficiency due to speed and tractive effort.

By averaging all samples of η_i for each consecutive speed interval, Δv, of 1.0 m/s and a tractive force, ΔF_{mot0}, interval of 10 kN respectively, the mean efficiency, $\bar{\eta}$ is stored in a 2-dimensional matrix $\boldsymbol{N_0}$:

$$\boldsymbol{N_0} = \begin{array}{c|cccc} & & \Delta v \text{ (m/s)} & & \\ \Delta F_{mot} \text{ (kN)} & \Delta v_1 = 0 - 1.0 & \cdots & \Delta v_{34} = 33.0\text{-}34.0 \\ \hline 0 - 10 & \bar{\eta}_{11} & \cdots & \cdots \\ \vdots & \vdots & \vdots & \vdots \\ 250 - 260 & \cdots & \cdots & \bar{\eta}_{2634} \end{array}$$

For simulation purposes, the mean efficiency for each time step, i, is retrieved from the matrix $\boldsymbol{N0}$.

The locomotive alone can run at speeds of up to 37.5 m/s (135 km/h). A freight train does normally not exceed the speed of 31 m/s (110 km/h) during normal operation.

It is not possible to evaluate from the measurements the efficiency when P_{mot0} and v are close to zero. Therefore, when P_{mot0} and v are close to zero, the efficiency in this region gives, as on average, a small relative error of approx. 1 - 3 ‰, in total determined energy consumption for one hour of running time.

7.6 Running resistance model

The results of running resistance tests are presented and discussed in Chapters 3 - 5. For simulation purposes, the model of the running resistance must include resistance due to grades and curves. Moreover, it should be applicable to more freight train types of different configurations, than tested. For clarity, curve resistance, F_C, is here separated from the ordinary mechanical resistance.

The total running resistance is expressed by:

$$F_{RT} = F_{MA} + F_M(v) + F_D(v) + F_D(v^2) + F_C + F_G \tag{7-17}$$

The speed independent part of the mechanical resistance, F_M, of the locomotive and the tested freight wagons are determined by:

$$F_{MA} = n_{loco} \cdot 2000 + (65 + 0.6 \cdot 10^{-3} Q) n_{ax} \text{ (N)} \tag{7-18}$$

where Q is the average axle load of the freight wagon. Resistance due to curves and grades is dependent upon curve radius, R, and track inclination G, respectively, which is necessarily not constant along a train. Therefore, curve and grade resistance is calculated individually for each vehicle, j, in the train set, by

$$F_C + F_G \approx \sum_{j=1}^{n_{loco}+n_{wag}} gK_C M_j \frac{0.65}{(R_j - 55)} + \sum_{j=1}^{n_{loco}+n_{wag}} gM_j G_j \quad \text{(N)} \tag{7-19}$$

where M_j is the individual vehicle mass and $K_C = 0.7$. The curve resistance is basically according to Röckl's formula [63] and is valid for $R \geq 350$ m, however a correction factor K_C is introduced. Curve resistance tests performed by Lukaszewicz [49] for ore trains shows that the original Röckl formula overestimates the resistance. By reducing the original formula by 30 %,

a better agreement between simulations and measurements is achieved on parts of the track where curves are present, see Section 8.4.

The linearly speed dependent mechanical and aerodynamic resistance is determined by

$$F_M(v) + F_D(v) \approx (-22 + 0.6L_T)v \quad \text{(N)} \tag{7-20}$$

where L_T is the total length of the train. The part of aerodynamic resistance which depends on the speed squared, is calculated by

$$F_D \approx (5.4 + K_D L_T)\left(v^2 + vv_w + \frac{v_w^2}{2}\right) \quad \text{(N)} \tag{7-21}$$

Since the evaluated influence of measured head or tail wind from full scale test is approximately half of the calculated in Section 5.1, only half of the contribution should be added to the drag.

The value of K_D depends upon the freight train configuration. In order to make the aerodynamic resistance applicable to more configurations than tested, the value of K_D is calculated for different percentages of covered and uncovered open type wagons in a train set according to Table 7-1. These values are used in Chapter 11, where calculated results of energy consumption and running time of different freight trains, by means of simulations, are compared with full scale measurements.

Table 7-1 Values of K_D for different percentages of covered and open type wagons in a freight train consist.

K_D	Covered (%)	Open type (%)	Comment
5.2×10^{-2}	87.5 - 100	0.0 - 12.5	K_D from measured SJ *Hbis*.
6.9×10^{-2}	62.5 - 87.5 (75 ± 12.5)	12.5 - 37.5 (25±12.5)	Calc. mean value from SJ *Hbis* and mixed config.
8.6×10^{-2}	37.5 - 62.5 (50 ±12.5)	37.5 - 62.5 (50 ±12.5)	K_D from measured mixed config.
9.2×10^{-2}	12.5 - 37.5 (25±12.5)	62.5 - 87.5 (75 ± 12.5)	Calc mean value from mixed config. and SJ *Oms*.
9.7×10^{-2}	0.0 - 12.5	87.5 - 100	K_D from measured SJ *Oms*.

8 A general description of the simulation model used

8.1 General

The simulation model used in this work consists basically of four parts as shown in Figure 8-1.

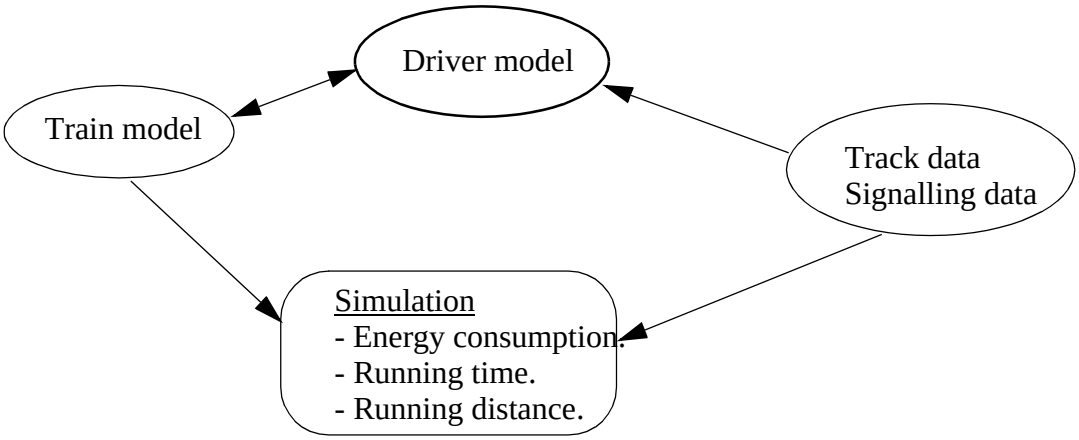

Figure 8-1 Base elements of the simulation model.

The *train model* which is used in the simulation program is a distributed mass model and consists basically of modules or functions which calculates:

- Tractive forces at wheel rims, F_w
- Braking forces at wheel rims, F_{brk}
- Total running resistance, F_{RT}
- Mechanical and electrical efficiency, incl. auxiliary power, η
- Running time, running distance and energy consumption, E_{tot}.

The *driver model* decides

- When to brake, coast or power.
- Duration and level of braking or powering.

The driver model will be further defined in Chapter 10.

A *train data base* and a *track data base* are used, containing:

- Different freight trains, including train lengths, number of axles, axle loads, wagon types.

- Track data and fixed signalling data.

Output data from the train and driver model is used in the *simulation* program to calculate:

- Energy consumption.
- Running time.
- Running distance.

8.2 Equations of motion

The acceleration during propulsion (powering) for each time step Δt_i is calculated by

$$a_i = \frac{F_{w(i)} - F_{RT(i)}}{M_{t\alpha} + (M_T - M_{t\alpha})(1 + H)} \tag{8-1}$$

where $M_{t\alpha} = M_{loco}$ if all axles are driven. During coasting by

$$a_i = \frac{-F_{RT(i)}}{M_T(1 + H)} \tag{8-2}$$

and during braking

$$a_i = - \frac{F_{brk(i)} + F_{RT(i)}}{M_{brk\alpha} + (M_T - M_{brk\alpha})(1 + H)} \tag{8-3}$$

where $M_{brk\alpha} = M_T$ if all axles are braked. M_T is the total train mass and H is the relative factor accounting for rotational inertia of the unbraked wheel sets. Speed is calculated for each time step, i, by

$$v_{i+1} = v_i + a_i \Delta t_i \tag{8-4}$$

and the travelled distance is

$$\Delta x_i = \left(v_i + \frac{a_i}{2}\Delta t_i\right)\Delta t_i \tag{8-5}$$

8.3 Energy consumption and running time.

Total energy consumption, E_{tot}, at the locomotive's pantograph is divided into two cases. One case is valid for $v > 0$ and $F_w > 0$, and the other case for $F_w = 0$ or $v = 0$, during coasting or idling, according to Eq. (8-6).

$$E_{tot} = \begin{cases} \sum_{i=1}^{n} \dfrac{(F_{w(i)} + K_j a)v_i(1+\zeta)\Delta t_i}{\eta_i}; & v > 0, \quad F_w > 0 \\ \sum_{i=1}^{n} P_{0(i)}\Delta t_i; & F_w = 0, \text{ or } v = 0 \end{cases} \tag{8-6}$$

P_0 = 66 kW, and is an empirical mean value originating from idling electrical losses and auxiliary power of the locomotive.

Total running time, T, is calculated by Eq. (8-7).

$$= \sum_{i=1}^{n} \Delta t_i \tag{8-7}$$

and total running distance, S_{tot}, by Eq. (8-8).

$$S_{tot} = \sum_{i=1}^{n} \Delta x_i \tag{8-8}$$

8.4 Verification and calibration of the train model in simulations

It is possible to verify the model, by synchronising in a simulation the virtual train, with a real train, with respect to the real trains data, geographical starting position, powering level, braking level and initial speed for time step number 1. After the synchronisation, only the measured line

voltage, braking and powering levels of the real train are used as input signals into the simulation.

The train model should be calibrated with respect to running resistance of the real train and available adhesion. Otherwise, it is not possible to make any correct comparisons between the model and the real train regarding the tractive and braking force, as applied by the driver.

The assumed running resistance of the train in the model can be compared to the resistance of the real train *during coasting*. If the train accelerates more in the simulation than the real train does, for the same track section and same initial speed, then the assumed running resistance is most likely too low, provided the track data is correct. This can be approximately corrected for by rising the air drag for the model. Different train configurations, wagon types and influence of ambient wind makes this approach sometimes necessary.

Once the running resistance is approximately calibrated, it is possible to approximately calibrate the adhesion level. This can be done by comparing simulated accelerations with accelerations of the real train at full powering while travelling uphill in a grade. If the simulated tractive forces and accelerations are too low, then it is most likely that the assumed adhesion level is also to low. Simulations done in this manner are called *calibrated simulations*.

After the calibration is made, it is possible to compare and tune in the braking gain and release time. It is also possible to approximately determine the curve resistance when running through curves. This has resulted in the *empirical constants* , λ_{gain}, λ_{rel}, and K_{brk} in the braking model in Eqs. (7-10) - (7-12) and the empirical curve resistance constant, K_C, in Eq. (7-19).

A comparison between simulation and measurement is shown as an example in Figure 8-2. The simulated speed and running distance is corrected for slippage.

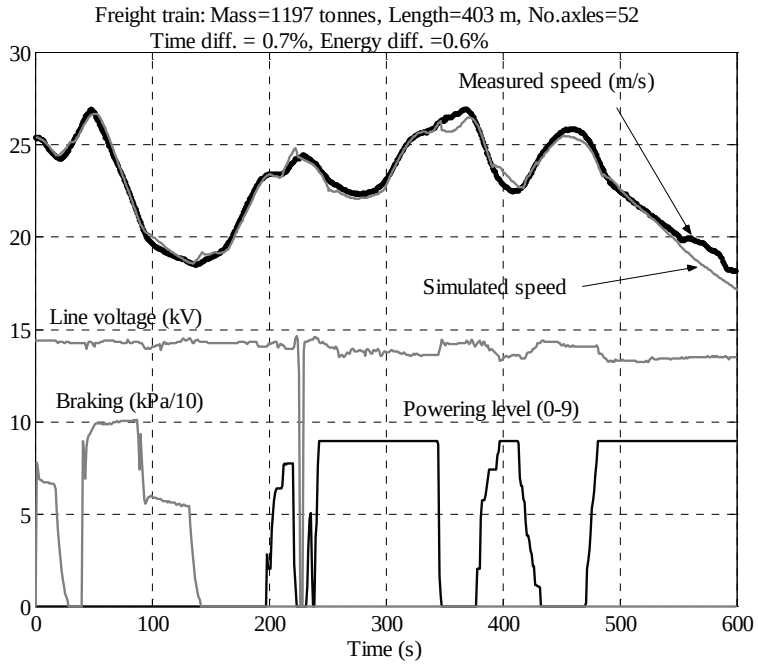

Figure 8-2 ***Example of comparison between simulation and measurement.***
Measured line voltage, powering and braking levels are used as input to the simulation

The model, calibrated with respect to running resistance and adhesion, has been tested for several cases. It is concluded that the average difference, with standard deviation, is 0.3 ± 1.0% in energy consumption and 0.1 ± 0.6%, in running time compared to measurements. This is well within the range of the measurement error of 1 - 2 % for the energy consumption.

Figure 8-3 shows the results of a large number of simulations with different freight trains on different tracks.

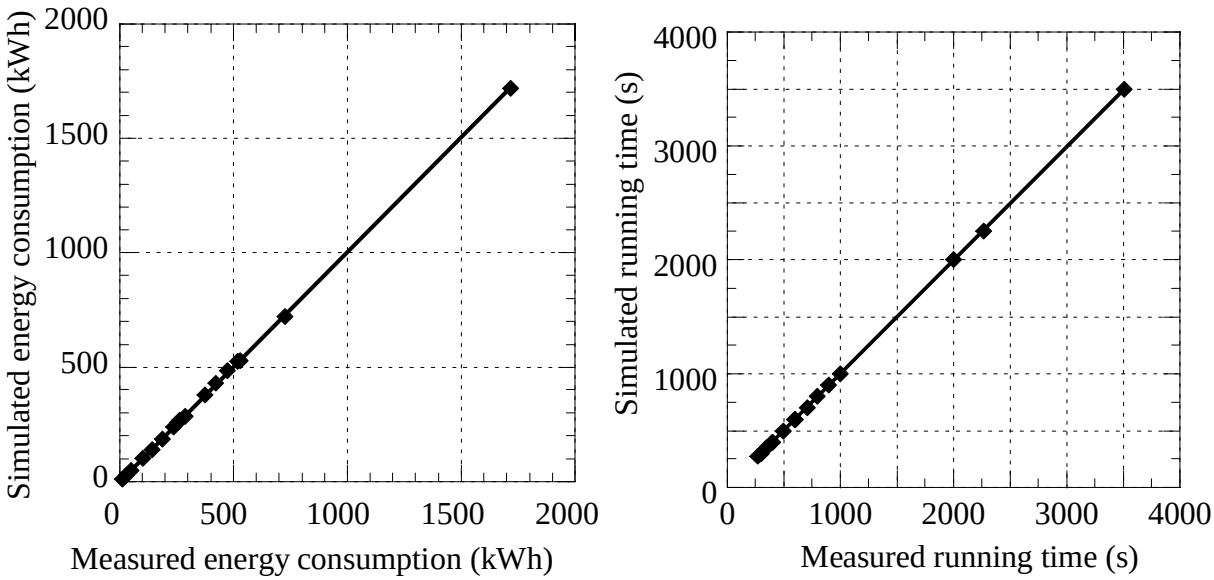

Figure 8-3 Simulated energy consumption and running time compared to measured.

Non calibrated models are verified in Section 11.2.

9 The driver

Driver behaviour may have a significant influence on energy consumption and running time of trains. This is why it is necessary to make use of a driver model in simulations. Before such a model can be constructed, some driver describing parameters must be determined and defined. This is done in the following chapters.

The definitions and analysis of driver describing parameters in this work are mainly based on the full scale recordings and observations which are described in Chapter 6.

It is pointed out here again, that the drivers are driving the trains as they are used to do and are not instructed to make any precautions due to the recordings. Also, the trains are run throughout the whole Sweden on tracks having relatively large grades in the northern part of Sweden and on tracks having relatively small grades in the southern part.

9.1 Driver behaviour and driving modes

9.1.1 Observations on real driving

From the full scale tests, the following main observations, A - C, are made and defined:

A. The train can be handled in three different ways or *driving actions*

1. *Powering*. Tractive force is applied by the driver or a power control unit.
2. *Braking*. Braking force is applied by means of mechanical brake by the driver or the ATC.
3. *Coasting*. The train is moving forward without any powering or braking.

B. There are basically three *driving modes* which are making use of the driving actions:

1. *Acceleration* up to the nominal speed which is v_{ATC}.
2. *Speed holding*.
3. *Retardation* of train down to nominal speed or stop.

For heavy freight trains, acceleration up to nominal speed is achieved mostly by means of full available powering which is limited by adhesion and line voltage. Retardation of the train is normally achieved by means of braking. Coasting may also be used for retardation, if the train is running uphill or on a horizontal track, and for deliberate energy saving or prolonging the running time.

C. The driving is *restricted* by:

1. Speed restrictions or stops, indicated by signalling and ATC.
2. Time table.

Two examples of typical driving are shown in Figure 9-1 and Figure 9-2. The driver observations are discussed in more detail in the following Sections 9.1 - 9.6.

Figure 9-1 shows a typical example of how a real speed pattern of a train differs from the nominal speed which is denoted by ATC. The powering is conducted manually by the driver. During the first 500 s, the train is loosing speed despite of full powering. This is due to insufficient tractive force when negotiating the severe grade of approx. 17 ‰. The actual train has a mass of 1197 tonnes, including locomotive.

The powering level set by the driver, can be overruled by the traction and automatic speed control system. Thus, the tractive force is not always corresponding to the manual powering setting.

A very interesting effect of braking can be noticed in Figure 9-1. Despite the driver has stoped braking, it takes some time to release the brakes completely. According to the empirical model in Section 7.2, the release time for the braking is in the order of approximately 30 s.

.

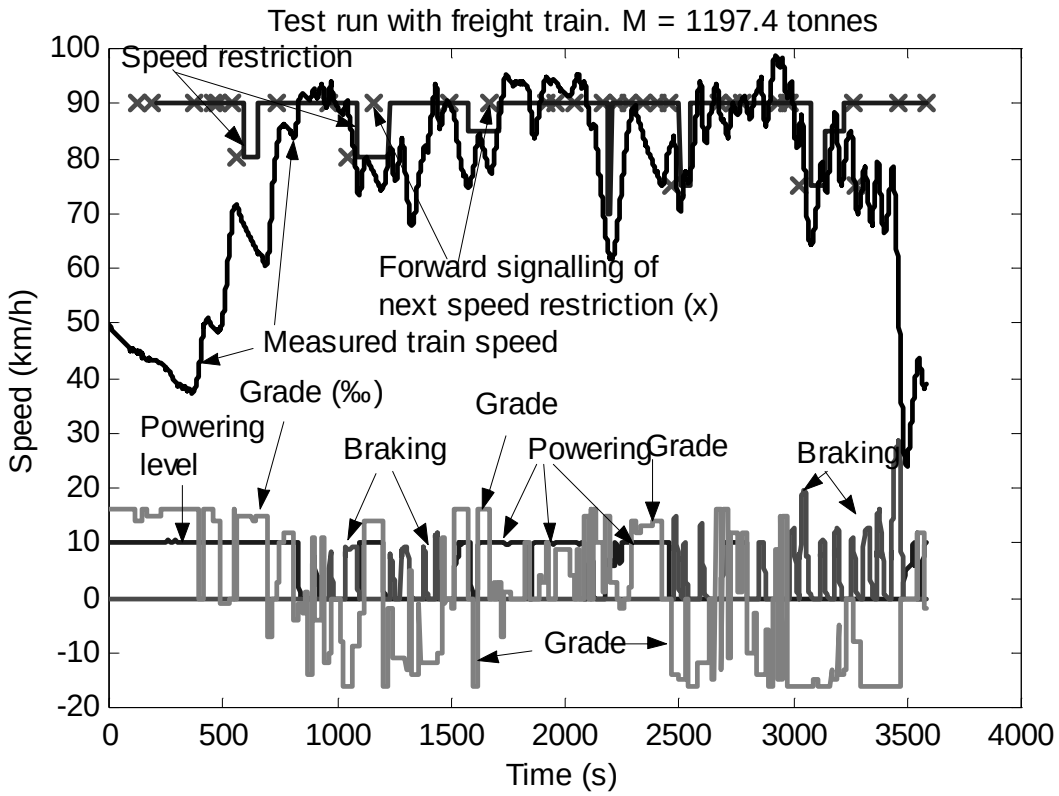

Figure 9-1 ***Example of typical measured speed profile together with grades, present speed restriction and forward signalling.*** *Driver' s manual powering and braking are scaled for clarity.*

Figure 9-2 shows an another typical example of driving where the powering is conducted by the automatic speed control. The speed is almost constant and set by the driver to be maintained above the nominal speed, which is denoted by the ATC. It is possible to exceed the speed restriction by approx. 2.8 m/s (10 km/h) without automatically entering the full braking mode.

9.1.2 Idealised driving - minimum time driving

In estimation and simulation of energy consumption and running time it is frequently assumed that the train is driven on minimum running time, defined as driving with maximum acceleration, followed by speed holding close to the nominal speed, v_{ATC}, until full or nominal braking is necessary. For example, coasting is normally not applied except in downhill grades where the running resistance is compensated by the negative grade resistance.

In the following Sections 9.2 - 9.4, it is shown that real driver behaviour differ from the idealised driving, based on the above mentioned idealised assumptions.

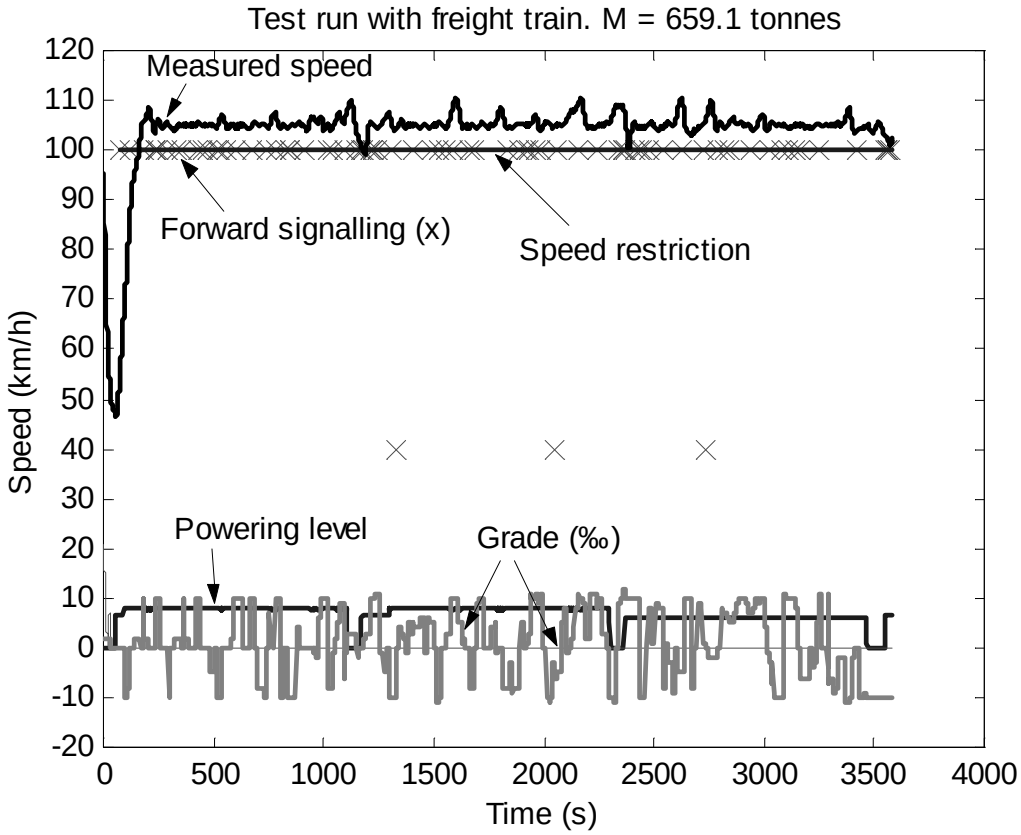

Figure 9-2 Example of typical driving with automatic speed control where the speed restriction is being constantly exceeded.

9.2 Acceleration

Acceleration can only be done by means of powering or if the train travels downhill by means of coasting.

In this section, tests are evaluated in order to determine and quantify how much power, during acceleration, is *applied by the driver of the total maximum available.*

The *powering ratio* during acceleration up to nominal speed, v_{ATC}, is introduced here for speed, $v > 0$ and acceleration $a > 0$ as:

$$\sigma_{pwr} = \frac{\text{power utilised}}{\text{Maximal avaliable tractive power}} = \frac{P_{mot0}(t)}{P_{t0}(\gamma=\max, U_L)} \tag{9-1}$$

P_{mot0} is estimated by Eq. (6-3) and P_{t0} by Eq. (7-3). The catenary voltage drop is accounted for in Eq. (9-1) and P_{t0} is not limited by adhesion. However, P_{mot0} may be limited by adhesion. The driving should *not* be in the *speed holding mode* which is described in Section 9.3.

It should be noted that although the powering ratio is determined through measured power, it also shows the tractive effort ratio, i.e. tractive effort in relation to maximum tractive effort.

Figure 9-3 shows the powering ratio in relation to maximum for a total of 193 test runs of a total running time of 175 h, with different drivers and train configurations and on different track sections. For each test run, of approx. 1 h, the powering ratio is measured during the acceleration mode and then averaged.

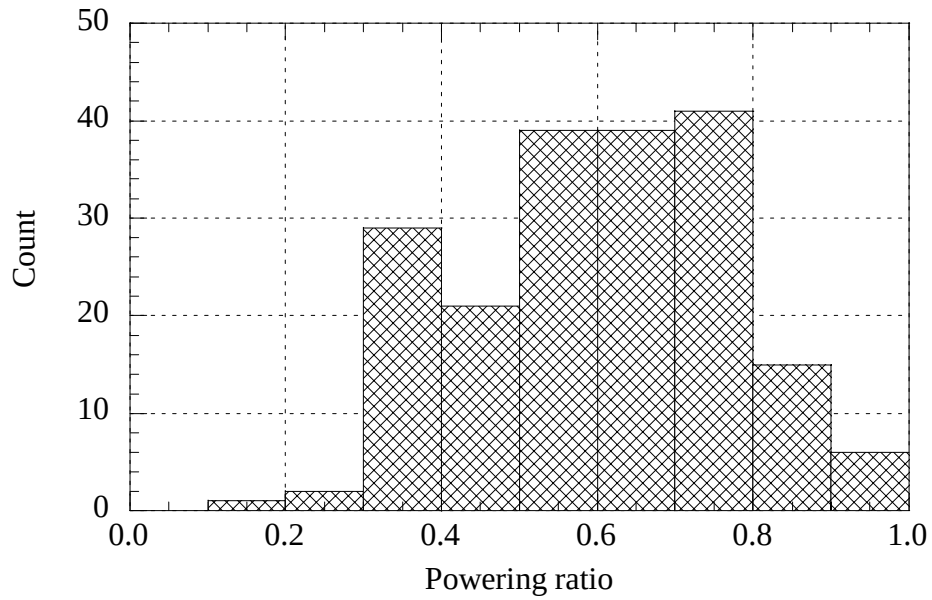

Figure 9-3 Distribution of powering ratio in relation to maximum for 193 test runs of total 175 h running time.

In Figure 9-4 and Figure 9-5, the measured powering ratio is shown together with train mass and mean grade of the evaluated running distance, respectively. Each data sample represents a mean value evaluated during approx. 1 h of running with various train configurations and drivers. The powering ratio, as shown in Figure 9-4, is increasing with respect to train mass. This shows that the driver or the power control unit is not using full powering as on average.

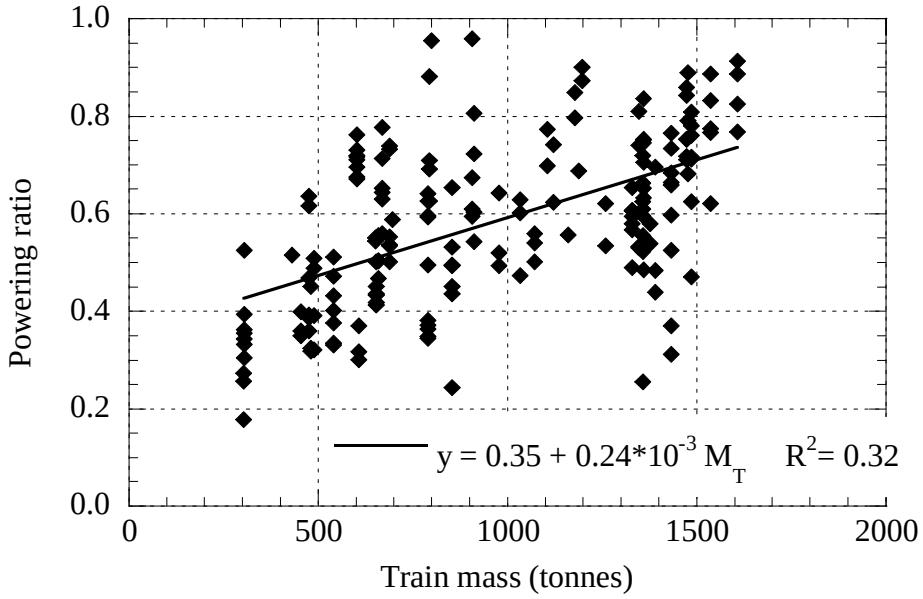

Figure 9-4 Measured powering ratio with respect to train mass.

The mean grade, $\overline{G}$, is calculated from the difference in track altitude between the positions of the locomotive where the measurements start and end. This difference is then divided by the total measured running distance, S_{tot}.

$$\overline{G} = \frac{h_{end} - h_{start}}{S_{tot}} \text{ (‰)} \qquad (9\text{-}2)$$

In Figure 9-5, the powering ratio is shown with respect to mean grade of different track sections having lenghts in the range of 40 - 100 km. No significant variation of powering due to mean grade is detected.

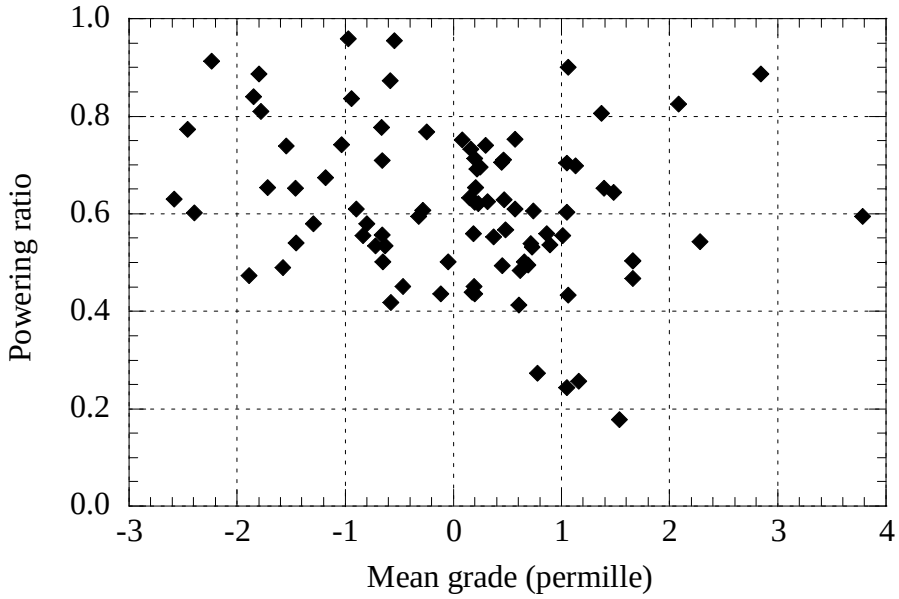

Figure 9-5 Measured powering ratio with respect to mean grade.

The nominal speed restricted by the ATC for a freight train is normally 22 - 28 m/s, (80 - 100 km/h). If the mean speed is less than 20 m/s, (70 km/h), then it is probable that the train is subject to speed restrictions or stops, thus reducing the speed from nominal. This could lead to more powering from the driver who wants to catch up time. However, no significant variation of the powering ratio due to mean speed can be detected in Figure 9-6.

.

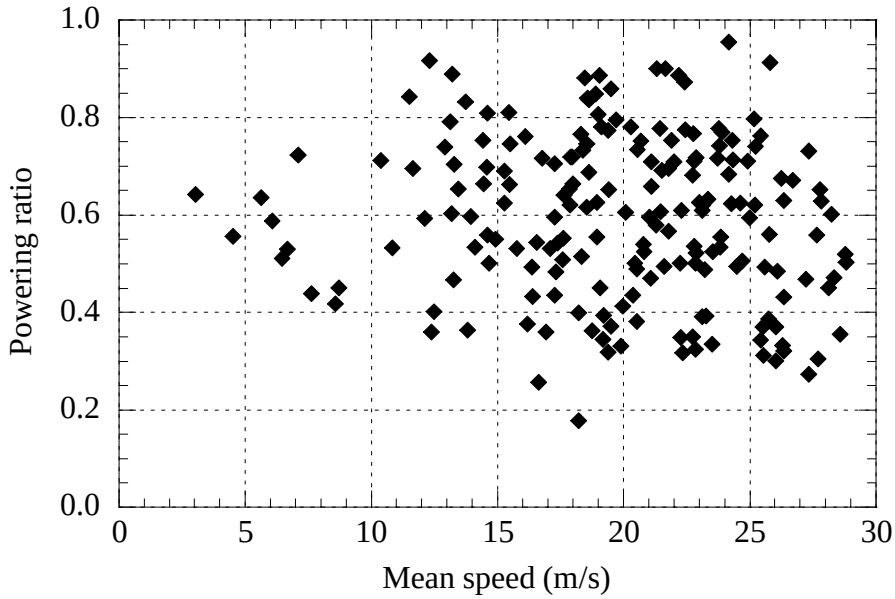

Figure 9-6 Measured powering ratio with respect to mean speed.

Taking all the samples in Figure 9-4 into consideration, measurements show that the *average powering ratio is approximately* 0.6. F_{mot}, thus P_{mot}, is limited not only by the power control, handled by the driver, but also by the speed control unit, catenary voltage drop and available adhesion which is random in behaviour and cannot be measured by simple means. However taking only the drivers power control into consideration, it is observed that the power control during acceleration, up to the speed restricted by ATC, is set by the driver frequently at the maximum powering notch (notch = max).

One contributing factor for the quite low powering ratio is the available adhesion. At low speed the maximum tractive effort is 250 kN, see Figure 7-1, corresponding to an adhesion utilisation of more than 0.3. Therefore, during starting or at low speeds, the tractive force is frequently limited by the adhesion. By assuming an adhesion of 0.20, a quite low but common level, the maximum tractive force available is approximately

$$F_w = min(F_t, F_{t\alpha}) \tag{9-3}$$

$$F_{t\alpha} \approx g \cdot M_{t\alpha} \cdot \alpha = 9.81 \cdot 79 \cdot 0.20 = 155 \text{ kN} \tag{9-4}$$

Note that 155 kN of tractive force is about 60% of maximum 250 kN. See Figure 7-1 in Section 7.1.

9.3 Speed holding

Speed holding can be attained either manually by the driver or by means of automatic speed control. However, if the train is driven manually, the train's speed profile is not following the nominal speed, v_{ATC}, exactly as given by the ATC. This is clearly shown in Figure 9-1. In many simulation programs the train's speed profile is assumed to be identical to that of v_{ATC}.

It is normally possible to drive a train up to 2.8 m/s (10 km/h) above the nominal speed restriction before the train enters automatically into the full braking mode. If the speed excess is more than 4.2 m/s (15 km/h) the train enters into the emergency braking mode [61]. This gives the possibility to drive faster than v_{ATC} and gain time, if for example the train is behind its time schedule. An example of such driving has been shown in Figure 9-2.

Hence it is important to find how much the driver allows the train speed to exceed or drop below v_{ATC}, before a driver action is executed. The train speed above the nominal speed where a driver action is executed is in this work defined as the *upper speed action limit,* v_a^+.

$$\text{Upper speed action limit: } v_a^+(t) = v(t) - v_{ATC}(t) \; ; \; v \geq v_{ATC} \tag{9-5}$$

For instance, if the train speed exceeds v_a^+, then the driver starts decelerating by means of braking, or if applicable, by means of coasting.

It is exemplified in Figure 9-2 that upper speed action limit is about 1.4 m/s (5 km/h) for normal operation. If the train is behind time schedule then the train speed is quite often 1.4 - 2.8 m/s (5 - 10 km/h) above v_{ATC}.

9.4 Coasting

9.4.1 Degree of coasting

To quantify the coasting in relation to the total measured running distance, the *degree of coasting* is introduced here as:

$$\text{Degree of total coasting: } \delta_{cst} = \frac{\text{Total coasting distance}}{\text{Total running distance}} = \frac{\sum S_{cst}}{S_{tot}} \qquad (9\text{-}6)$$

Figure 9-7 shows the degree of coasting for a total of 204 test runs with different train configurations and different drivers and on different track sections. Each test run is about 1 h.

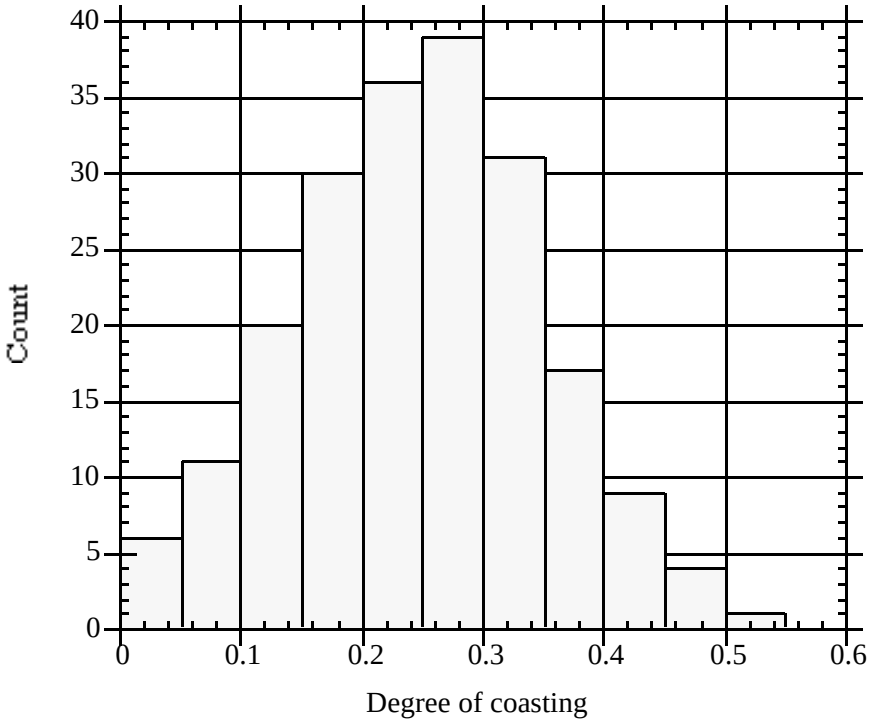

Figure 9-7 Distribution of degree of coasting.

It is shown from evaluated test data in Figure 9-8 and Figure 9-9 that the degree of total coasting does not show any significant variation due to the mean grade or total train mass. Hence, it is therefore probable that the degree of coasting is, on average, normally not much affected by train mass or grades, at least within the range of grade and train mass encountered in the observed train operation.

The results are somewhat surprising regarding grades since the negative mean grades (downhill) do not cause higher degree of coasting. However, it may be that larger and longer grades, not experienced in the present tests, would have caused a more significant influence.

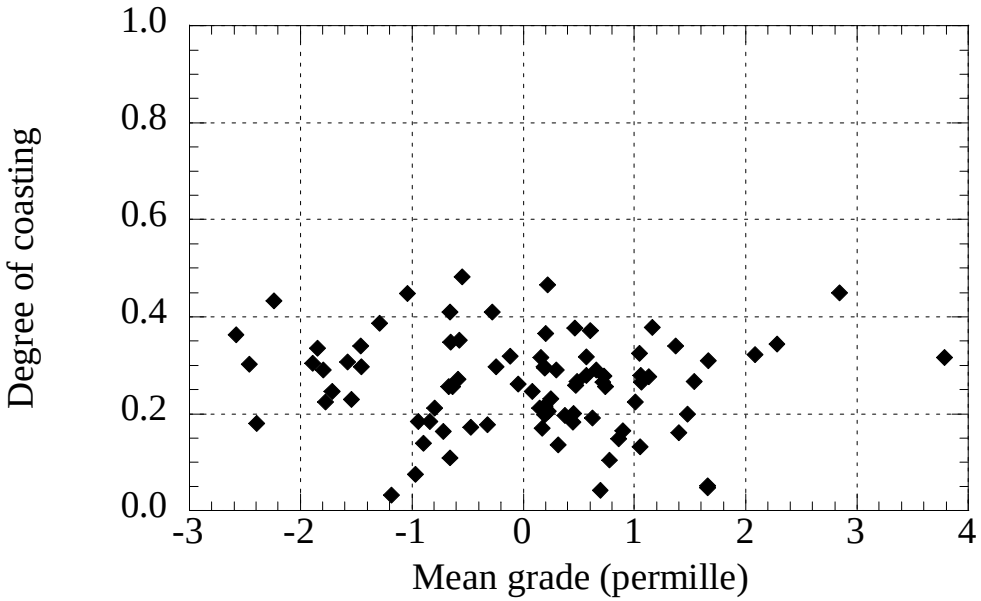

Figure 9-8 Measured degree of coasting with respect to mean grade.

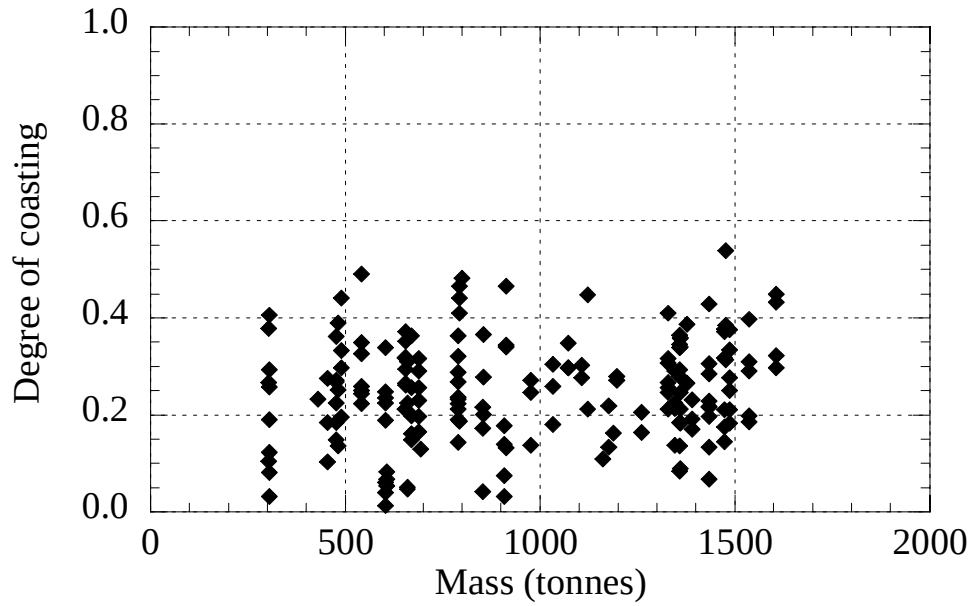

Figure 9-9 Measured degree of coasting with respect to train mass.

Taking all the samples into consideration, measurements show that the mean degree of coasting with standard deviation is 0.25±0.10.

To examine at which speed coasting is interrupted, the *lower speed action limit* is introduced in this work as:

$$\text{Lower speed action limit: } \bar{v_a}(t) = v(t) - v_{ATC}(t);\ v < v_{ATC} \tag{9-7}$$

For instance, if the train speed is lower than $v_{ATC} + \bar{v_a}$, then the driver starts powering so that the train speed reaches v_{ATC}.

For coasting, it is shown in Figure 9-10 and in Figure 9-11 that the train speed may as on average drop by 1-7 m/s from v_{ATC} before any action is taken. In this case is the average value with the standard deviation of the lower speed action limit $\bar{v_a} \approx 3.2 \pm 1.5$ m/s.

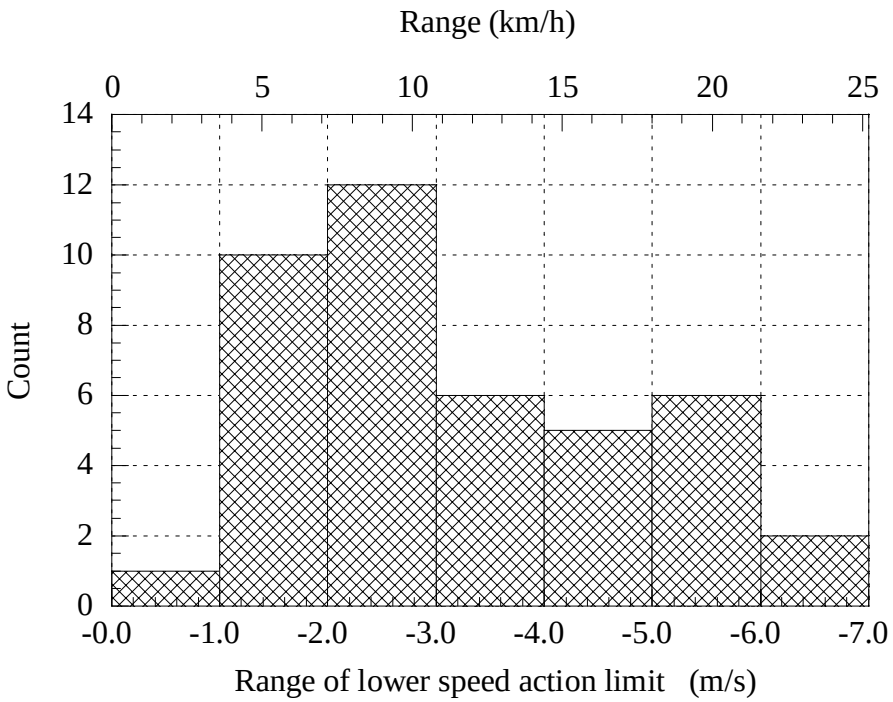

Figure 9-10 Mean lower speed action limit.

Figure 9-11 show that mean grade and train mass has no detectable influence on the drivers tendency to coast.

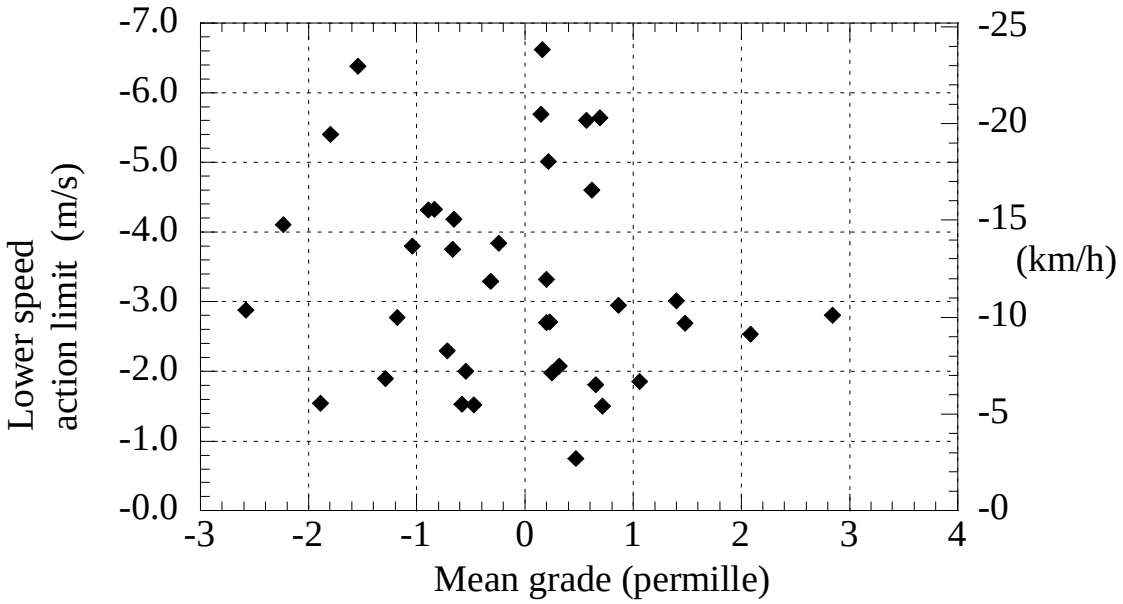

Figure 9-11 Lower speed action limit, with respect to mean grade.
Each sample represents a mean value evaluated during 1 hour of running time with different trains and different drivers.

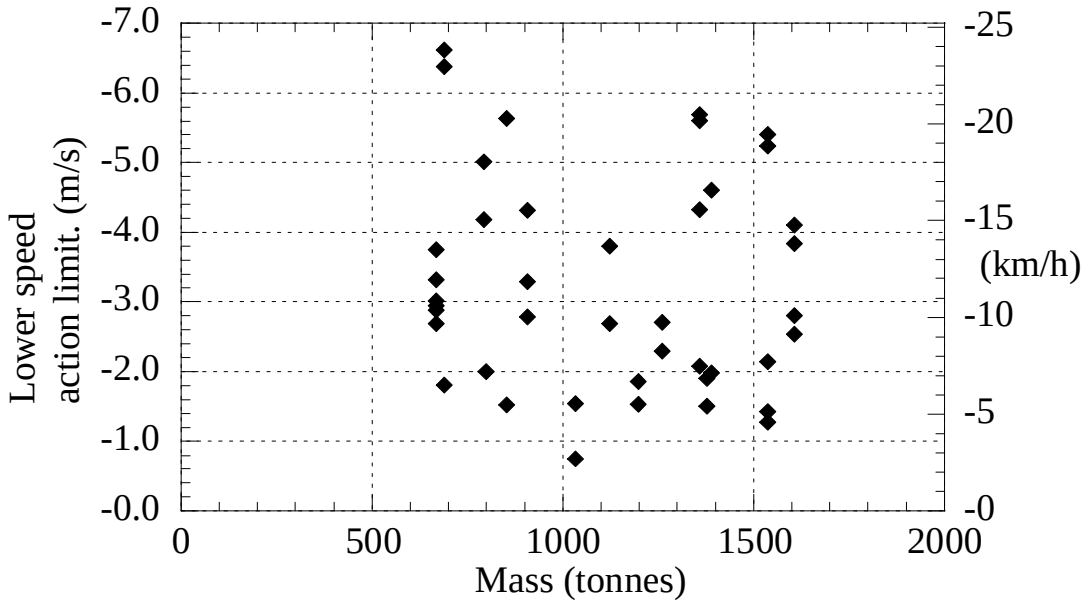

Figure 9-12 Lower speed action limit with respect to total train mass.

9.4.2 Deliberate energy saving or prolonging the running time

The degree of coasting has an impact on the energy utilised for propulsion. Figure 9-13 shows the specific energy consumption, energy per gross-ton-km, with respect to the degree of coasting.

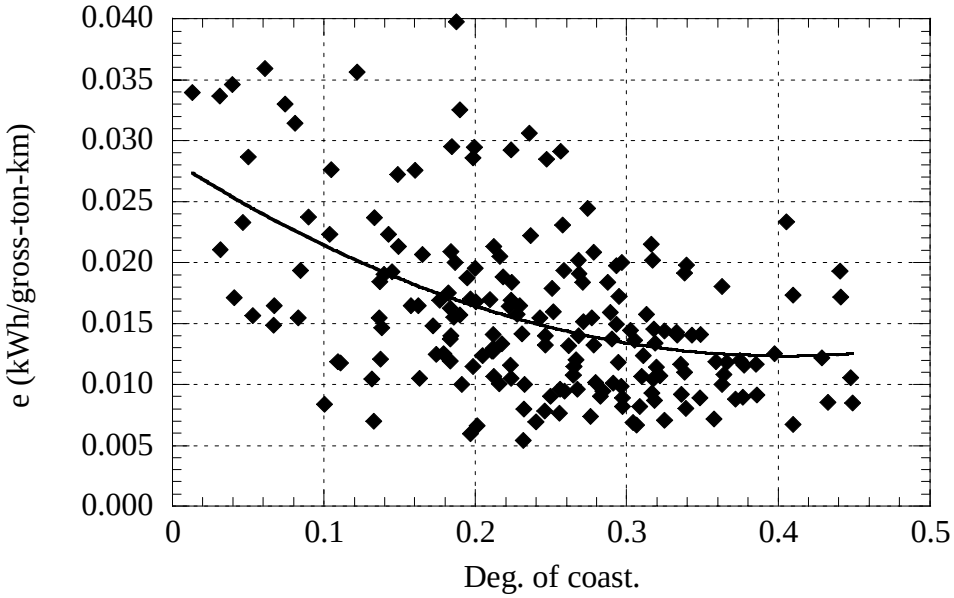

Figure 9-13 Specific energy consumption with respect to degree of coasting.

Even though the data is scatterous, it is possible to distinguish a clear tendency in how the degree of coasting affects the specific energy consumption for freight trains.

9.5 Braking

Braking is applied either by the driver or the ATC which applies the brakes at their maximum level, if the speed restriction is exceeded by 2.8 m/s (10 km/h). The braking level compared to maximum, is the braking ratio:

$$\sigma_{brk} = \frac{\beta}{360} \tag{9-8}$$

Maximum braking ratio, $\sigma_{brk} = 1.0$, corresponds to a pressure reduction in the main air-pipe by 150 kPa. This corresponds to a braking pilot pressure of 360 kPa. The applied braking ratio for 183 test runs of approx. 160 h of running time is shown in Figure 9-14. Taking all the samples into consideration, measurements show that the relative brake ratio, with standard deviation, has a mean value of 0.35 ±0.07.

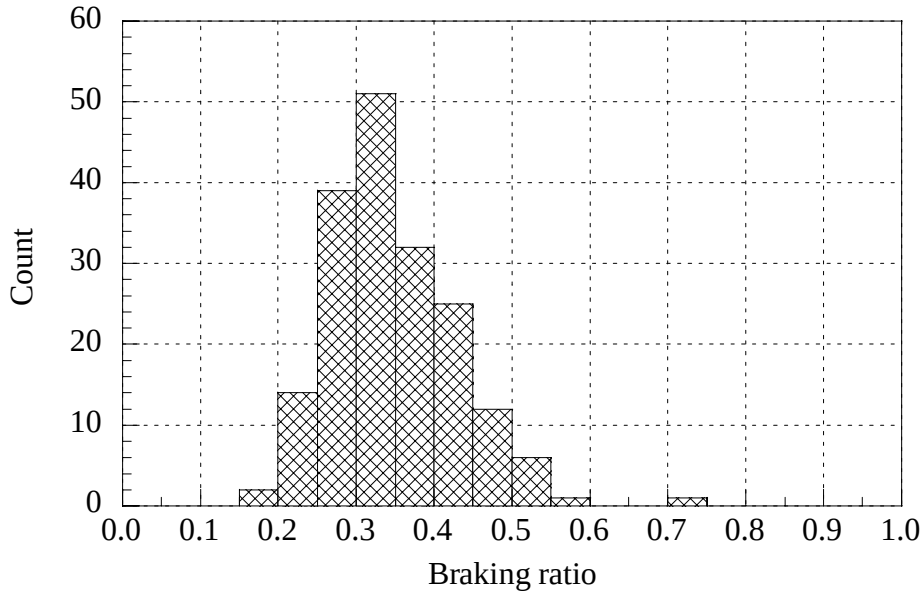

Figure 9-14 Distribution of braking ratio for 183 test runs with different trains, drivers and track sections.

In Figure 9-15 and Figure 9-16 it is shown that the braking ratio does not vary significantly with train mass or mean speed-

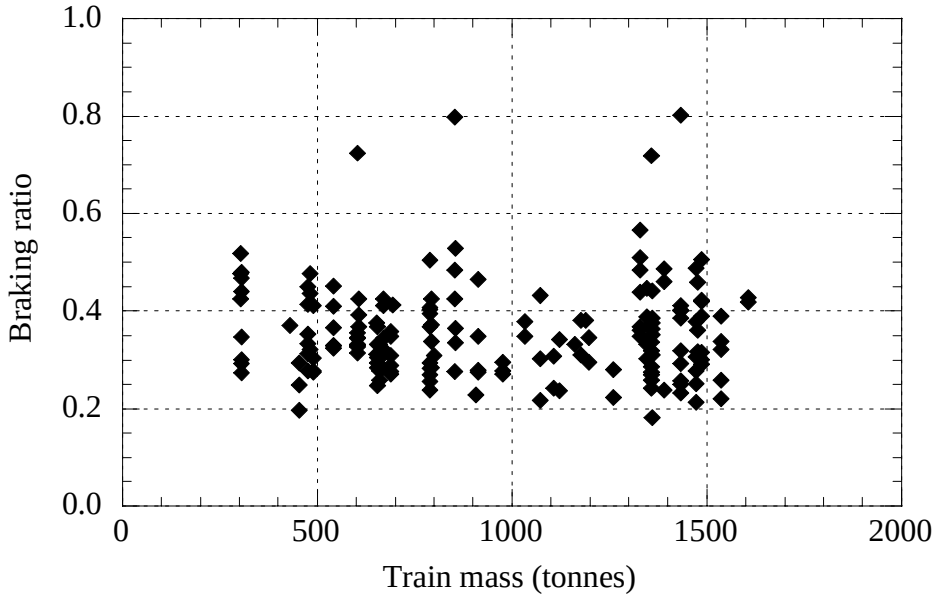

Figure 9-15 Measured braking ratio with respect to train mass.

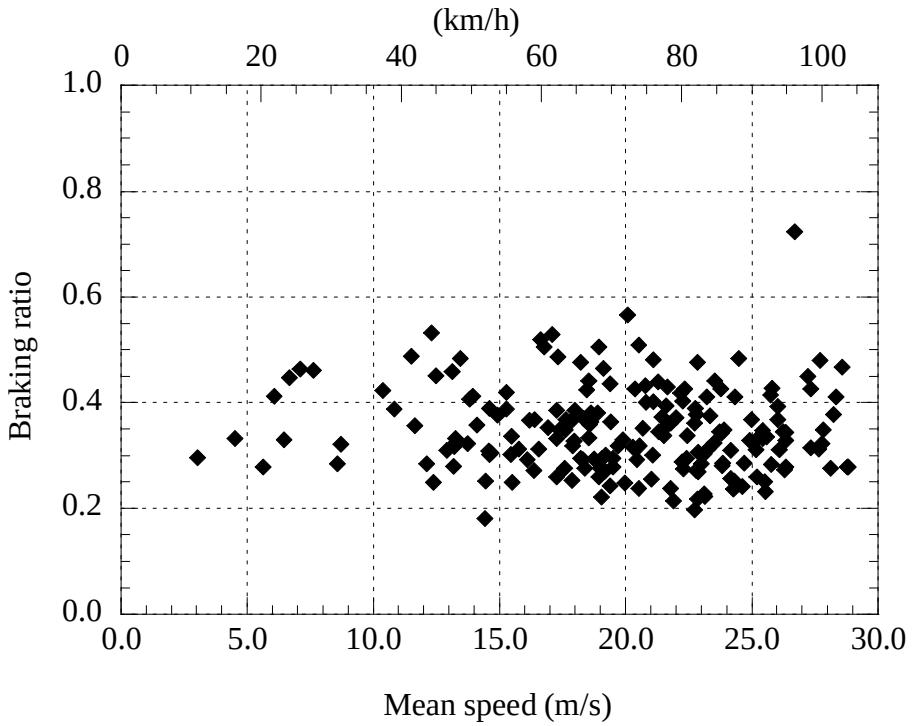

Figure 9-16 Measured braking ratio with respect to mean speed.

9.6 Conclusions

Five driving describing parameters are defined and analysed from full-scale observations. These parameters are useful for simulation purposes. These parameters can be used for *designing a driver model* which predicts freight train driving approximately as an *average* driver, or in any other way, thus *comparing* different ways of driving in further studies.

The big scatter in observed data is due to different conditions regarding trains, track, etc., but is also due to variation in individual driver behaviour.

The driving describing parameters, in freight train operation, are found to have the following characteristics:

- *Powering ratio*, has a mean value of 0.6 and is typically in the range of 0.5 - 0.8 of maximum. It is also increasing with respect to increasing total train mass, as on average.

- *Braking ratio*, shows a mean value of 0.35 of maximum. This indicates that the drivers preferably brakes gently and avoid long braking recovery times.

- *Degree of coasting* has a mean value of 0.25. This relatively high value indicates that coasting is used frequently and also leading to energy savings. The degree of total coasting has a big influence on energy consumption.

- *Upper speed action* limit is assumed to be in the range of 1.4 - 2.8 m/s, since the driver must not exceed the speed restriction by 2.8 m/s (10 km/h).

- *Lower speed action limit* has a mean value of 3.2 m/s and is typically in the range of 1.0 - 6.0 m/s.

The driving analysis of measured data from train operation shows no significant variance due to mean grade or mean speed. Also, driving parameters are not influenced by the train mass except the powering ratio.

It is also shown that the average driver applies a considerable amount of coasting, in addition to that the braking distance is longer than nominal due to a low braking ratio.

10 Driver model

By making use of the *driving describing parameters* as summarised in Section 9.6, a general driver model is developed in this chapter which simulates *normal manual driving*. Another model which simulates the *minimal time driving* is also developed. The two models are thus:

1. *Normal Manual Driving*, NMD.
2. *Minimal Time Driving*, MTD, by means of automatic speed holding. This model is more simple than the model for NMD and is not further described in this section. This model is developed only for this work as a special case, and the automatic speed control is not the same as the one on a real train. The description and flow charts of this model can be seen in APPENDIX D.

As a consequence of the driving describing parameters, NMD allows the speed to fluctuate about the nominal speed so that the simulated speed pattern resembles the speed pattern of a manually driven real train. The train speed fluctuates normally around v_{ATC} and is limited by upper and lower speed action limits.

MTD is achieved by means of suitable mixing of powering, braking and coasting so that the speed fluctuates as little as possible around the nominal speed, v_{ATC}, which is normally given by the ATC. This is simply achieved for the train model in this work, by balancing the required tractive force at the wheel rims of the locomotive with the calculated instantaneous running resistance. Acceleration is done at maximum powering, and the braking is done at nominal braking, i.e. 2/3 of full braking.

10.1 Normal Manual Driving model, NMD

Because of long braking and acceleration distances and relatively long response times of the train to powering and braking, the driver must plan in advance how to drive. When approaching a speed restriction, a strategic decision must be made how the driving should proceed. It is therefore natural to include a *lead distance,* or a look ahead distance, for the driver in the NMD model. The main benefit of this is that coasting can be utilised as a means for deceleration if the conditions are favourable. A “blind model” follows the speed restriction strictly and the deceleration is made frequently by means of mechanical braking.

It is observed in Section 9.4 that *coasting* is frequently utilised. The mean degree of coasting is 0.25. It is therefore important to include criteria in the model for when to start or stop coasting. Also, a model for how *powering and braking* are handled by the driver must be included.

Hence, the model for NMD consists of 3 main blocks or modules:

1. *Lead module*. This module determines how to drive when approaching next speed restriction.
2. *Coasting decision module*. Decision is made whether to start or stop (interrupt) coasting.
3. *Manual Speed Control module*, MSC. The level for powering and braking is determined in this module.

Figure 10-1 shows the flow chart for the NMD model. The different modules and variables are explained in the following sections.

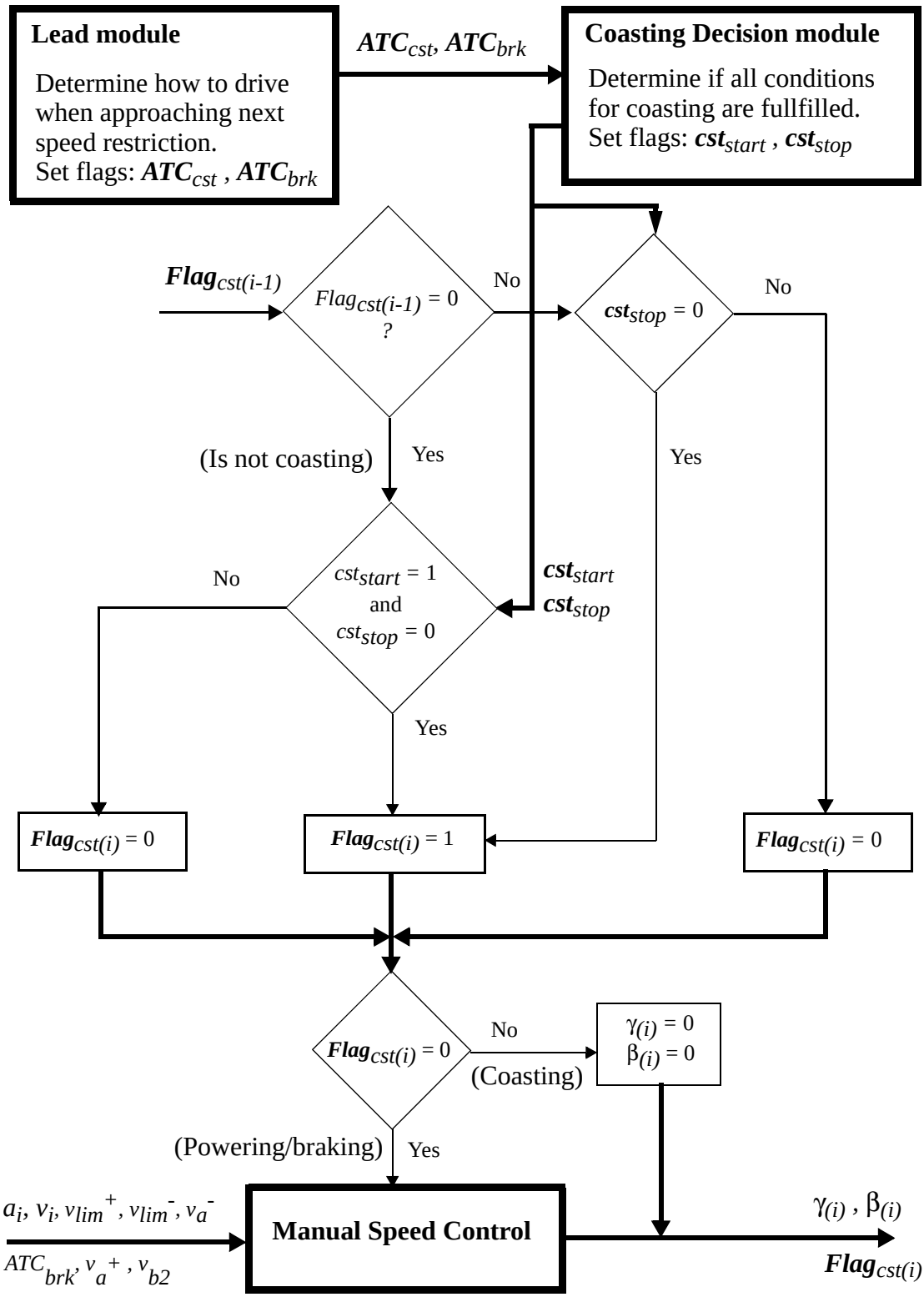

Figure 10-1 Main flow chart of the Normal Manual Driving model, NMD.

10.2 Lead module

In the *Lead Module*, it is suggested how to drive with respect to how the situation looks ahead by letting the driving model "see forward" a distance, S_{lead}. Depending on the decision, two flags, $\boldsymbol{ATC}_{cst}$ and $\boldsymbol{ATC}_{brk}$, are each set to a value of 0 or 1, see the flow chart in Figure 10-3. $\boldsymbol{ATC}_{cst}$ is a flag which is set to 1 if coasting is suggested. $\boldsymbol{ATC}_{brk}$ is a flag which is set to 1 if the train must brake. They are otherwise set to 0. If for example $\boldsymbol{ATC}_{cst} = 1$ and $\boldsymbol{ATC}_{brk} = 0$ it means that it is suggested to coast. The final decision, however, is made in the Coasting Decision module.

The total lead distance, S_{lead}, for the driving, is the sum of the look forward distance, S_{frw}, and the operational braking distance, S_{brk}, see Figure 10-2.

v_{b2} is the speed limit where the train automatically enters full braking mode, according to Section 6.3.

$$v_{b2} = v_{ATC} + 2.8 \text{ m/s} \tag{10-1}$$

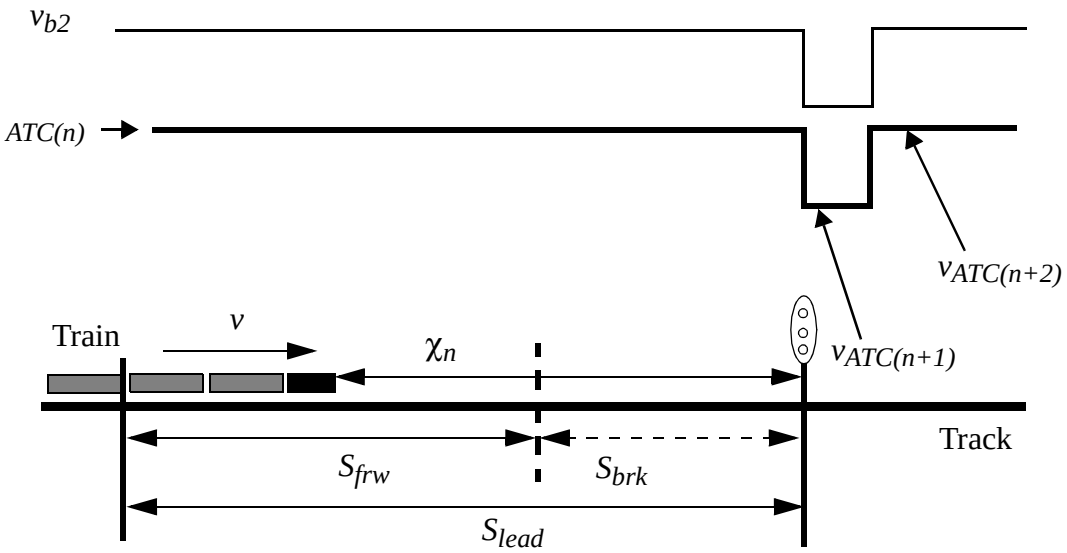

Figure 10-2 Train approaching a speed restriction.

S_{frw} is a forward distance to the position on the track where the train must enter the braking mode. As long as the train's position, χ_n, is in the S_{frw} section, it is possible to utilise powering, enter the coasting mode or brake at a further lower braking level than the normal operational level. The flow chart of the lead module is in Figure 10-3.

If the train is decelerating in the S_{frw} section, the starting point for S_{brk} is moving forward, since the braking distance becomes smaller, see Eq. (10-9).

S_{brk} is determined from Eq. (10-7) and depends on the mean grade between the trains actual position and the position of next signal and on the actual speed difference v_i - $v_{ATC(n+1)}$. The trains deceleration due to braking force and gradient is determined in Eq. (10-2). The effect of running resistance is not included because of safety reasons. In real operation and for rare conditions, air drag can be compensated for by a strong tail wind. F_{brk} is calculated from Eq. (7-10).

The total retarding force, due to mechanical braking in normal operation, and mean gradient is:

$$F_{brk} + F_G = -M_T \cdot g \cdot \left(\sigma_{brk} \cdot K_{brk} \cdot \frac{t_i - t_{b0}}{\lambda_{gain}} + \frac{G}{1000} \right) \quad \text{for } t_{b0} \le t_i \le t_{gain} \tag{10-2}$$

and

$$F_{brk} + F_G = -M_T \cdot g \cdot \left(\sigma_{brk} \cdot K_{brk} \cdot \frac{G}{1000} \right), \text{ for } t_{gain} < t_i \le t_{rel} \tag{10-3}$$

The utilised acceleration during operational braking is thus:

$$a_{brk} = \frac{F_{brk} + F_G}{M_T} = \left\{ \begin{matrix} \sigma_{brk} = 0.35 \\ K_{brk} = 0.092 \\ t_{gain} < t_i \le t_{rel} \end{matrix} \right\} = -g\left(0.032 + \frac{G}{1000} \right) \tag{10-4}$$

The values in Eq. (10-4) are empirical according to Section 7.2.

The braking distance can be divided into two parts:

1. The brakes are applied linearly until the braking force, thus *a*, reaches its final value after time $\Delta t = \lambda_{gain}$. During this part, the total decrease in speed is $\Delta v = \frac{-a_{brk}}{2} \Delta t$ and the travelled distance is:

$$\begin{aligned} S_1 &= v_i \Delta t + \int_0^{\Delta t} a(t) t dt = v_i \Delta t + \int_0^{\Delta t} \frac{F_{brk} + F_G}{M_T} dt \\ &= v_i \Delta t - \frac{g}{6} \left(\frac{3G}{1000} + \sigma_{brk} K_{brk} \right) \Delta t^2 \end{aligned} \tag{10-5}$$

2. Thereafter, the braking force, thus a_{brk}, is at its final value according to Eq. (10-4) and the initial speed is $v_i - \Delta v$. The travelled distance during this second part is:

$$S_2 = \int_{(v_i - \Delta v)}^{v_{ATC(n+1)}} \frac{v}{a_{brk}} dv \tag{10-6}$$

Using the same empirical values in Eq. (10-5) and Eq. (10-6) as in Eq. (10-4) gives the total braking distance:

$$S_{brk} = v_i \Delta t - \left(\frac{4.9G}{1000} + 0.05\right)\Delta t^2 + \frac{1}{2} \cdot \frac{(v_i - \Delta v)^2 - v_{ATC(n+1)}^2}{g\left(0.032 + \frac{G}{1000}\right)} \tag{10-7}$$

where

$$\Delta v = \frac{-a_{brk}}{2}\Delta t = \frac{g}{2}\left(0.032 + \frac{G}{1000}\right)\Delta t \text{ (m/s)} \tag{10-8}$$

The lead distance is then:

$$S_{lead} = S_{frw} + S_{brk} \text{ (m)} \tag{10-9}$$

As mentioned before two flags, $\boldsymbol{ATC}_{cst}$ and $\boldsymbol{ATC}_{brk}$, are each set to a value of 0 or 1, depending on whether certain conditions are fulfilled. The flow chart in Figure 10-3 explains how the flags are set.

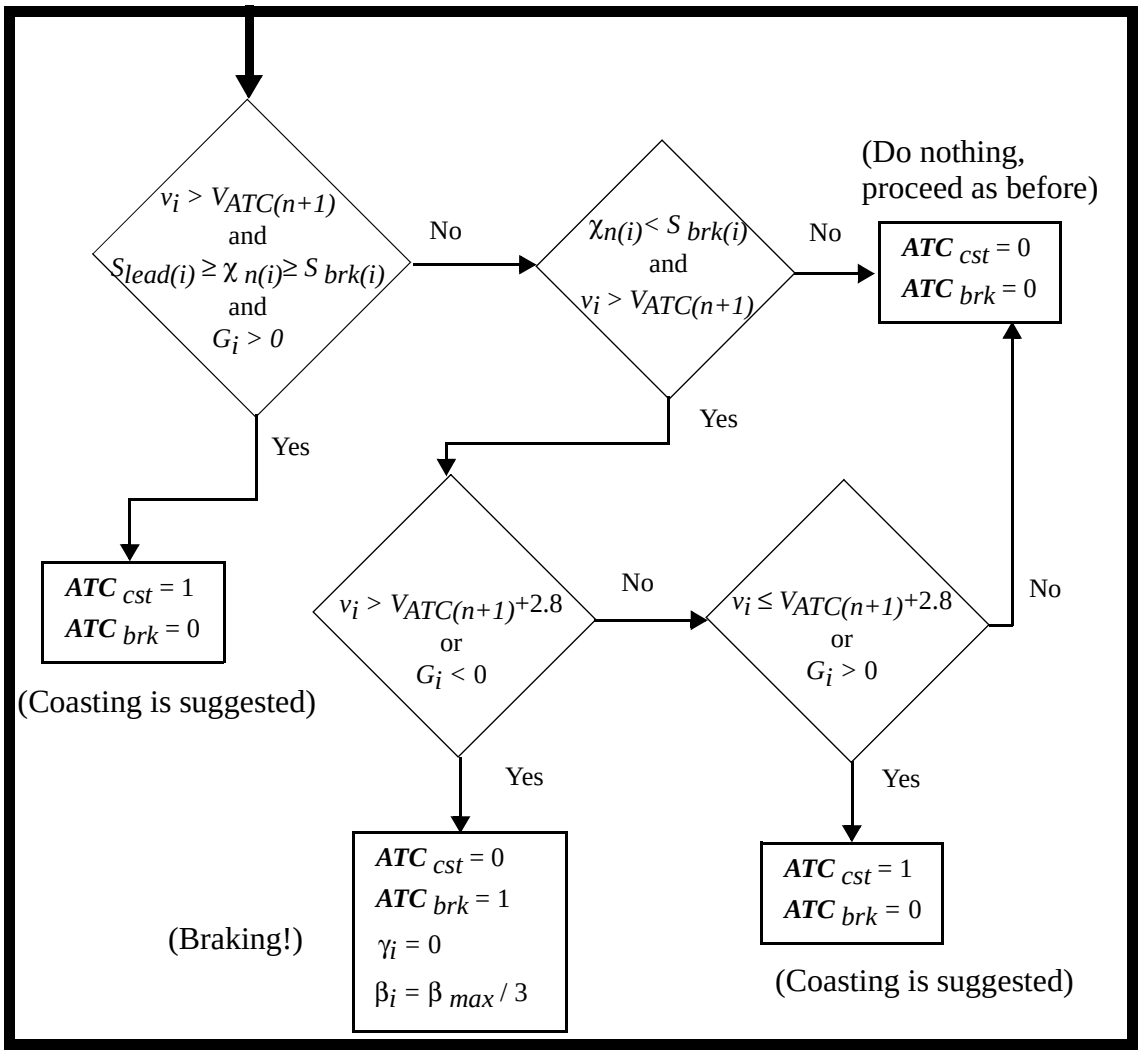

Figure 10-3 Flow chart of the Lead module.

10.3 Coasting Decision module

The flags $\boldsymbol{ATC}_{cst}$ and $\boldsymbol{ATC}_{brk}$ are used as input data into the *Coasting Decision module* which finally decides whether the train should start coasting by setting flag $\boldsymbol{cst}_{start} = 1$ or stop coasting, if the train already is in the coasting mode, by setting flag $\boldsymbol{cst}_{stop} = 1$. The flow chart in Figure 10-4 describes how the flags are set. v_{b1} and v_{cst} are explained in Section 10.4

Depending on how $\boldsymbol{ATC}_{cst}$ and $\boldsymbol{ATC}_{brk}$ are set, it is decided if the train should be in the coasting mode or powering/braking mode by setting the flag $\boldsymbol{Flag}_{cst}$ to 1 or 0, respectively.

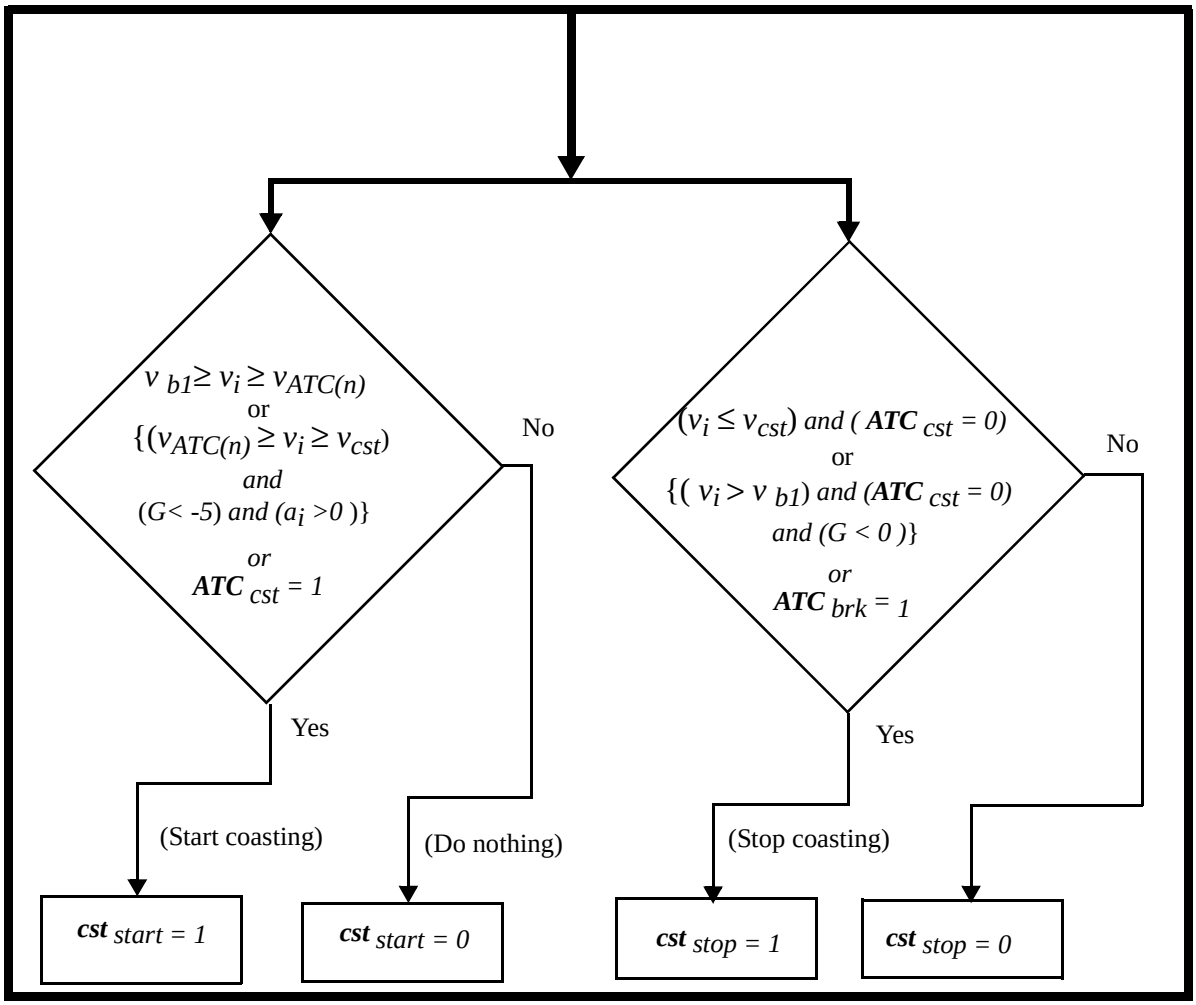

Figure 10-4 Flow chart of the Coasting Decision module

10.4 Manual Speed Control module

The driving enters the *Manual Speed Control module* if $\boldsymbol{Flag}_{cst} = 0$. Figure 10-5 shows a general situation when a train approaches a signal which is restricting the speed v_{ATC}. v_{b1} is a speed limit where the driver takes precautions not to exceed the speed limit of v_{b2}. If the train speed exceeds v_{b2}, the train enters automatically the full braking mode.

It is assumed that the speed limit v_{b1} is at the upper speed action limit

$$v_{b1} = v_{ATC} + v_a^+ \text{ m/s} \tag{10-10}$$

A typical value for v^+_a is 1.4 m/s (5 km/h) according to Section 6.3, in the Swedish ATC system.

$$v_{b2} = v_{ATC} + 2.8 \text{ m/s} \tag{10-11}$$

v_{lim}^+, v_{lim}^- and v_{lim0} are speed limits used only for speed control, internally in the Manual Speed Control module which is further described in APPENDIX D by the flow charts in Figure D-1 and Figure D-2. When the speed is in the range of v_{lim}^- to v_{lim}^+, the change in powering and braking level is made subtle in small steps, so that the speed is approximately maintained at v_{ATC}. When the speed is below v_{lim0} the increase in powering is made in bigger steps so the train speed reaches v_{ATC} more quickly. If the train is in coasting mode, it is not affected by v_{lim}^+, v_{lim}^- or $v_{lim0.}$ The train coasts until the speed reaches v_{cst} which is the limit given by the lower speed action limit v_a^-.

$$v_{cst} = v_{ATC} - v_a^- \text{ m/s} \tag{10-12}$$

The empirical mean value for v_a^- is 3.2 m/s. See Section 9.4.

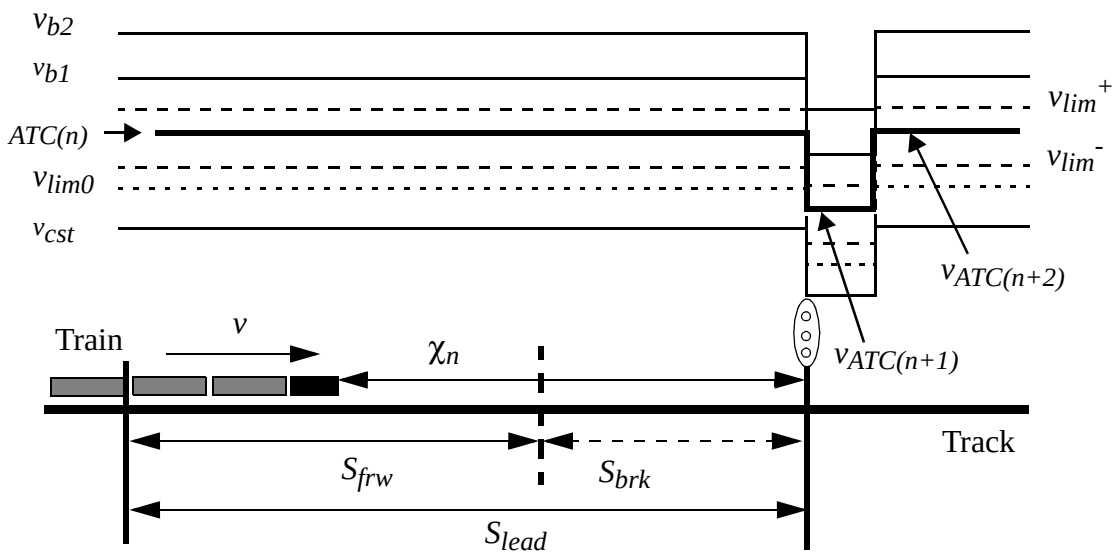

Figure 10-5 Speed limits and variables used in the NMD model.

Input data into the NMD model is:

- ***Flag***$_{cst(i-1)}$: This flag tells the model whether the train was in coasting mode or not at former time step i-1.

- v_i: Present train speed at time step *i*.

- v_{lim}^{+}, v_{lim}^{-}: Speed limits used internally in the Manual Speed Control module for speed control purposes. The values are empirical and found by means of trial-and-error from simulations.

- a_1, a_2, a_3: Acceleration limits used internally in the Manual Speed Control module for speed control purposes. They have empirical values, estimated by trial-and-error from simulations.

- $v_{ATC(n+1)}$, $S_{ATC(n+1)}$: Signalled speed and position on the track of next signal n+1.

- s_i: Present train position.

- S_{frw}: This is a constant distance used in the Lead Module where the total lead distance is calculated.

- G_i: Mean grade.

- $\gamma_{(i-1)}$, $\beta_{(i-1)}$: Former level settings of powering and braking at time step i-1.

- v_a^{+}, v_a^{-}: Upper and lower speed action limits.

Output data is:

- γ_i, β_i: powering and braking level used for calculating the tractive force or the braking force in the train model.

- $\boldsymbol{Flag}_{cst(i)}$: Flag which decides whether the train is in coasting mode or manual speed holding mode. The flag also tells the NMD module at next time step, i+1, whether the train is in coasting mode or not.

11 Verification of the driver model

The train model combined with the driver model is compared with full-scale measurements made with different trains run on different tracks with different drivers.

11.1 Conditions

The simulated train's initial value of starting position on the track, speed, powering and braking levels must be the same as for the real train. Table 11-1 shows the number of comparisons made, with corresponding train masses and the mean grades of the track sections.

Table 11-1 Number of comparisons, train masses and mean grade of track sections.

Mean grade (‰)	600-800 t	1100 - 1400 t
0.0 - 1.5	4	3
-2.6 - 0.0	3	2

11.2 Non-calibrated train model

The train model for each case is not calibrated with respect to running resistance and adhesion. Running resistance is calculated according to Section 7.6, and line voltage according to Eq. (7-1).

The relative difference, with standard deviation, between measured and simulated energy consumption is 1.7 ± 3.5 %, and the difference for the running time is 1.1 ± 2.6 %.

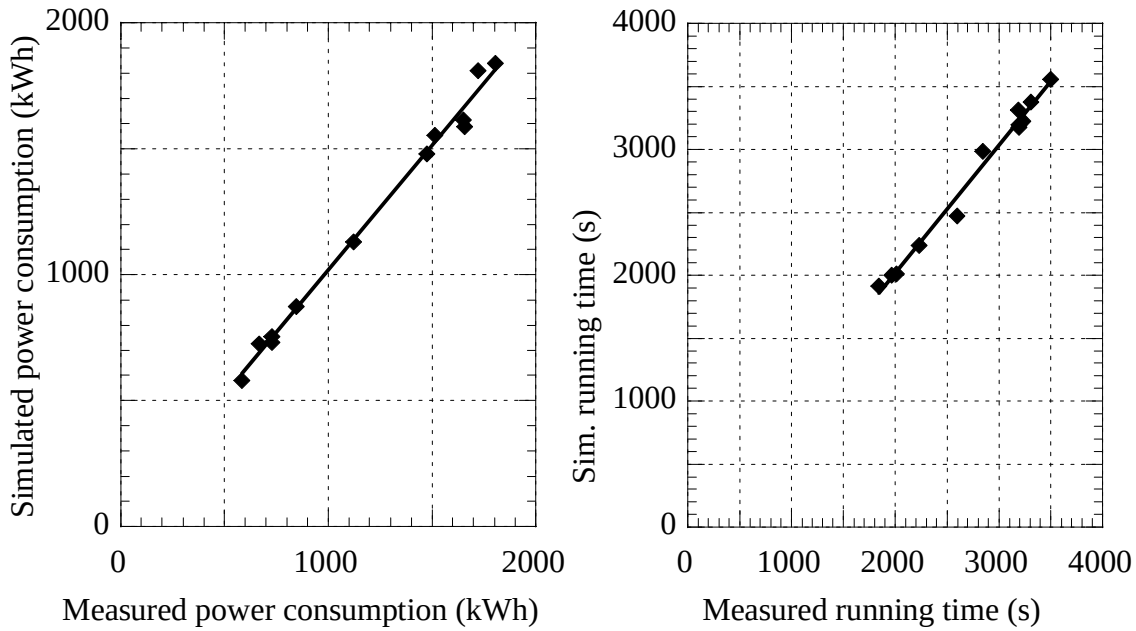

Figure 11-1 Comparison between measurements and non-calibrated simulations of energy consumption and running time.

The virtual driver is driving a freight train approximately as a real average driver. An example of this is shown in Figure 11-2 where the real train is running on a track section containing grades up to ± 17 ‰. The train mass is 670 tonnes. Effects of wind, slippery tracks due to rain, faulty track data giving errors in grades and curve radii are factors which are not always possible to account for.

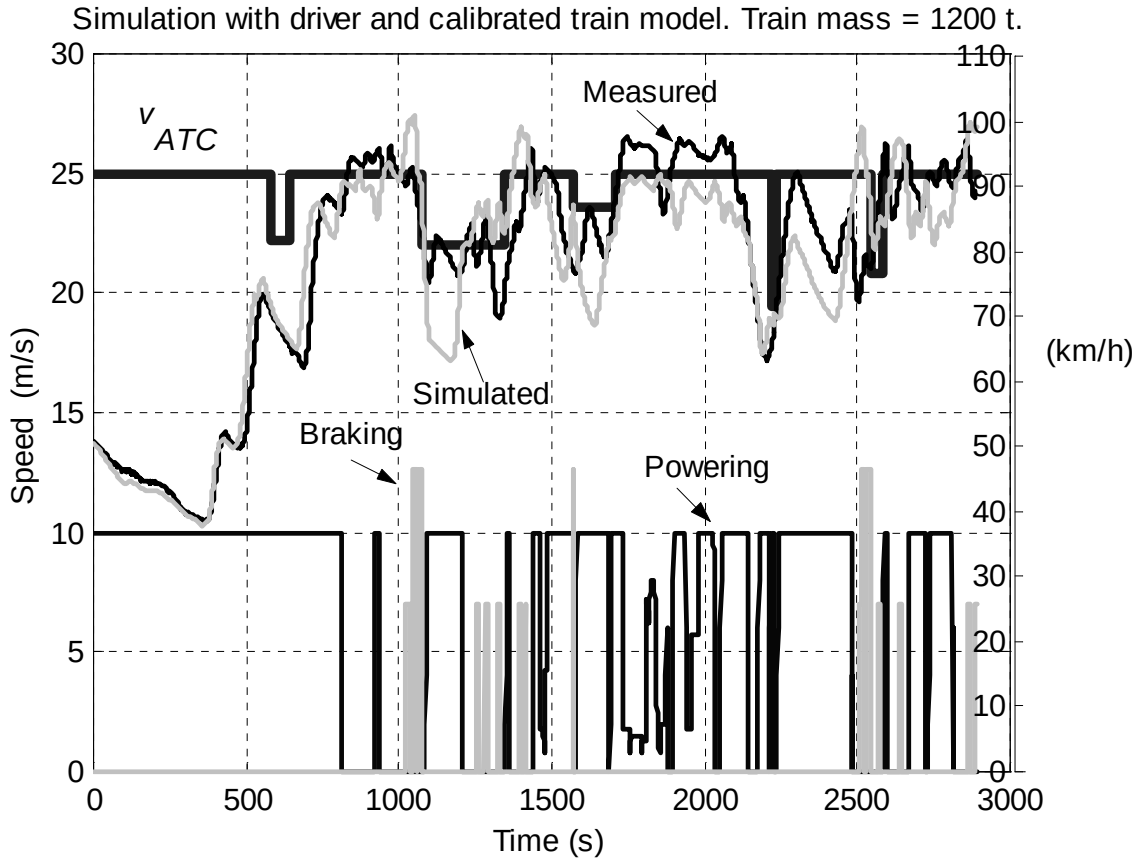

Figure 11-2 Example of simulation with a non-calibrated train model. *The powering and braking levels are scaled for clarity.*

11.3 Calibrated train model

If the model is calibrated as described in Section 8.4 with respect to running resistance and adhesion, the relative difference, with standard deviation, in energy consumption is 0.1± 1.2% and in running time 0.1 ± 1.1%. This is within the accuracy in the measurements of ± 1 - 2 %.

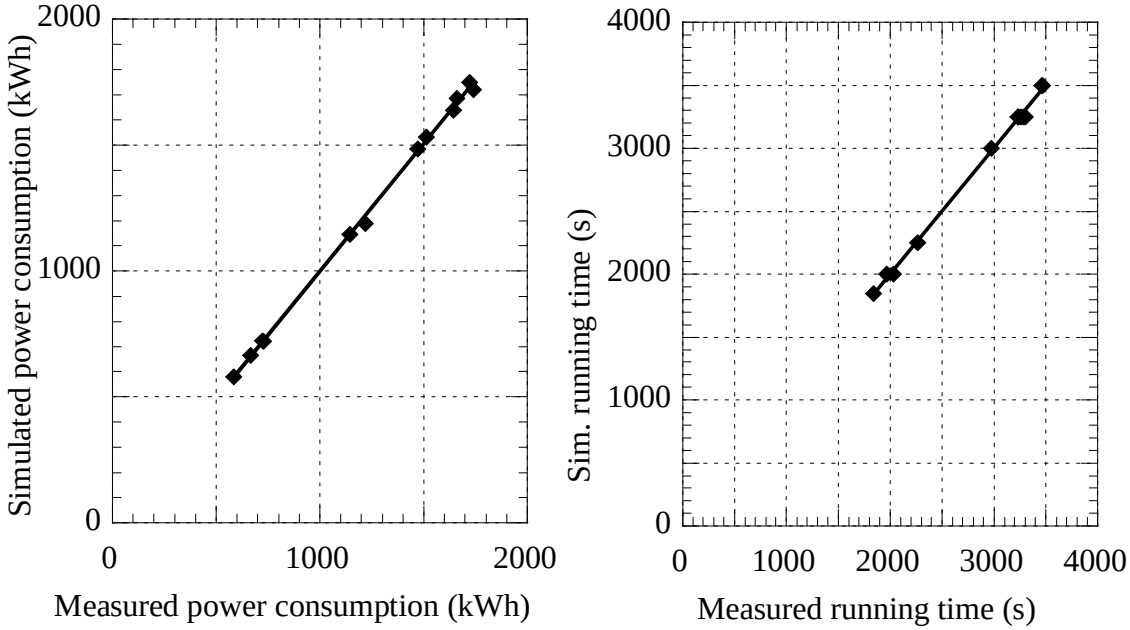

Figure 11-3 Comparison between calibrated simulations and measurements of energy consumption and running times.

12 Parametric study on influence of driver behaviour

The study presented is this Chapter is performed by means of simulation, using the models and simulation package as developed according to Chapter 7, 8 and 10. Investigations on the principal influence from different driving describing parameters on energy consumption and running time are performed in Sections 12.2 - 12.6. In Section 12.1 simulated trains, track sections and ambient conditions are introduced.

12.1 Trains track sections and ambient conditions

All investigations in this Chapter will be made with a typical example of a Swedish freight train having characteristics according to Table 12-1

Table 12-1 Train used in simulation

Type	Config.	Length	Mass	Trailing axles	K_D	Loco	Max train speed
Freight	Mixed	413 m	1197 t	52	8.6×10^{-2}	1 *SJ Rc4*	27.8 m/s 100 km/h

The trains are run over three different track section, two of them being idealised track and one being real track sections with various changing gradients and speed restrictions and real signalling.

Table 12-2 Track sections

T1 Idealised track section with a constant nominal allowed speed of 27.8 m/s (100 km/h) and a constant positive or negative grade (or zero grade)

T2 Idealised track section (length 75 km) with a maximum nominal allowed speed of 100 km/h except two speed restrictions to 72 km/h (20 m/s) and another two speed restrictions to 36 km/h) 10 m/s. Constant positive or negative grades. See Figure 12-2 for details.

T3 Real "hilly" track (length 40 km) with real signalling. Grades up to approx. ± 18 ‰. See Figure 12-1 for details. maximum nominal speed of 25 m/s (90 km/h) with six speed restrictions ranging from 20 m/s (70 km/h) to 23.6 m/s (85 km/h).

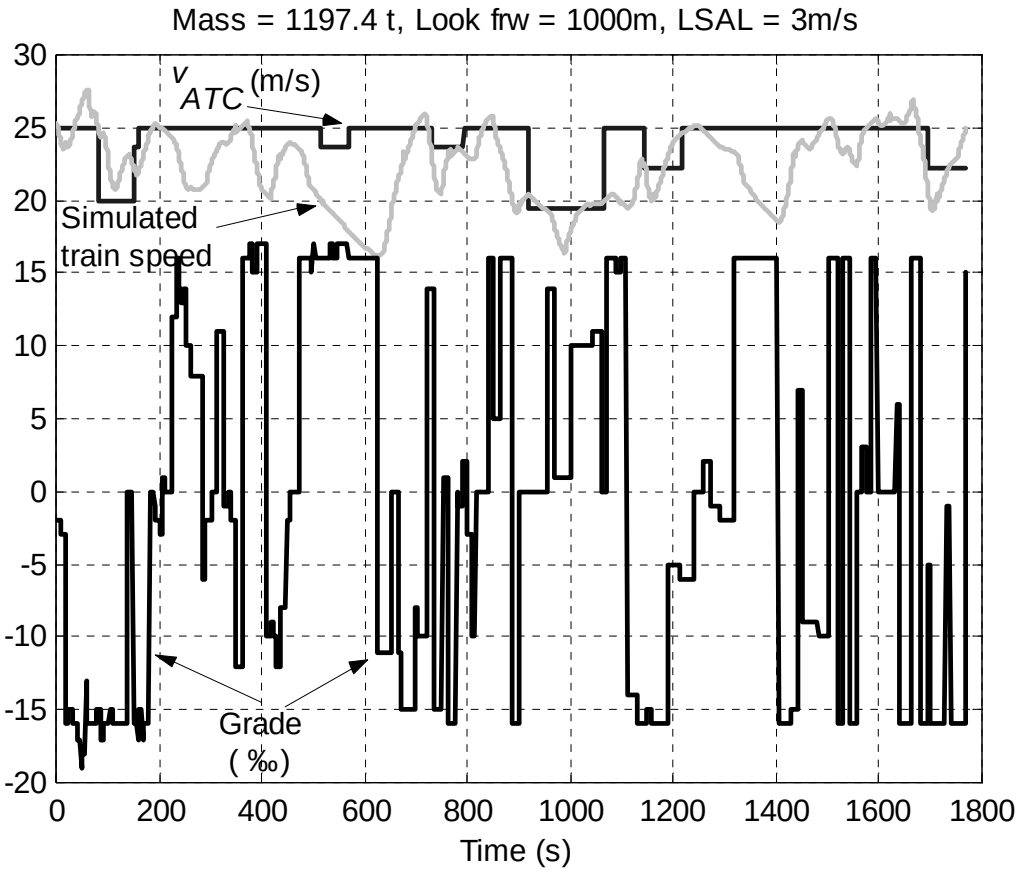

Figure 12-1 Track T3. Speed restrictions and grades, with an example of simulated train speed.

Table 12-3 Ambient conditions.

Adhesion	Wind	Temp	P_{atm}
dry rail	no	20 C	1013 hPa

12.2 Influence of look ahead and coasting before braking

As reported in Chapter 9, *coasting* is a quite usual driving action, constituting some 25 % of total running distance as an average, as reported from the real freight train operations in Chapter 9. Coasting can sometimes be made as part of the "speed holding" mode as a means of keeping speed around the nominal allowed speed. Such driving behaviour will be investigated further on in Section 12.3.

Very frequently coasting is part of the retardation mode before a speed restriction or stop, where coasting starts at a certain *look forward distance* S_{frw} before the driver applies the brakes. This is described in Sections 9.3 - 9.4 and in 10.2 - 10.4. The influence of such driving will be investigated in this section. By choosing a coasting distance long enough it is possible to avoid some braking and to avoid powering the whole time before braking.

The investigation of coasting before braking is firstly made on idealised track *T2* with speed restrictions, to demonstrate the principal influences. This is shown in case 1 as described below.

Case 1 Effect of look forward distance S_{frw} *, on idealised track T2.*

- The grade is set to 2 ‰ in order to reduce the coasting distances.
- Upper and lower speed action limits are zero.
- Powering ratio is 0.85 throughout the simulations.
- Braking ratio is 0.35.
- The coasting distance before a speed limit or braking due to speed reduction is varied from 0 to 4000 m in steps of 400 m.

By choosing a coasting distance long enough it is possible to avoid some braking. This is shown in Figure 12-2 and Figure 12-3. The effect of brake recovery time is encircled in Figure 12-2. Despite the driver has stopped braking, it takes some time to release the brakes completely. This leads to a speed drop below the nominal speed resulting in increased energy consumption and running time. Some examples of this speed drop is shown in Figure 9-1 and Figure 12-20.

The analysis in Figure 12-4 shows that a relatively big reduction in energy consumption can be achieved if braking is avoided, which in this case occurs for $S_{frw} \geq 2400$ m . The sudden reduction in energy consumption, marked with a circle in Figure 12-4, is due to the absence of the speed drop caused by the braking recovery time. In this example, the reduction in energy consumption is 18 % and the increase in running time is 5 %.

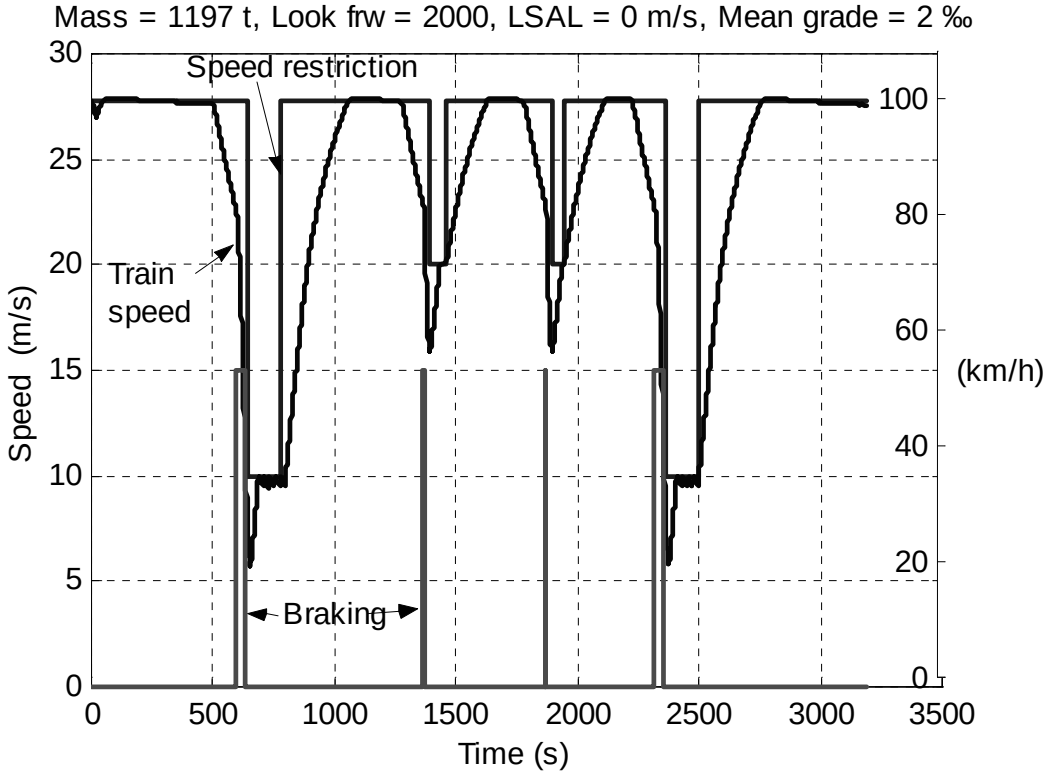

Figure 12-2 S_{frw} = 2000 m, is not long enough for avoiding braking at t = 1350 s and t = 1850 s.

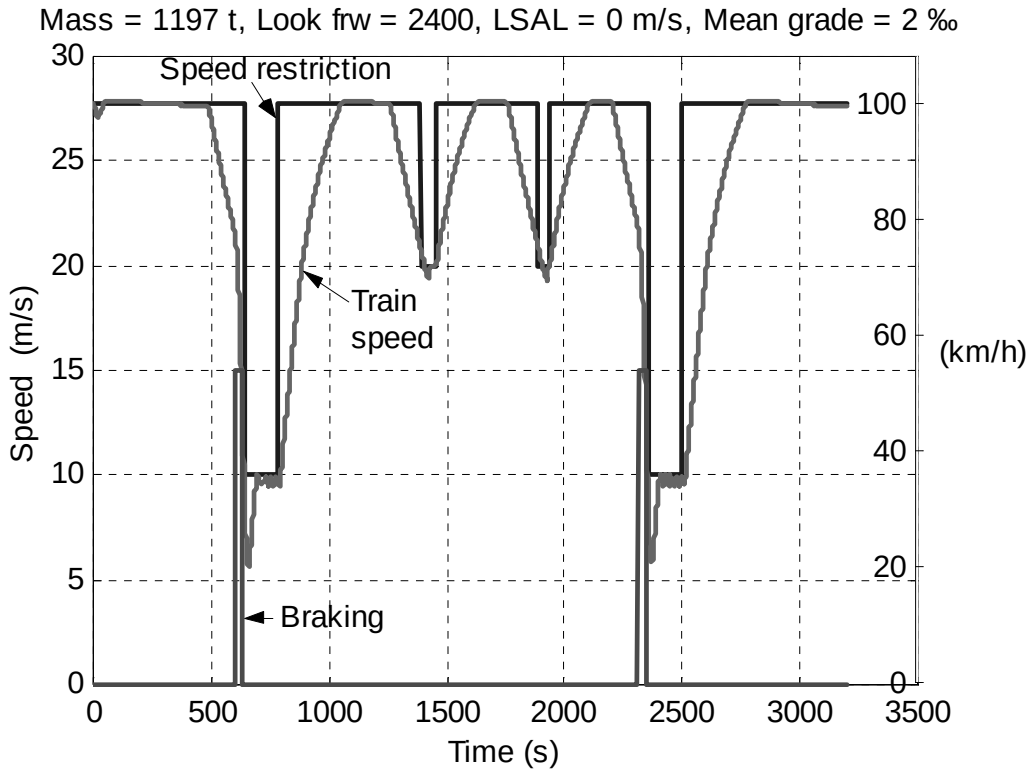

Figure 12-3 S_{frw} = 2400 m, is long enough for avoiding braking at t = 1350s and t = 1850s.

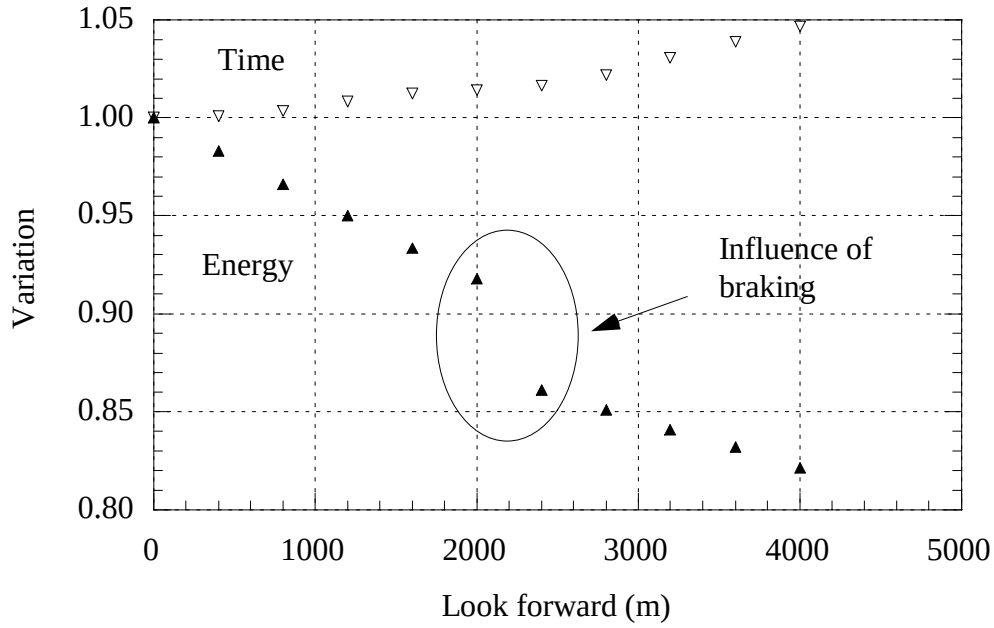

Figure 12-4 Influence of Look forward distance, S_{frw}, on energy consumption and running time. The gap in energy consumption shows the influence of braking

Case 2 Effect of look forward distance S_{frw}, on real "hilly" track T3.

- Upper and lower speed action limits are 1.4 m/s and 3.0 m/s, respectively.
- Powering ratio is 0.85 throughout the simulations.
- Braking ratio is 0.35.

An example of a simulation for this case is shown in Figure 12-1.

Figure 12-5 shows that a reduction in energy consumption of 17 % can be achieved by increasing the look forward distance, compared to the reference case with a look forward distance of 0 m.

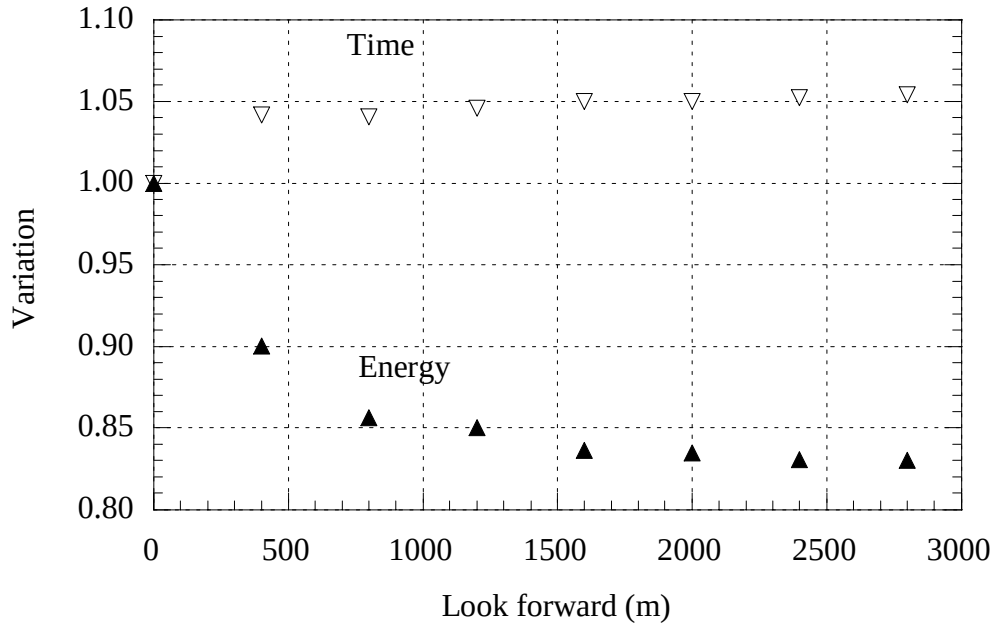

Figure 12-5 Influence of Look forward distance, S_{frw}, on track T3.

The effect of the look forward distance on coasting before speed limit or stop can be expressed by Eq. (12-1).

The *degree of coasting before speed limit or stop* is in this work defined as:

$$\delta_{cst-brk} = \frac{\text{Coasting distance before speed lim.}}{\text{Coasting distance before speed lim. + Braking dist.}} \qquad (12\text{-}1)$$

Example of the influence of $\delta_{cst\text{-}brk}$ on energy consumption and running time is shown in Figure 12-6. It is the same train and track as used in Figure 12-4.

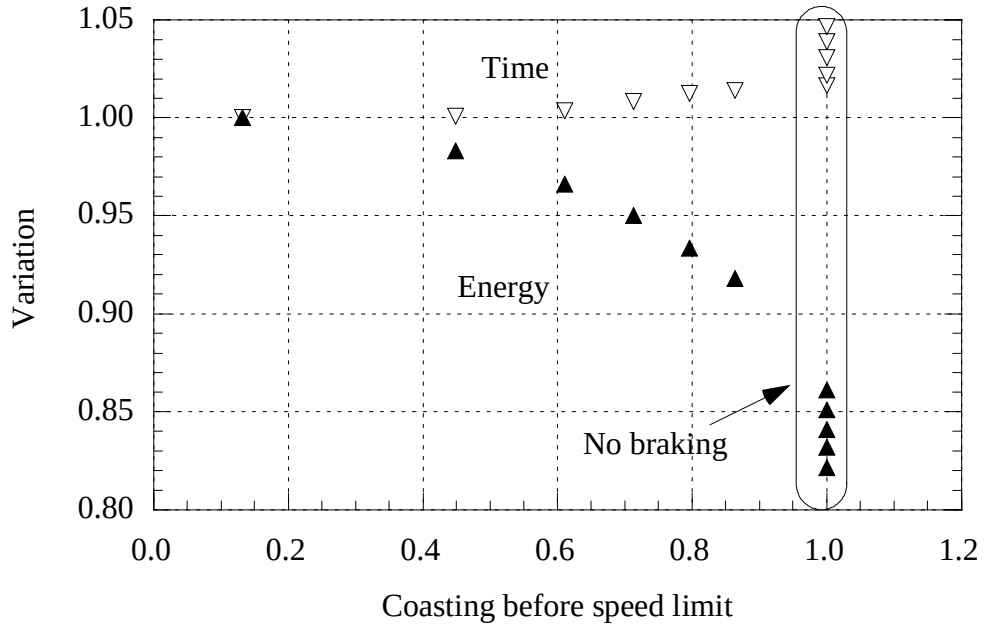

Figure 12-6 Influence of coasting before speed limit, $\delta_{cst\text{-}brk}$, on energy consumption and running time for track T2.

Conclusion

The energy consumption is sensitive to the choice of the look forward distance. By making an appropriate choice, it is possible to reduce the energy consumption by 10 -15 % while the running time increase is relatively small, 1 -5 %, compared with a reference case having a look forward distance of 0 m.

If unnecessary braking can be avoided, an energy saving of 5 - 7 % can be achieved, without increasing the running time.

12.3 Influence of lower and upper speed action limits

As pointed out earlier, coasting can be part of the “speed holding” driving mode as a means of keeping speed around the nominal allowed speed. In this case the (average) driver tolerates a certain drop in speed below the nominal allowed speed, before he starts powering again. As described earlier it is assumed that the speed is allowed to drop with an amount of v_a^- defined as the *lower speed action limit*. Also, the drivers quite frequently exceed the nominal allowed speed limit with a certain amount, still allowed within the ATC margin before the brakes are applied automatically. It is assumed that the (average) driver tolerates the speed to rise above the nominal allowed speed with an amount of v_a^+ defined as the *upper speed action limit*. The influence of these driving parameters will be principally investigated in this section.

By altering the lower speed action limit, v_a^- , in relation to v_{ATC}, it is possible to investigate the influence of v_a^- on train energy consumption and running times.

The investigation of the lower and upper speed action limits is firstly performed on idealised track *T1*, just to make a demonstration of different ways of manual speed holding. This is shown in cases 3 and 4, as described below. Secondly, the influence of lower and upper speed action limits on a the real track *T3* is demonstrated as an example in cases 5 and 6.

Case 3 Effect of lower speed action limit v_a^- , on idealised track T1.

- Upper speed action limit is 0 m/s.
- Powering ratio is 0.85 throughout the simulations.
- Braking ratio is 0.35.

Figure 12-7 shows an example of simulated speed pattern for a straight and level track. The powering is reduced to zero when the speed reaches v_{ATC} thus making the train start coasting. When the train speed drops to v_{cst} , due to running resistance, the powering is increased to maximum. This is commonly called *Bang-Bang driving* since the powering level is either at its maximum or zero. No restrictions due to signalling are present for this case.

Variation in running time and energy as a function of the lower speed action limit is shown in Figure 12-9, on level track.

.

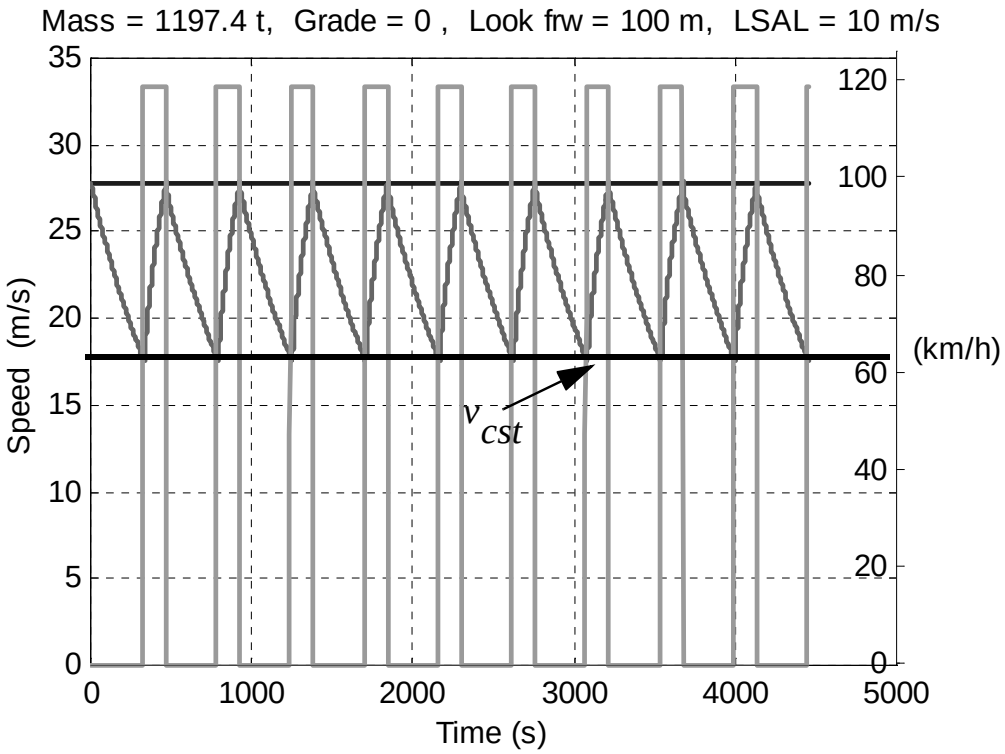

Figure 12-7 Example of Bang-Bang speed pattern from simulation on level track where lower speed action limit is 10 m/s.

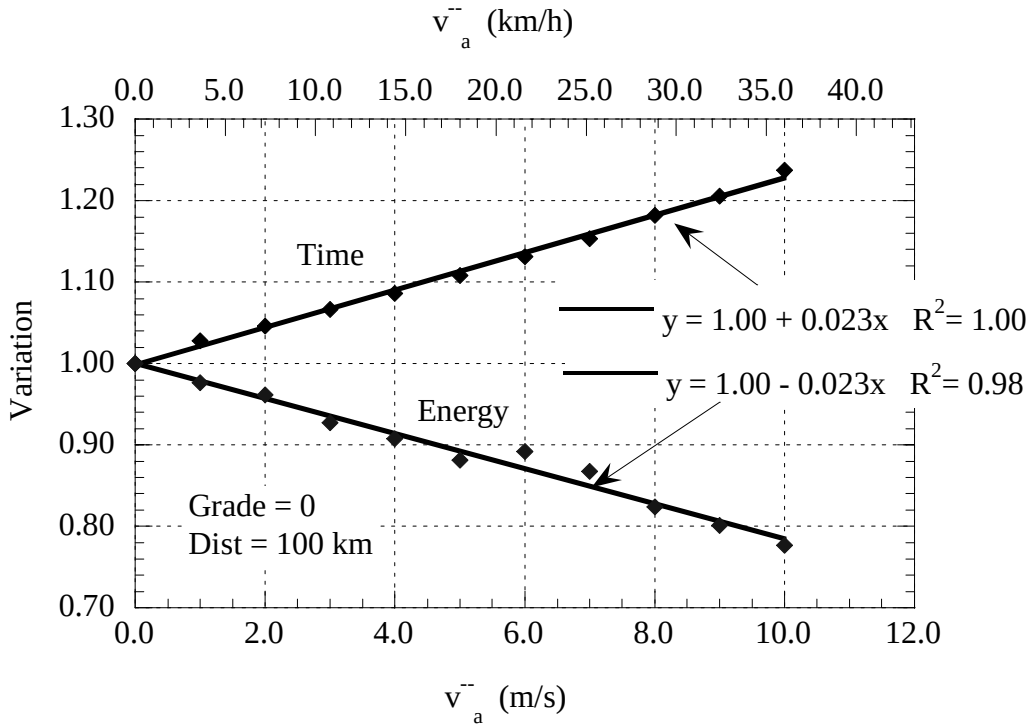

Figure 12-8 Change of total running time and energy consumption due to change in lower speed action limit for Bang-Bang driving on a level track T1.

Variations in running time and energy for other mean grades are shown in Figure 12-10.

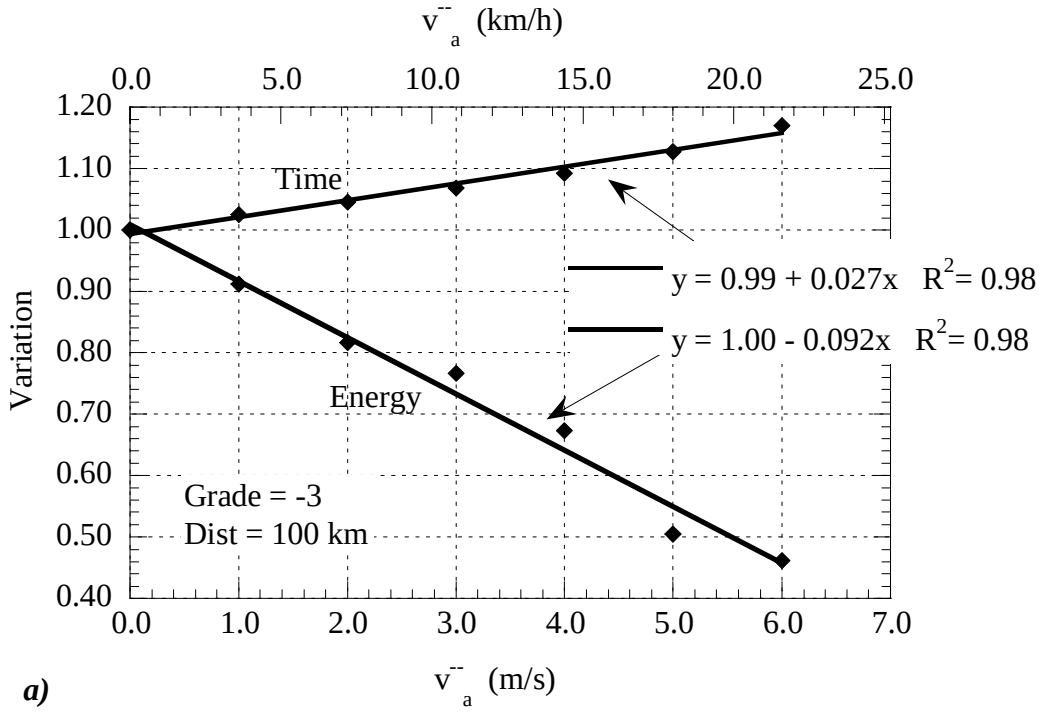

a)

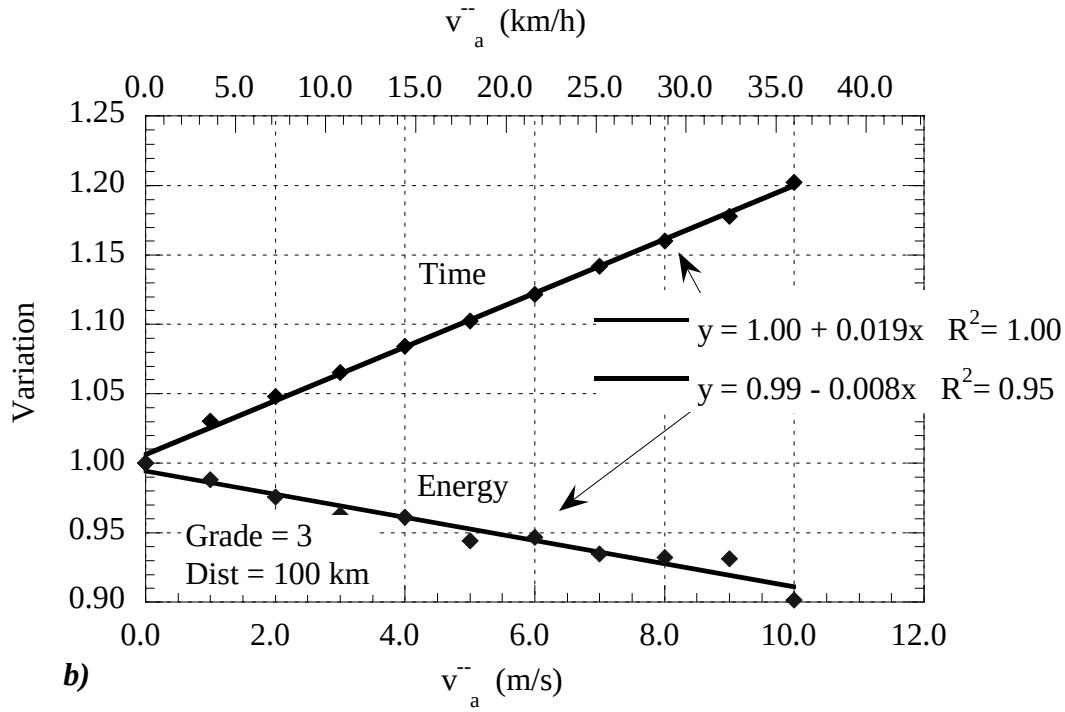

b)

Figure 12-9 Variation of total running time and energy consumption due to change in lower speed action limit for Bang-Bang driving on track T1 with a grade of
a) -3 ‰.
b) 3 ‰.

Figure 12-8 and Figure 12-9 shows the results from simulations made for different mean grades of a straight track *T1*. Figure 12-9 shows that the reduction in energy consumption compared to the increase in total running time is most favourable when the mean grade is less than 0, i.e. when travelling downhill. If the train travels on a level track, Figure 12-8, the rate of the change of running time is of the same order as for the change in energy consumption

Case 4 Effect of lower speed action limit v_a^- *combined with a positive upper speed action limit* v_a^+ *, on idealised track T1.*

- Upper speed action limit is 1.4 m/s.
- Powering ratio has a mean value of 0.85.
- Braking ratio is 0.35.

This case shows, see Figure 12-10, that energy consumption for the *same running time* and mean speed, is almost the same.

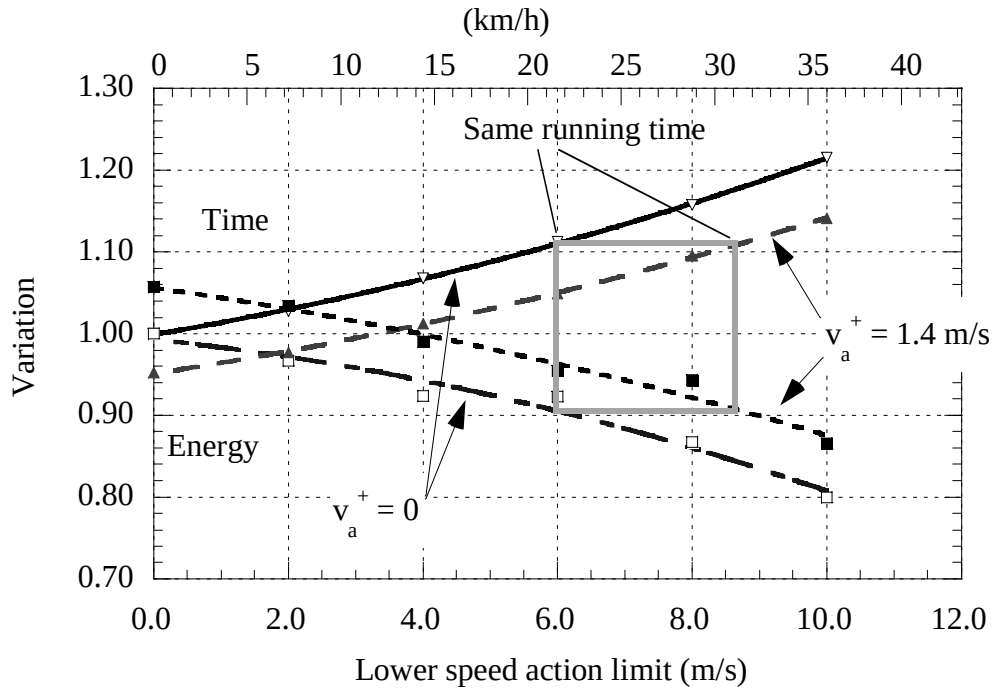

Figure 12-10 Comparison of energy consumption and running time for different upper and lower speed action limits for an idealised track T1.

Case 5 Effect of lower speed action limit v_a^- *, on real"hilly" track T3.*

- Upper speed action limit is 0 m/s.
- Powering ratio has a mean value of 0.85.

- Braking ratio is 0.35.
- Look forward is 1000 m.
- The results are presented compared to minimum time driving and v_a^- = 0 m/s.

It is shown in Figure 12-11 how the simulated change of running time and energy consumption on a real track section, having real signalling, is influenced by the lower speed action limit. The energy consumption decreases and the running time increases as the v_a^- increases. This reduction in energy consumption, is due to a decrease in the mean speed, which decreases the running resistance, as the lower speed action limit increases. It is also shown that compared to minimum time driving, the energy consumption is reduced by 11 % if a lower speed action limit of 1.0 m/s is introduced. The total running time remains almost unaffected.

.

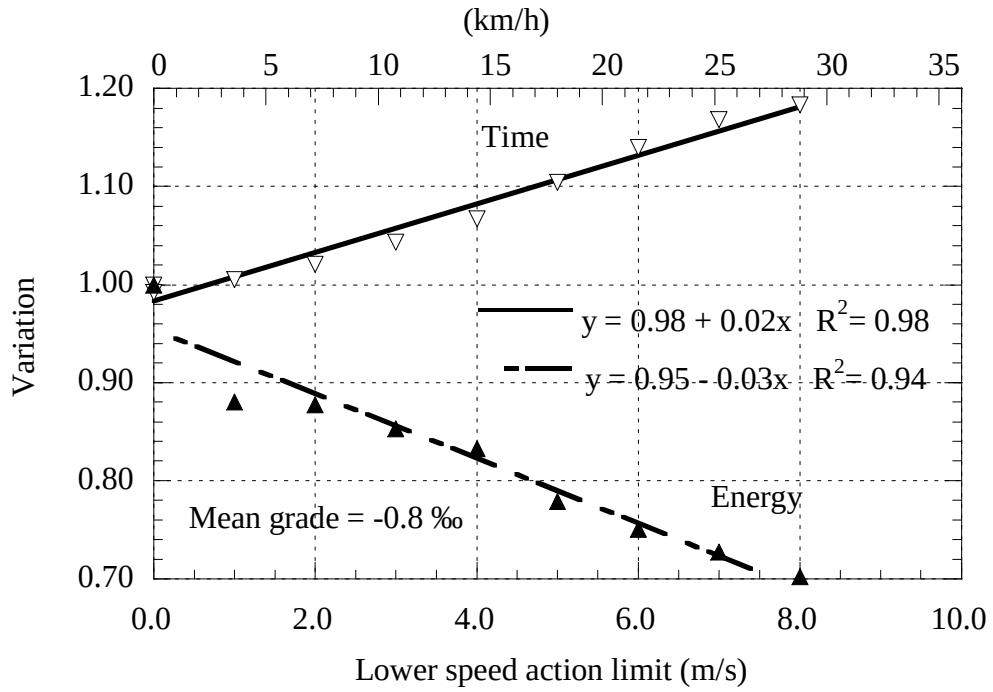

Figure 12-11 Influence of lower speed action limit on real track T3.

Case 6 Effect of lower speed action limit v_a^- combined with a positive upper speed action limit v_a^+ , on real"hilly" track T3.

- Upper speed action limit is 1.4 m/s.
- Powering ratio has a mean value of 0.85.

- Braking ratio is 0.35.
- Look forward is 1000 m.
- The results are presented compared to normal manual driving and v_a^- = 0 m/s

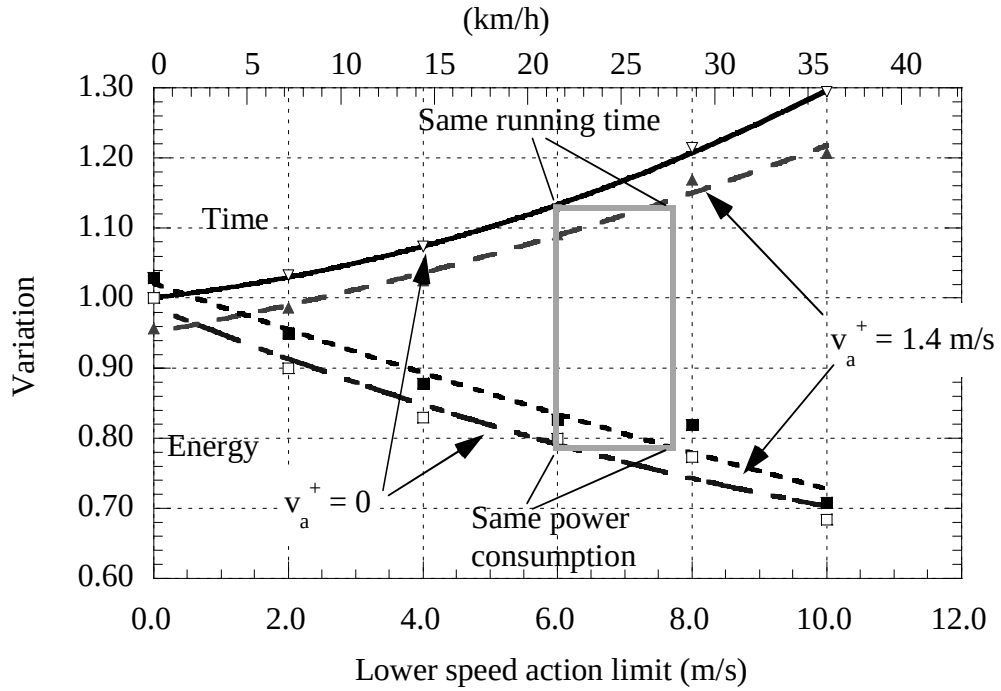

Figure 12-12 Comparison of energy consumption and running time for different upper and lower speed action limits for a real track T3.

Conclusions

A train running at low values of v_a^- has about the same energy consumption as a train running at higher values of v_a^- , provided the mean speed is the same for the two trains. The mean speed can be increased for the train having higher values of v_a^- by increasing the upper speed action limit v_a^+.

12.4 Influence of powering ratio

As determined in Chapter 9 the average powering ratio is approximately 0.6, i.e. some 40 % less than the used locomotive *Rc4* is able to produce. This may be due to the driver only, but also in many cases to the amount of available adhesion.

The investigation of the influence of powering ratio, σ_{pwr}, is firstly performed on idealised track *T1* without speed restrictions, in manual speed holding. The driver is alternating between maximum available powering and coasting, so called *"Bang-Bang driving"* . This is shown in case 7, as described below. Secondly, the influence of powering ratio is also demonstrated on the idealised track *T2* with speed restrictions and on a the real "hilly" track *T3* in cases 8 and 9 respectively. The principal effect of lower adhesion, which limits the tractive force at low speeds, is demonstrated in Case 10.

Case 7 Effect of powering ratio σ_{pwr} , on idealised track T1.

- Lower speed action limit is maintained at 3 m/s throughout the simulations
- Upper speed action limit is zero.
- The tractive force is varied from 1.0 F_w down to 0.7 F_w in steps of 0.1.
- Bang-Bang driving.

The results in Figure 12-13 shows that the powering ratio has negligible influence on energy consumption and running time for Bang-Bang driving.

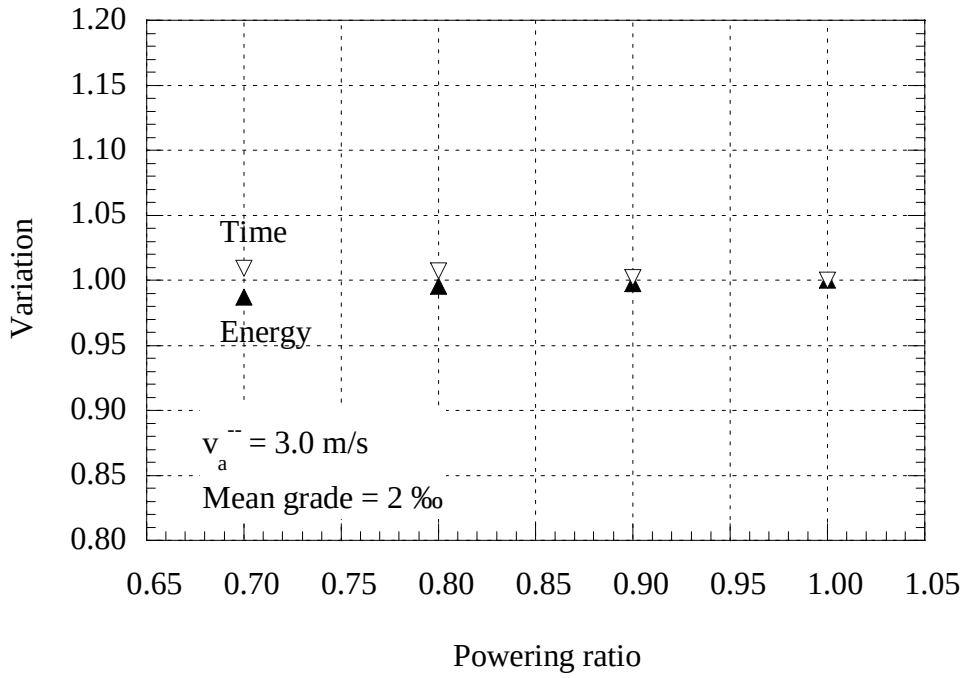

Figure 12-13 Influence of the powering ratio on energy consumption and running time when alternating between powering and coasting (Bang-Bang driving) on track T1. The lower speed action limit is 3 m/s and the mean grade is 2 ‰.

Case 8 Effect of powering ratio σ_{pwr} , on idealised track T2.

Lower and upper speed action limits are zero, causing the driving to be speed holding.

- Look forward distance is 800 m.
- Braking ratio is 0.35.
- The tractive force is varied from 1.0 F_w down to 0.5 F_w in steps of 0.1.

Figure 12-14 and Figure 12-15 shows the simulated speed pattern for σ_{pwr} = 1.0 and σ_{pwr} = 0.6, respectively. For σ_{pwr} = 0.6 it is impossible for the train to reach the nominal speed v_{ATC}. The influence of the powering ratio on relative energy consumption and running time is shown in Figure 12-16. The powering ratio has a bigger influence on the energy consumption and running time than in case 7. This is explained by a lower mean speed in this case because of insufficient tractive force leading to slow acceleration.

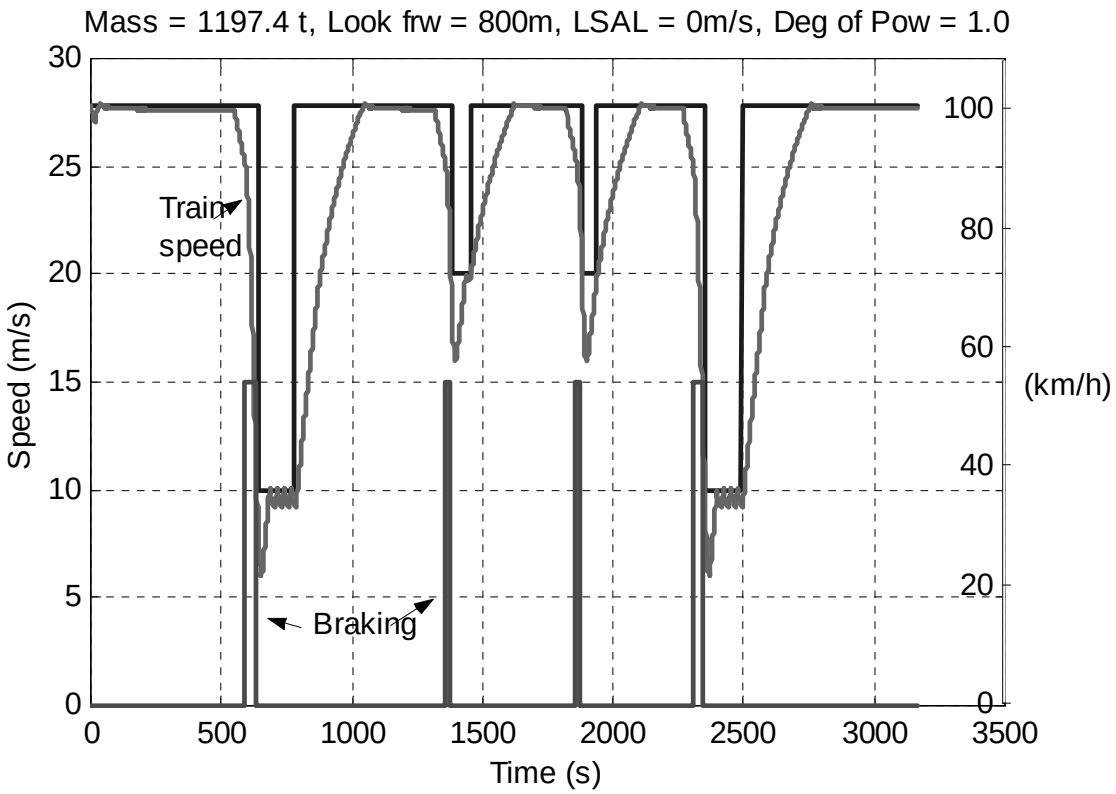

Figure 12-14 Example of speed pattern for a powering ratio of 1.0.

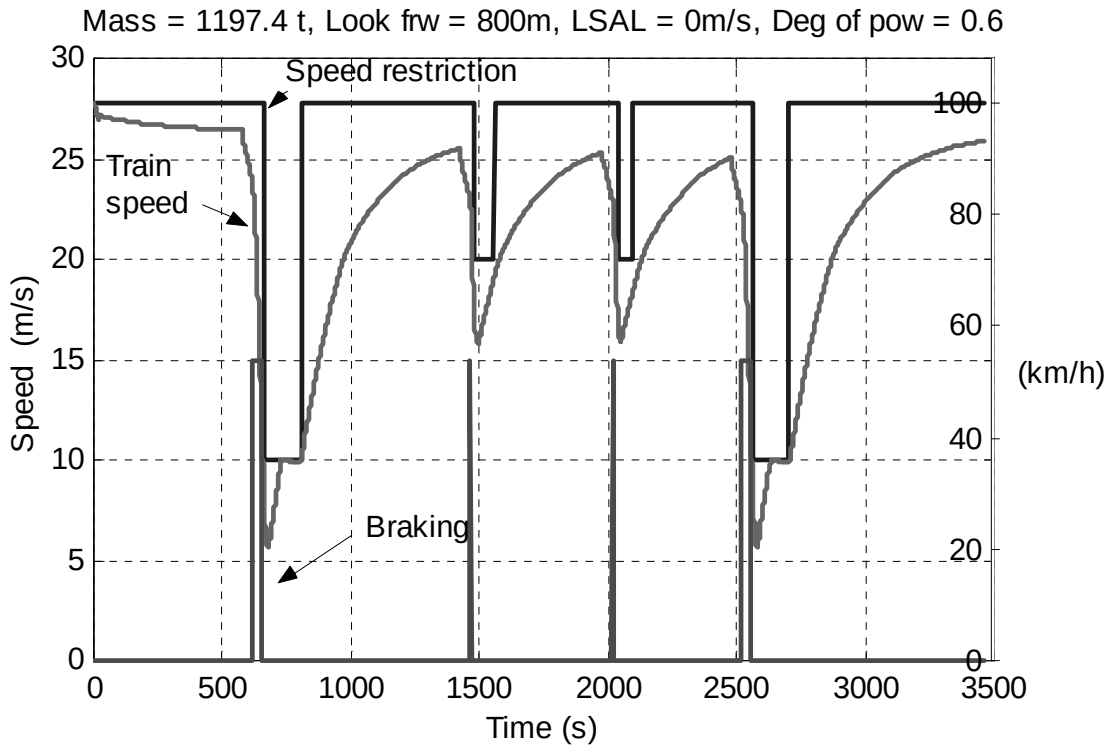

Figure 12-15 Example of speed pattern for a powering ratio of 0.6.

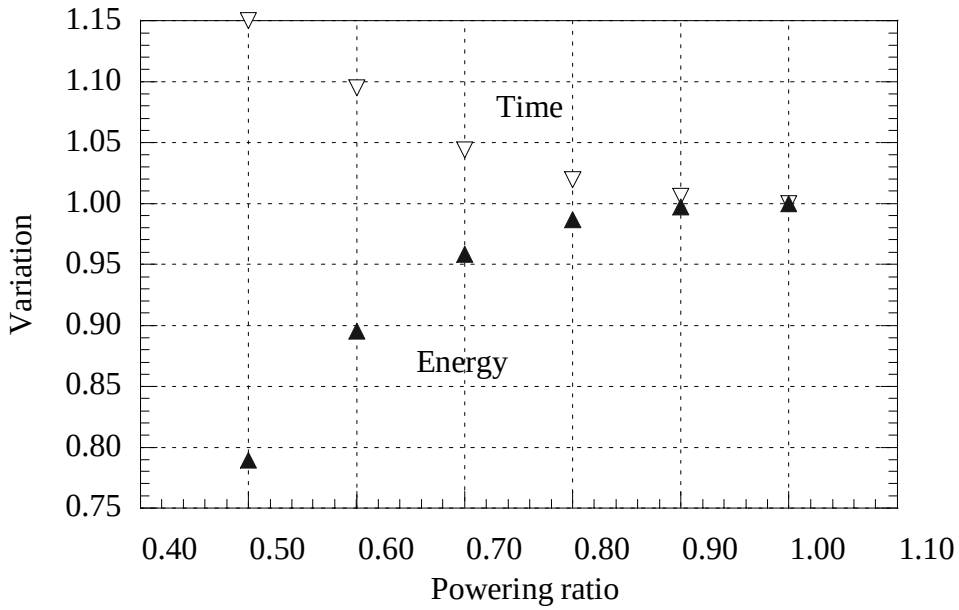

Figure 12-16 Influence of the powering ratio on energy consumption and running time.

Case 9 Effect of powering ratio σ_{pwr} , on real"hilly" track T3.

- Lower and upper speed action limits are 3.0 m/s and 1.4 m/s, respectively.
- Look forward distance is 800 m
- Braking ratio is 0.35.
- Normal manual driving.

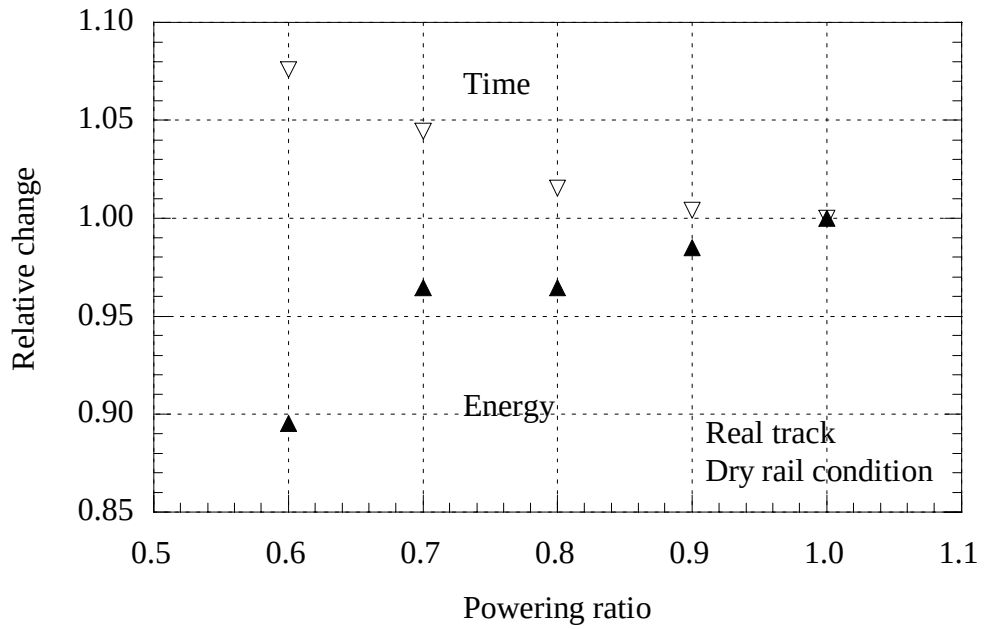

Figure 12-17 Influence of the powering ratio on energy consumption and running time for real track T3.

Case 10 Effect of adhesion level on real track T3.

- Lower and upper speed action limits are 3.0 and 1.4 m/s.
- Look forward distance is 1000 m.
- Braking ratio is 0.35.

Influence of adhesion, α, on energy consumption and running time is shown in Figure 12-18.

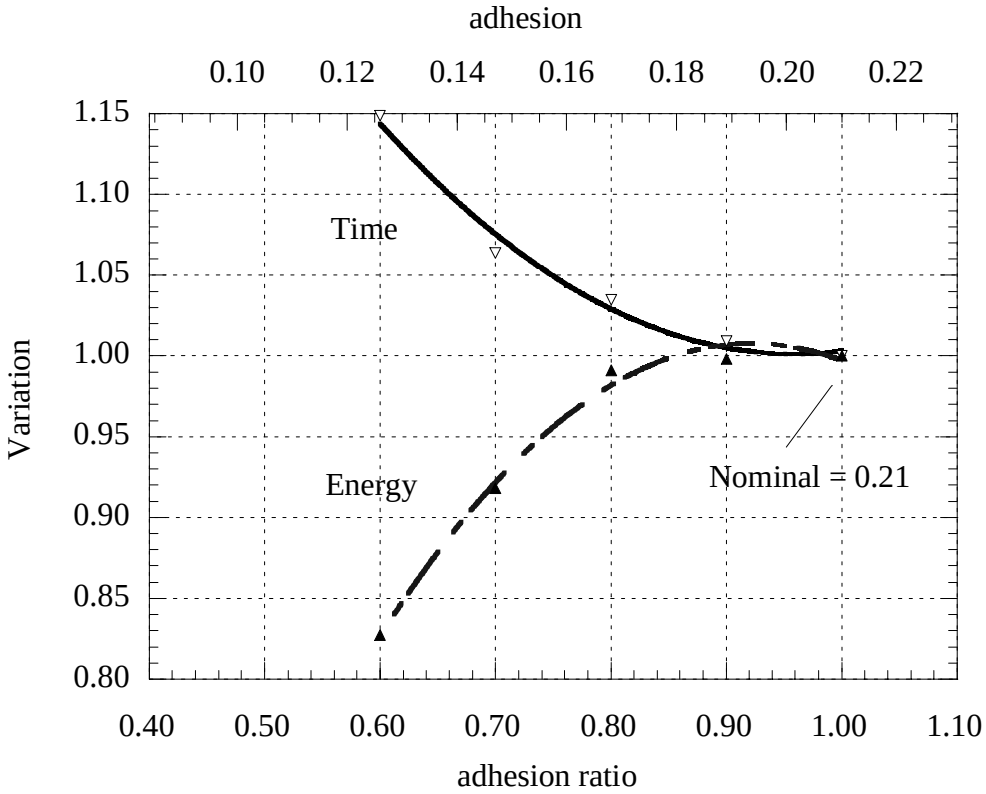

Figure 12-18 Influence of adhesion on energy consumption and running time for track T3.

Lowering the available adhesion in the model reduces the energy consumption and increases the running time. Below 60% of nominal adhesion, the slippage is severe and the available tractive force is not big enough for overcoming grades.

The influence of adhesion on energy consumption and running time is basically the same as the influence of the powering ratio.

12.5 Influence of braking ratio

As determined in Chapter 9 the average driver apply an average braking ratio of approximately 0.35, i.e. some 65 % less than the maximum braking effort of the train.

C*ase 11 Influence of braking ratio* σ_{pwr} *performed on real track T3.*

- Lower and upper speed action limits are 3.0 and 1.4 m/s.
- Look forward distance is 1000 m.
- Normal manual driving.

The influence of the braking ratio on energy consumption and running time is shown in Figure 12-19.

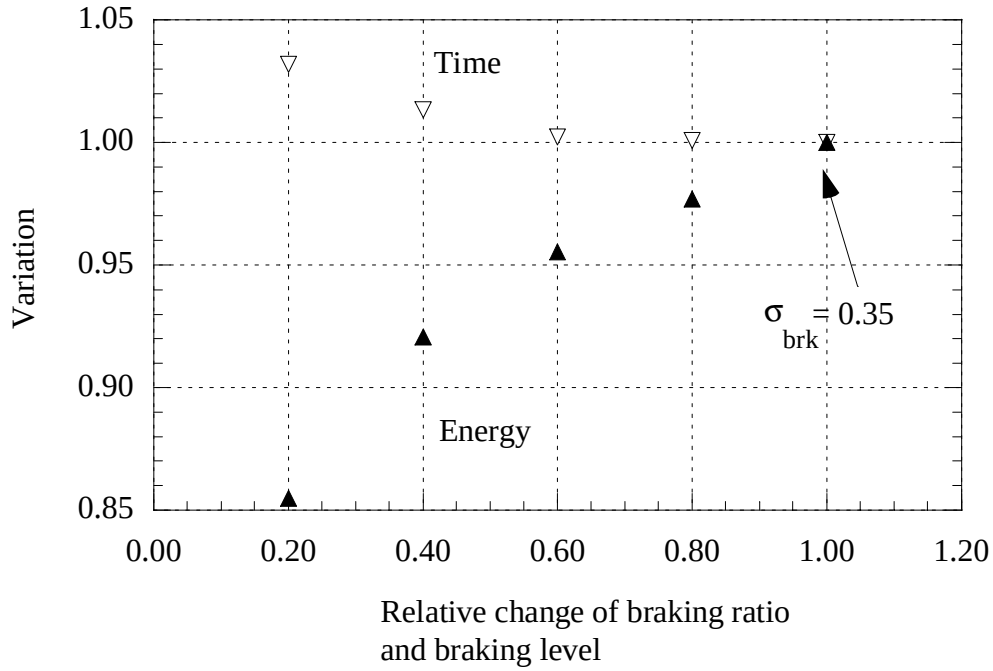

Figure 12-19 Influence of braking ratio on energy consumption and running time for real track T3.

A decrease in braking ratio, reduces the energy consumption more than it increases the running time.

12.6 Influence of some combinations of driving parameters

By combining the driving parameters according to the results in Section 12.2 - 12.5, it is possible to reduce the energy consumption of a train for a slight increase in running time.

Case 12 Effect of a combination of driving parameters for energy consumption and running time on a real track T3

- Lower and upper speed action limits are 6.0 and 2.0 m/s. To compensate the large v_a^- , the v_a^+ is increased by 0.6 m/s from the nominal 1.4 m/s.
- Look forward distance is increased from nominal 1000 to 2000 m. This allows longer coasting distances before a speed restriction.
- Braking ratio is 0.21 (60 % of nominal). Braking ratio has a bigger influence on energy consumption than on running time.
- The powering ratio is 0.85.

Figure 12-20 shows a comparison between measured train speed and a simulation made, for this case, with optimised driving parameters. The energy consumption is reduced by 9.4 % and the running time is increased by 3.0 %.

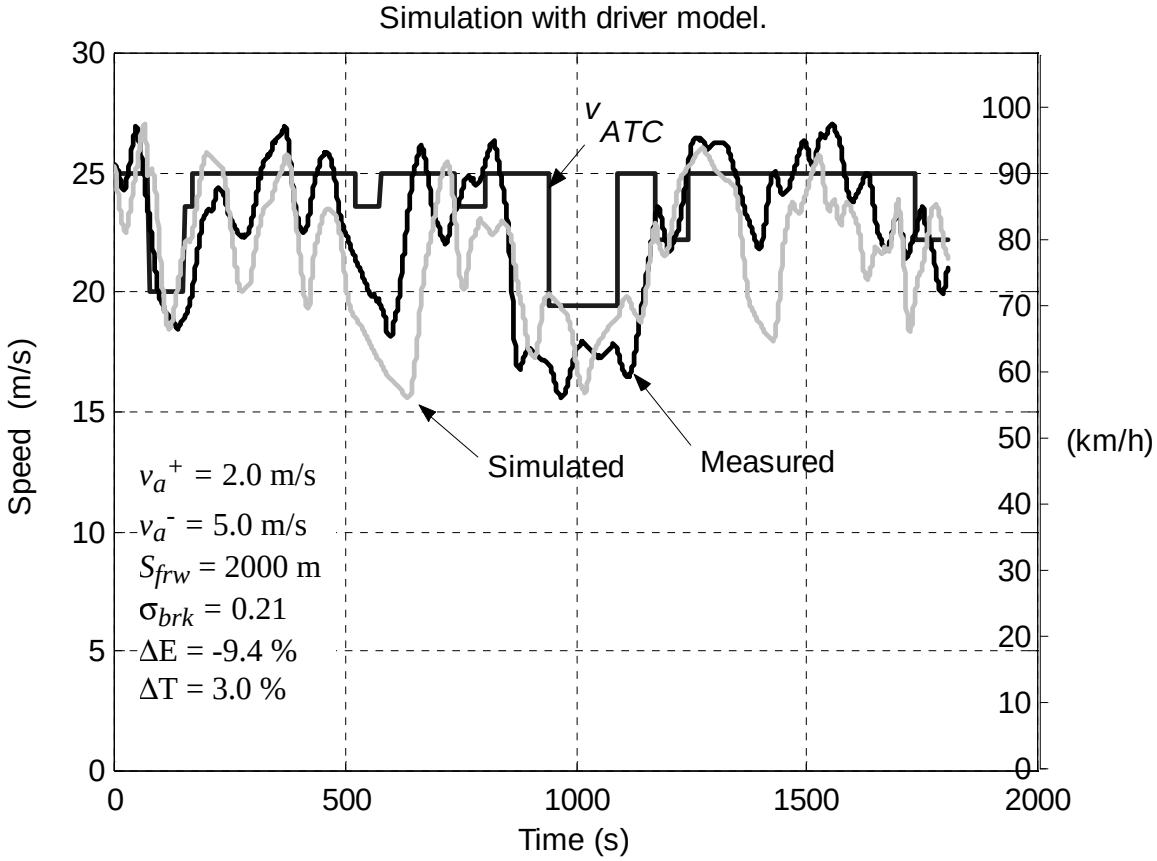

Figure 12-20 Comparison between measured train speed and a simulation made with optimised driving parameters.

Conclusions

This case shows that it is possible to reduce the energy consumption significantly by means of combining the driving describing parameters. Also, the running time is maintained at almost the same as for the measured train.

The running time is less affected than the energy consumption by the driving describing parameters.

13 Concluding remarks

13.1 Conclusions and discussion

Methodology for determining running resistance

In this work, a methodology for determining running resistance is developed and described. The methodology is introduced as the *Energy Coasting Method.* Due to its simplicity, and absence of complex measuring equipment, relatively few error sources can affect the results. This method needs only the accurate information on total train mass, track altitude data and determined train speed, as input data.

The method is sensitive, like all other methods, to precision errors in *speed* and in determined *track altitude*. This can be coped with by choosing an appropriate *evaluation distance*. The scatter of the data from which a running resistance polynomial is fitted, decreases with increasing evaluation distance. However, for obtaining (enough) output data for low speeds, v < 10 m/s, a short evaluation distance is necessary, at low speeds.

The method for determining the influence of measured ambient wind shows good agreement with test results.

Results from running resistance tests

The Energy Coasting Method, is used for determining *running resistance* of high speed trains, ordinary passenger trains and different freight trains. The running resistance for each train type is parameterised and expressed as a function of speed, train length, number of axles, axle load, curve radius and grade.

Running resistance is just slightly affected by the axle load on modern tracks. For freight trains with 36 trailing axles and covered *Hbis* wagons, an increase of about 150% in axle load, from 73 to 183 kN, raises the running resistance by about 2.5 kN, which is about 10% of running resistance at 25 m/s (90 km/h).

The full scale tests with freight trains on *Track 1* and *Ore* wagons on *Track 4*, indicate that *no systematic variation* of coefficient B, due to variation of axle load occurs, at least not on *Track 1* and *4*. The linear term, *Bv*, which is found to be affected by ambient wind, may contain a part of the aerodynamic drag not covered by the quadratic term, Cv^2. Negative values of coefficient *B* from test results are not unusual.

Running resistance of passenger train *P3*, loco + 9 cars, is higher on a jointed track on gravel than on modern continuous welded track. The increase affects in particular the *B coefficient*, which rises from B = 48 Ns/m on track 1 to B = 113 Ns/m on *Track 2*, i.e. an increase of 135%. The *A* coefficient increases by 15%.

Coefficient *B* increases approximately *linearly* with train length for passenger and freight trains.

Coefficient *C* (aerodynamic drag) increases approximately *linearly* with train length for passenger and freight trains.

With respect to total frontal area, the aerodynamic drag of open type *Oms* wagons with vertical poles is much higher than the aerodynamic drag of covered type *Hbis* wagons.

The effect of head and tail wind upon aerodynamic drag for passenger trains can be approximately calculated, if the vertical distribution of the airflow above ground is considered, thus giving good agreement with test results. The resulting influence of head and tail wind is considerably lover than estimated from the conventional method by considering relative speed between train and wind.

Train model

The train model contains many different factors and variables that will significantly degrade the accuracy and performance of the model if these factors are not modelled correctly.

It is most important to include *catenary voltage drop* in the *traction model* of the locomotive of type Rc4. A voltage drop from 15 kV to 12 kV reduces the tractive force by about 25 % at a speed of 20 m/s (70 km/h). The empirical linear model used for determining the voltage drop as a function of total power intake for the simulations, needs to be improved.

The change in tractive force is lagging in time compared to the change in powering level, set by the driver. The *time lag* is about 10 s. This lag should be implemented in the model, otherwise an offset will be introduced from the point along the track where the driver stars powering.

The tractive force is frequently limited by the *adhesion*. The conventional adhesion formula according to Curtius- Kniffler shows good agreement with measurements.

The *braking model* is empirical and is not describing the real braking system of a train in detail. However, the model contains verified brake gain time, brake release time and braking levels. The braking model shows satisfactory results in simulations when compared to measurements.

Slippage of the loco's four axles is determined. If the slippage is not introduced in a model, an error of 2 - 4 % may occur in determined speed or running time, compared with measurements.

By *verifying the train model with measurements*, it is concluded that the accuracy in the train model is within the accuracy of the measurements, i.e. a few percent, with respect to energy consumption and running time.

Driver model and driver behaviour

Five *driving describing parameters* are introduced and defined in this work:

- *Powering ratio*, has a mean value of 0.6 and is typically in the range of 0.5 - 0.8 of maximum. It is also increasing with respect to increasing total train mass, as on average.

- *Braking ratio*, shows a mean value of 0.35 of maximum. This indicates that the drivers preferably brakes gently and avoid long braking recovery times.

- *Degree of coasting* has a mean value of 0.25. This relatively high value indicates that coasting is used frequently. It is shown that coasting is also leading to energy savings. The degree of coasting has a significant influence on energy consumption.

- *Upper speed action* limit is assumed to be in the range of 1.4 - 2.8 m/s, since the driver must not exceed the speed restriction by 2.8 m/s (10 km/h).

- *Lower speed action limit* has a mean value of 3.2 m/s and is typically in the range of 1.0 - 6.0 m/s.

The analysis of measured data from train operations shows no significant variance due to mean grade or mean speed. Also, driving parameters are not influenced by the train mass except the powering ratio.

The *driver model* developed, is making use of the driving describing parameters and decides when to enter into the powering mode, coasting mode or the braking mode.

Comparison with measurements shows that the energy consumption and running time can be determined with good accuracy if the train model is combined with the driver model. It is therefore concluded that the simulation model can be used to successfully study driver behaviour.

Some examples are shown in this work how different driving describing parameters influence energy consumption and running time. In principal, coasting and low braking ratio is favourable to reduce energy consumption. To gain time, the upper speed action limit should be quite high. It is shown that it is possible to reduce energy consumption by 10 - 15 % with just a few percent in time penalty.

13.2 Further research

It is believed that further studies and optimisation would make it possible to improve the balance between energy consumption and running time.

Driver behaviour is studied only for ordinary freight trains. It is desirable to include into this research other type of trains, in particular those equipped with regenerative braking systems.

A more detailed model of the braking system and the variation of line voltage, is an issue for futher development.

14 References

[1] Andersson, E.: Energy Consumption and Air Pollution of Electric Rail Traffic. The Swedish Case. KTH. Stockholm 1994. TRITA-FKT Report 9446, ISSN 1103-470X.

[2] Gunther Ellwanger: Railway energy consumption, Challenges and state of the art. Energy Research Policy Conference - ERRI, Amsterdam 21, 22 October 1997.

[3] Muhlenberg: Resistance of a Freight Train to Forward Motion, vol I. Methodology and Evaluation. Mitre Corp., Metrek Div., Report no FRA/ORD-78/04.I. National Technical Information Service, Springfield 1978.

[4] Davis, W.J, Jr.: The tractive resistance of electric locomotives and cars, *General Electric Rewiew,* vol. 29, October 1926.

[5] Hara, T., Ohkushi, J., Nishimura, B: Aerodynamic Drag of Trains.
QR of RTRI Vol. 8 No. 4,1967.

[6] Guiheu, C.: Resistance to forward movement of TGV-PSE trainsets: Evaluation of studies and results of measurements. *French Railway Review*, Vol. 1. No. 1. 1983.

[7] Peters, J-L.: Optimising aerodynamics to raise IC performance. *Railway Gazette International*, October 1982.

[8] Gawthorpe, R.G.: (1983) 'Train drag reduction from simple design changes', *Int. J. of Vehicle Design*, Technological Advances inVehicle Design Series, SP3, Impact of Aerodynamics Vehicle Design, pp. 342 - 353.

[9] Peters, J-L.: Aerodynamics of very high speed trains and maglev vehicles: State of the art and future potential. Int. J. of Vehicle Design, Special Publication SP3, 1983.

[10] Chambadal, M.: Railway aerodynamics. French Railway Review, Vol 1. NO.5 1983.

[11] Peters, J-L.: Measurement of the influence of tunnel length on the tunel drag of the ICE/V train. Elsevier Science Publishers Ltd. England. *Aerodynamics and Ventilation of Vehicle Tunnels*, 1991, pp. 739-756.

[12] Lukaszewicz, P., Andersson E.: Running Resistance of Swedish Passenger Trains- measurements, methodology and results (in Swedish. Institutionen för Flygteknik avd Järnvägsteknik, KTH, Stockholm 1992. ISRN KTH/FPT/AR 65 SE.

[13] Lukaszewicz, P.: Running resistance of X2 in higher speed (in Swedish). KTH Järnvägsteknik 1993.

[14] Line tests with a view to reducing the aerodynamic drag of freight vehicles, *report ERRI A 168.2/RP 8*, Utrecht 1992.

[15] Lukaszewicz, P.: Running Resistance of Passenger and freight trains. Methodology and Test Results. KTH. Stockholm 1995. TRITA-FKT report 1995:16. ISSN 1103-470X.

[16] Lukaszewicz, P.: Train Running Resistance- A litterature survey with comparative examples (in Swedish). KTH Stockholm 1991. ISRN KTH/FPT/AR 64 SE.

[17] Lukaszewicz, P.: Train Running Resistance, energy consumption and Running Time (in Swedish). VTI och TFBs forskardagar 1992, pp 222. ISSN 1101-2986.

[18] Railway aerodynamics: Resume of test methods to determine the aerodynamic drag of a train in the open air. *Report ERRI C 179/RP 9*, Utrecht, april 1993.

[19] Determination of train resistance in the open air over typical track, using the coasting method (BR analysis): *ORE question C 179, report No. 2*, Utrecht 1991.

[20] SIMON User's Manual (in Swedish). Handbok BVH 723.002 1995-06-01. *Banverket.*

[21] SIMTRAC User's Manual (in Swedish). Technical description. *Balfour Beatty* 2001-03-28.

[22] Mera J.M et al.: Railway lines operation simulator: GifTren. Computers in Railways VII. WIT press 2000. ISBN: 1-85312-826-0.

[23] Arman Marofi: Personal communication, SJ.

[24] Barter W.A.M: Multi-train simulation: verification and accuracy. Computers in Railways VII. WIT press 2000. ISBN: 1-85312-826-0.

[25] Drish W.JR.: Train Energy Model (TEM) A State-of-the Art Simulator for Predicting the Fuel Consumption of a Train. Presented at the *Winter Annual Meeting* Miami Beach, Florida-November 17-21, 1985. The American Society of Mechanical Engineers WA/RT-13.

[26] Galdi V., Ippolito, L., Piccolo, A .: AC Railway Systems Simulation. World Congress on Railway Research, WCRR-97. The Congress Proceedings Vol C, pp 93 - 104. Firenze 16-19 November -1997.

[27] Kloster, S., Haugli, J. P.: Energiökonomisering i Baneströmforsyning og togframföring. NSB 1994.

[28] Howlett, P: Optimal Strategies for the Control of a Train. *Automattica,* Vol.32, No. 4 pp 519-532, 1996.

[29] Jiaping, Z.: Centralized Computation of Optimal Power reductions in a Railway System. TRITA-MAT-1989-6. april 1989.

[30] Yasukawa, S., Fujita, S., Hasebe, T., Sato, K.: Development of an On-Board Energy-Saving Train Operation System for the Shinkansen Electric Railcars. *QR of RTRI*. Vol 28, No. 2 - 4, '87 Nov.

[31] Schuler-Hainsch, E. : Einsparung von Traktionsenergie im Schienenfernverkehr durch Optimierung der Fahrweise. *ETR* 37 (1988, H.12-Dezember.

[32] Young, J.D., Boumester, H. J., Michaud, C., English, G.W.: Railway Linehaul Energy Intensity: Development of an Enhanced Train-Handling Module for the AAR Train Energy Model. CIGGT Report No. 89-19, Transport Canada Report No. TP 8677E. March 1990.

[33] Analysis of the railways replies to the questionnarie concerning the use of technical measures for achieving optimum driving from the point of energy consumption. *ORE question A 168*, report No. 5. Utrecht, september 1989.

[34] Andersson, E., Lukaszewicz, P.: Energy Studies for Current and Future High Speed Trains. *World Congress on Railway Research*, WCRR-94. The Congress Proceedings Vol 2, pp 1359 - 1361. SNCF. Paris 1994.

[35] Hammit, A.: Aerodynamic Forces on Freight Trains, vol. I, *Report no FRA/ORD-76-295.I*. National Technical Information Service, Springfield 1976.

[36] Beckwith, T. Marangony, R. Lienhard, J: Mechanical Measurements. 5th ed. Addison-Wesley Publishing Company, Inc. 1993.

[37] Hay W: Railroad Engineering, John Wiley & Sons, Inc, New York 1982.

[38] Koffman J.L: Tractive resistance of rolling stock, Rail Engineering International, April/ May 1973.

[39] Andersson, L: Personal communication, SJ/MTL Laboratory.

[40] Ingemarson, I: Laboratorierapport 9610-59E9, SJ (in Swedish).

[41] Ingemarson, I: Rapport MT 67555, SJ 19997-02-19 (in Swedish).

[42] Ahmed S, Gawthorpe R, Mackrodt P: Aerodynamics of Road and Rail Vehicles, Vehicle System Dynamics, vol. 14 (1985, pp. 319-392.

[43] Bernsteen A: A theoretical analysis of the rolling resistance of railway vehicles from fundamental mechanics, UMI Dissertation Services 1980.

[44] Ågren J: Train Running Resistance, especially analysis of resistance due to friction (in Swedish, Tågets gångmotstånd, särskilt analys av friktionsmotstånd.

[45] Zachrisson, P: Personal communication. Banverket/TBG.

[46] Andersson, E: Personal communication. KTH (Royal Inst. of Tech. dept. of Railway Technology.

[47] Lilliesköld, O: Personal communication. ABB Traction AB.

[48] Track data provided by Swedish National Rail Administration, Banverket/BD F.

[49] Lukaszewicz P: Running resistance of Ore trains (in Swedish), report from field mesurements. KTH 1995.

[50] Lukaszewicz P: Gångmotstånd för person och godståg, Sammanfattning av utförda prov, KTH/SJ/ABB/Banverket, 1991- 93.

[51] Wan Changsen. Analysis of Rolling Element Bearings, Mechanical Engineering publications LTD, London.

[52] SKF product catalogue (in Swedish, SKF Huvudkatalog 1992.

[53] Scibor - Rylski, A.J: Road Vehicle Aerodynamics, Pentech Press, London 1984

[54] Andersson, E. & Berg, M: *Railway systems and rail vehicles*, (in Swedish) Part 1. KTH Railway Technology, Stockholm 1999.

[55] Andersson, E. & Berg, M: *Railway systems and rail vehicles*, (in Swedish) Part 2. KTH Railway Technology, Stockholm 1999.

[56] Ohyama, T: Adhesion Characteristics of Wheel/Rail System and its Control at High Speeds. *QR of RTRI*, Vol. 33, No. 1, 1992.

[57] Olofsson M: Power flow analysis of the Swedish railway electrical system. Department of Electrical Power Systems. KTH, Stockholm 1993. TRITA-EES-9301, ISSN 1100-1607.

[58] Lunden, H., Personal communication. SJ Laboratory SJ Freight Transport Division.

[59] Computer program for calculating tractive force of modified locmotive *SJ Rc4*, by H Lunden SJ/MTL.

[60] Computer program for calculating tractive force of locomotive *SJ Rc4* from measured variables, by I Ingermansson, SJ.

[61] ATC manual, BVH 544.3 (in Swedish).

[62] Dayman B: Demonstration of the Coast-Down Technique for Determining Train Resistances, Jet Propulsion Laboratory, California Institute of Technology, Pasadena California, October 1983. JPL Publication 83-85.

[63] Sachs K: Elektrische Triebfahrzeuge, Band 1, Springer Verlag, Wien, 2. Auflage 1973.

[64] Hucho W-H: Aerodynamics of Road Vehicles, Butterworths, 1987.

[65] Simiu E, Scanlan R: Wind Effects on Structures. 2nd ed., John Wiley & Sons,

[66] Measurement of the boundary layer behaviour on a train in the open air by pressure tube techniques: ORE question C 179, report No. 5, Utrecht 1991.

[67] Lukaszewicz P: Driving techniques and strategies for freigth trains. Computers in Railways VII. *COMPRAIL 2000* Bologna.

[68] UIC Leaflets 540 - 549.

[69] Stichel, S.: Running behaviour of railway freight wagons with single axle running gear. KTH Railway Technology, Stockholm 1998. TRITA-FKT Report 1998-40.

APPENDIX A

Terminology, definitions and abbreviations

ABB Former Swedish-Swiss-German railway supplier; formed Adtranz (see below) in a joint venture with Daimler Benz, later Daimler Chrysler.

A.C. Alternating current.
Used for traction motors, catenary voltage etc.

D.C. Direct current.
Used for traction motors, catenary voltage etc.

Adhesion Part of friction between wheel and rail which is used to transfer tractive or braking forces (i.e. forces in longitudinal direction).

Adhesion coefficient
Utilized adhesion: Ratio between utilised total tractive force of a tractive unit and the adhesive load; see below. Sometimes adhesion coefficient is defined for braking instead of traction.
Available adhesion: Ratio according to above, between the maximum attainable tractive force and the adhesive load without excessive slippage (at the actual wheel and rail conditions).

Adhesive mass (or weight, or load)
Part of vehicle`s or train´s mass (or weight) supported by driven (or braked) axles. In accordance the *adhesive mass in traction* and the *adhesive mass in traction* are defined.

Adtranz Railway supplier, mainly trains and signalling systems, located in Västerås, Stockholm and many other places worldwide.
Until 2001-04-30 the legal name was Daimler Chrysler Rail Systems (Sweden). From 2001-05-01: see *Bombardier.*

Air brake Normally a braking system with compressed air as medium, for applying the necessary brake force to the wheels or to brake disc, and using pressure variations in a main air pipe along the train as signal for applying the brakes (reduced air pressure) or releasing the brakes (increasing pressure after a reduction).

Axle In this context usually the same as *wheel axle*; part of *wheelset*; often used in the same meaning as wheelset. See also *wheelset*.

ATC Automatic Train Control, safety system which supervise train motion on railway lines, and automatically brakes the train if necessary.

ATP Automatic Train Protection: internationally used word for ATC, essentially the same.

Automatic train control
See ATC.

Automatic speed control
Also sometimes called: *Speed cruising.control*.
Control system within the tractive unit, keeping the speed close to the predetermined speed.

Banverket The Swedish National Rail Administration.

Bias error A fault in measured data that gives a constant off set from the true value.

Bogie Running gear able to turn in the horisontal plane, when negotiating curves or large track irregularities. The *wheelsets* are mounted, guided and suspended in the *bogie frame*. The bogie mostly also contains brake actuators (air brake cylinders, appropriate linkage etc.). In many traction vehicles (for example the locomotives in this report) also the traction motors and transmission gear are mounted in the bogie frame.

Bombardier
In this context: *Bombardier Transportation*, rail vehicle supplier who has made a take-over of Adtranz (see above), effective from 2001-05-01.
The company´s origin is Canada.

Braking control lever
Lever in driver´s cab, used for maneuvering the brakes of the train.

Braking distance
In this report: the distance the train is running from the moment where braking is applied until the moment where the train has the desired reduced speed (or stop at zero speed). As an approximation in this report, braking distance is measured from the moment where the pilot pressure starts to change.

Braking level
Level of applied braking; in this context measured by the pilot pressure *Pcv*, with a certain delay nearly proportional to the position of the braking lever.
In the standardised European air braking system the following levels are distinguished:

- *Full braking*; the maximum attainable at full braking capacity.
  Main air pipe pressure is reduced from 500 kPa to 350 kPa. Pilot pressure *Pcv* is 360 kPa.
- *Nominal braking*, sometimes called *service braking*, has a braking level of 2/3 of full braking.

In this report also *operational braking* is defined. It means the average of observed braking levels during normal operation.

Braking ratio

Braking level in relation to the level at full braking.

Brake gain time

Time from the moment where the brakes are applied until the desired braking level is reached.

Brake release time

Time from the moment where the brake level start to be reduced, until the moment where the brakes are fully released, i.e. the total brake force in the train is zero.

Continuous welded rails (CWR)

Rails in the track are welded into long rail sections, sometimes up to about 2000 m. Cf: *Jointed rails.*

Catenary Overhead wire mounted 5 - 7 m above the track, from which electrical current and voltage is taken to an electric train.

Coasting Neither tractive nor braking forces affects the train; "*pure rolling*".

CWR See continuous welded rails.

Degree of coasting

Total coasting distance divided by total running distance.

Driving control lever

Lever in driver´s cab, used for maneuvering the traction of the train; i.e. the tractive forces.

Driving describing parameters

Also simplified to *Driving parameters*. In this report five driver parameters are introduced, describing drivers behavior, driving style or driving strategy.

Driving parameters

See driving disrobing parameters

Energy consumption

The intake of energy (in this report: electrical energy) to a tractive vehicle (locomotive etc.) for propulsion and other purposes. Sometimes energy consumption is measured "behind" the pantograph, at the intake to the rail system, or the equivalent energy input to a transmission line or even to a electric power station.

Energy consumption can be measured as the consumption for a certain run; a train with a given mass running a certain distance. It can also be measured as a *specific consumption*, *per train-km* or *per ton-km.* In the latter case the energy consumption can also be measured *per gross-ton* or *per net-ton*; see these words.

Equivalent conicity

Ordinary railway wheels have more or less *conical* wheel treads or running surfaces. Thus the actual wheel rolling radius at the wheel-rail point of contact is dependent on the lateral positions between wheels and rails.
In this context equivalent conicity expresses the ratio between lateral position of the wheels in relation to the rails and the actual rolling radius of the wheels.

Equivalent mass

The ratio between a force and the corresponding acceleration in longitudinal direction of a rail vehicle. The rotating masses of the vehicle makes the equivalent mass higher than the static (nominal) mass.

Grade Track inclination in longitudinal direction, defined positive upphills and negative downhills.

Gross ton Total weight of a train, including the tare (empty) mass of a train and the mass of transported payload.

Jointed rails

Also: *jointed track*. Rail sections having a length of 10 - 60 m are bolted together into longer sections. The bolted locations are called *rail joints.*

KFB In Swedish: Kommunikationsforskningsberedningen
In English: The Swedish Transport and Communications Research Board

Line current

Electrical current taken from the "overhead line", i.e. from the catenary to the pantograph.

Line voltage

Electrical voltage on the "overhead line", i.e. on the catenary and the pantograph.

Lower speed action limit
: Average speed difference between nominal speed, v_{ATC}, and the speed where the driver interrupts coasting.

Main air pipe
: A pressurised air pipe connected to the braking systems of the wagons. Braking is applied by lowering the air pressure in the pipe.

Measuring car
: Special railway car used for instrumentation, data recording and as the working place for measuring staff.

Motor current
: 1. Normally *rotor current:* current in the rotor windings in an electrical traction motor
  2. *Field current*: In a separately excited D.C. motor, the current taken to the stator, in order to excite the magnetic field.

Net ton The mass of transported payload.

Nominal speed
: Speed according to the ATC system.

Operational braking
: Determined mean braking level, or mean ratio, from measurements.

Pantograph Device collecting electrical current from the catenary during speed.
The pantograph is usually located on the roof.

Pilot pressure
: Pressure corresponding to the braking level.

Powering level
: The driver‘s order to the traction system to provide tractive forces up to the desired level. Scaled in notches, which can be discrete or continuous. The real tractive force may be less than the desired tractive force, for example due to adhesion limitations.

Powering ratio is the power utilised divided by the maximal avaliable tractive power at the maximum powering level.

Precision error
: Random error. Error that is stochastic.

Radial self-steering bogie or wheelset

Through the conical wheels connected by a "stiff" axle, the normal railway wheelset has a *self-steering ability*, aligning the wheelset approximately radially in the track, provided that the wheelset(s) are allowed to take up such an attitude due to its guidance stiffnesses in the bogie or the vehicle.

Relative error

Ratio between a measured value and the true value.

Rotating intertia

Rotating masses, such as wheelsets, transmission gear, traction motors, brake discs etc., which through rotation contribute to the total inertia and kinetic energy of a rail vehicle.

Running resistance

The (longitudinal) forces acting on a train against their direction of travel.

SJ Former *Swedish State Railways*, until 2000-12-31. Contained the Passenger Traffic Division, the Freight Transport Division, The rolling Stock Division and others.

Now divided into a number of stately owned companies:

- *SJ AB* for passenger traffic
- *Green Cargo AB* for freight traffic
- *TrainTech* and *Euromaint* for technical support and consulting, as well as for vehicle maintenance.

Specific energy consumption

See *energy consumption.*

Speed In this context and report there are different speeds:

-*Vehicle speed*, a purely longitudinal speed measured as the vehicle‘s real speed forward along the track. Can not be measured, just calculated.

- *Wheel speed:* axle rotational speed divided by the rolling radius of the wheels.
- *Radar speed*, vehicle speed measured by radar equipment in aboard the train.

Swedish State Railways

See *SJ*

Test car See measuring car.

Three-piece bogie

Two-axled (freight) bogie where the two wheelsets are connected and fixed via bearings into two side frames, connected by a transverse bolster. This arrange-

ment has some particular properties; for example these bogies are known to have a quite large running resistance in curves.

Total running resistance
: The sum of *mechanical resistance* (on straight track), additional *curve resistance, air resistance* (air drag) and *grade resistance*.

Track gauge
: Approximately: Lateral distance between the inner edges of the rails in a track.

Traction
: Propulsion of a train; providing sufficiently large tractive forces in order to bring the rail vehicle or the train into speed, or to haul the train, more or less overcoming the resistance against train motion.

Tractive force
: (Sum of) propelling forces (on all driven axles), produced in a self-propelling rail vehicle.

Tractive effort
: The maximum attainable tractive force for each traction system, at each condition of powering level, speed, line voltage, etc. The tractive force is not necessarily the same as the tractive effort, because it may be reduced by the available adhesion.

Upper speed action limit
: The speed difference between nominal speed and the train speed above the nominal speed where a driver action is executed.

Wheelset
: Two wheels connected by a wheel axle. Sometimes also other items stiffly coupled to the wheelset are included, such as bearings with housing, traction transmission gear and brake discs.

APPENDIX B

Notations

General rules

Bold indicates a vector or a matrix

Δ indicates a difference or a change

- above a letter indicates a mean value

Latin letters

a	Acceleration (m/s^2)
A	Speed independent resistance (N)
A_f	Frontal area (m^2)
B	Coefficient in resistance term which is linearly dependent upon speed (Ns/m)
C	Coefficient in resistance term which is dependent upon speed squared (Ns^2/m^2)
C_D	Air drag coefficient
$C_D A_f$	Drag area (m^2)
C_l	Total mean pressure and friction drag coefficient along the train
C_p	Total mean front pressure and rear suction dragcoefficient
C_u	Undercarriage drag coefficient
$\bar{c}_f$	Mean skin friction coefficient
E	Energy, energy consumption (kWh)
e	Specific energy consumption
$e_{\Delta(\Delta X)}$	Maximal error due to error in evaluation distance (N)
$e_{\Delta h}$	Maximal error due to error in altitude (N)
$_{\Delta m}$	Maximal error due to error in mass (N)
$_{\Delta(mH)}$	Maximal error due to error in rotating inertia (N)

$e_{\Delta v}$	Maximal error due to error in speed (N)
$e_{\Delta \bar{v}}$	Maximal error due to error in calculated mean speed (N)
F	Force, resistance (N)
F_C	Curve resistance (N)
F_D	Air drag, air resistance (N)
F_{Db}	Car body friction drag (N)
F_{Dint}	Air momentum drag (N)
F_{Droof}	Roof drag (N)
F_{Du}	Undercarriage drag (N)
F_{Dw}	Increment in air drag due to wind (N)
F_{Dwall}	Wall drag (N)
F_M	Mechanical resistance at wheel periphery (N)
F_w	Final calculated tractive force (N)
G	Grade (‰)
g	Acceleration of gravity (m/s^2)
H	Additional term taking rotational inertia into account
h	Altitude (m)
I_A	Rotor current of traction motor (A)
I_F	Field current of traction motor (A)
J	Inertia (kgm^2)
j	Index
K	Constant
K_{brk}	Empirical constant in braking equation
K_C	Empirical constant in curve resistance equation
K_D	Empirical constant in air drag equation
K_m	Motor constant
L	Length (m)
M	Mass (kg)
n	Number of, step number
$\boldsymbol{N_0}$,	Efficiency matrix
P	Power (kW)
P_0	Power drawn by loco during coasting or idling (kW)
Q	Axle load (N)
r	Radius (m)
R	Curve radius (m)

R^2	Coefficient of determination
S	Distance (m)
s	Position (m)
t	Time (s)
t_{b0}	Time when starts increasing
t_{gain}	Time when braking has increased to its final level
t_{rel}	Time when braking starts decreasing
U	Voltage (kV)
u	Gear ratio
v	Speed (m/s)
v_{ATC}	Speed restriction, according to ATC system (m/s) Nominal speed (m/s) or (km/h)
v_a^+	Upper speed action limit (m/s) or (km/h)
v_a^-	Lower speed action limit (m/s) or (km/h)
v_{b1}	Speed limit for driver action due to v_a^+ (m/s) or (km/h)
v_{b2}	Speed limit when full ATC braking is automatically activated (m/s) or (km/h)
v_h^+	Upper speed holding limit (m/s) or (km/h)
T	Running time (s)
X	Position along the track (m)

Greek letters

α	Wind direction in relation to track(°). Adhesion coefficient
β	Yaw angle of wind (°). Braking level (0-360)
χ	Distance to next speed restriction (m)
δ_{cst}	Degree of coasting
$\delta_{cst\text{-}brk}$	Degree of coasting before braking or stop
ΔX	Evaluation distance for running resistance
Φ	Tractive calculated force matrix
γ	Powering level
η	Efficiency
λ_{brk}	Empirical braking or releasing time constant (s)
σ_{brk}	Braking ratio
σ_{pwr}	Powering ratio
ω	Angular velocity (rad/s)
ψ	Air-gap flux
ζ	Slippage ratio

Indices

a	Position index, action limit
ATC	Automatic train control system
ax	Axles
bα	Braking (adhesive)
brk	Braking
C	Curve
c	Passenger cars or freight wagons
cat	Catenary
corr	Corresponding
cst	Coasting
D	Drag
F	Force

f	Frontal
frw	Look forward until braking
G	Grade
i	Time step number
I	Inertia
j	Axle or motor number
k	Increment
kin	Kinetic
L	Line, catenary
lead	Total look ahead, total lead
loco	Locomotive
M	Mechanical
mot	Determined from measurements in motor. Account is taken to the effect of rotating masse at acceleration
mot0	Determined from measurements in motor. Nominal, without account to the rotating massses
n	Number
p	Propulsive
pnt	Pantograph
pot	Potential
R	Running
r	Radar
rel	Relative
rot	Rotor
T	Total of a train
t	Calculated tractive, including rot. inertia
t0	Calculated in motor, not including effect of rotating masses.
*t*α	Tractive (adhesive)
tot	Total
v	Vehicles
w	Wheel, at wheels
x	Forward direction along the track.
α	Adhesion, limited by adhesion.

APPENDIX C

A step by step description of the energy method:

1. Choose a measuring section which has accurate track data with respect to grades and curves. The first measuring position, x_1, in the coasting direction, is the start of the measuring section.
2. Choose a point of reference on the test train.
3. Choose a measuring interval, Δx, which determines the distance between the consecutive measuring positions, at which the train's total energy will be determined, with respect to the measuring position on the train. For the tests as described in this work, Δx is 50 m.
4. For each measuring position along the measuring section and with respect to the train's point of reference, determine the *altitud*e of each vehicle's centre according to track data. Thus the *potential energ*y of the train is calculated by *distributin*g its mass along the section.
5. Accelerate the train to the desired speed.
6. Start coasting before the train's point of reference arrives at the start of the measuring section, in order to avoid oscillatory motions from sudden changes in tractive effort.
7. With the train's point of reference arriving at measuring position x_1, from that moment on the train's position along the track is determined, so the speed can be calculated at consecutive measuring positions, x_2, x_3,...

Note: it is important to check if the determined position and speed of the test train agree with the actual position and speed along the track. This check should be done before and after each test run.

8. By calculating the *speed* of the train as its point of reference is at each measuring position, the train's *kinetic energ*y is determined.
9. Calculate the train's total energy at each measuring position.
10. Choose an evaluation distance $\Delta X = k\,\Delta x$. For the tests, as described in this work, ΔX of 2000 m is a good choice with respect to errors in track data and speed.
11. Starting from measuring position x_1, calculate the *mean spee*d and *differenc*e in total energy of the train, between measuring position, x_1 and x_1+k, x_2 and x_2+k,..., etc., until the end of the measuring section is reached or the train stops by itself. Thus pairs of are formed for each ΔX, which propagates forward by Δx along the measuring section.
12. Use the pairs of to determine a second degree running resistance polynomial as function of speed.
13. Determine the mean wind speed and wind direction during the test.

14. Coast in the reverse direction on the same track section, and repeat the procedure, from step 5 to 13. Δx is the same but the measuring position x_1 is now at the start of the measuring section in the reverse direction.
15. Determine pairs of fitted polynomials with similar wind conditions with respect to the track, and calculate a mean polynomial.
16. Average all mean polynomials for each train consist.

APPENDIX D

Flow charts of driver model

The numerical values used in the flow charts, are empirical.

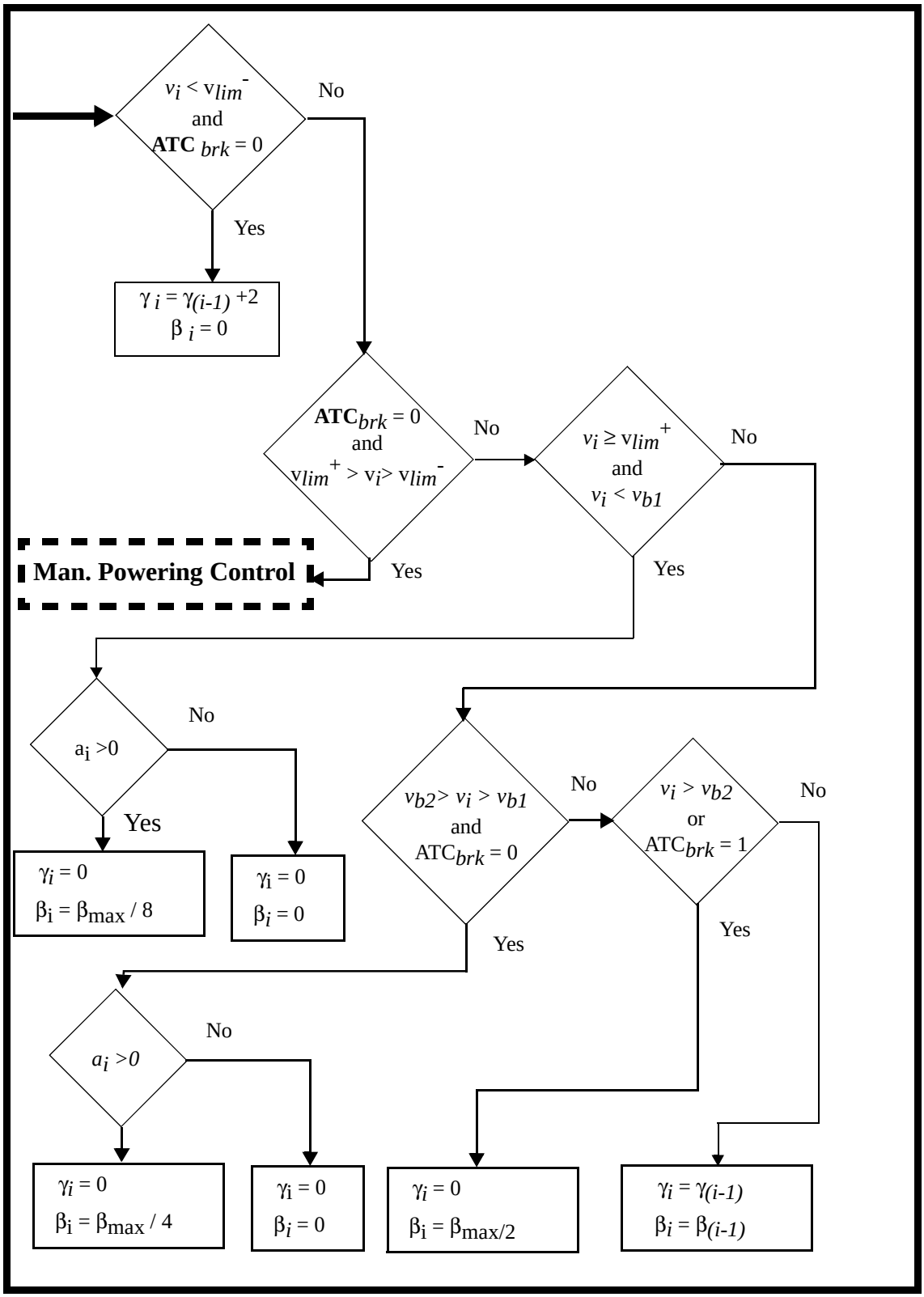

Figure D-1 Flow chart of the Manual Speed Control module.

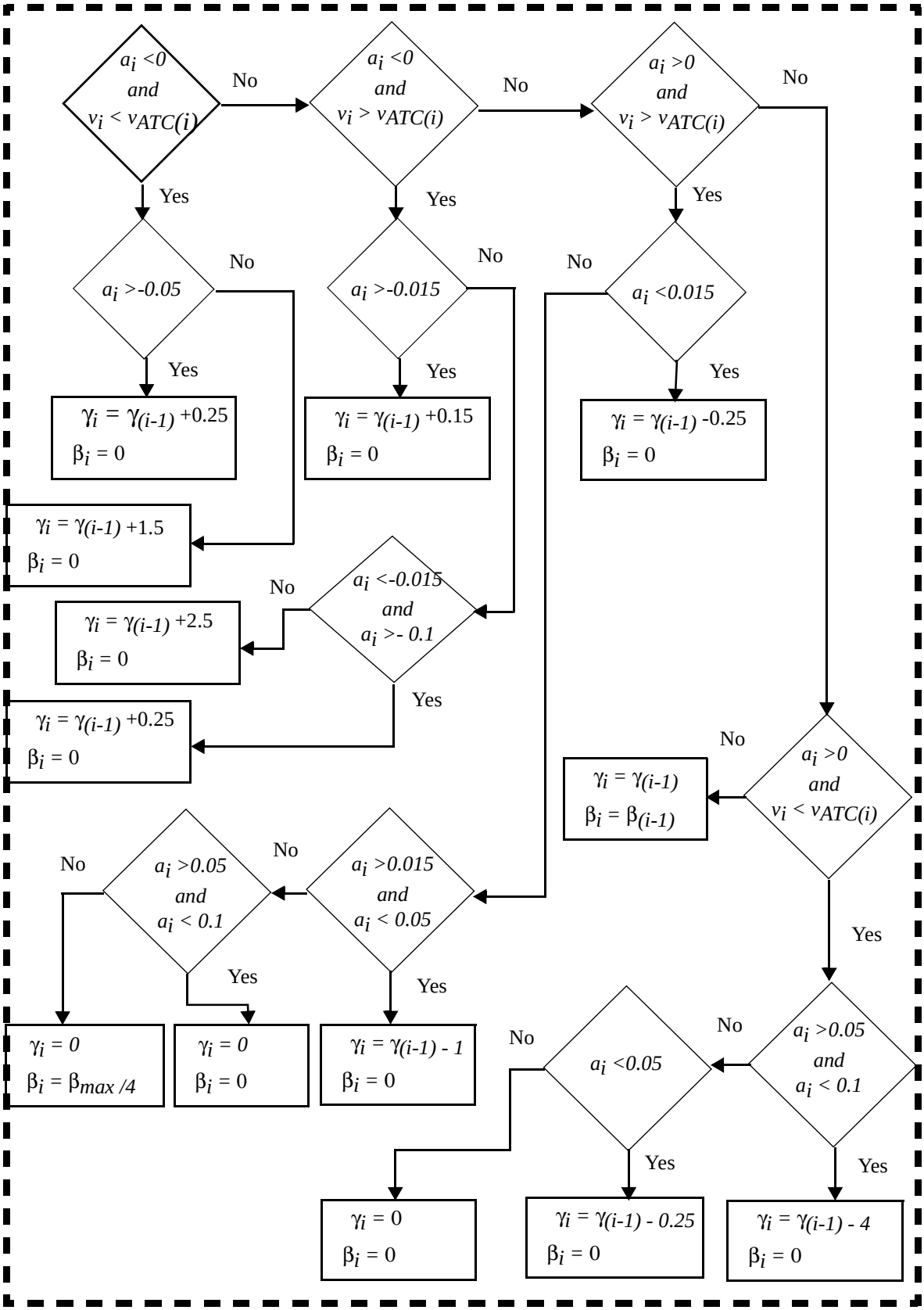

Figure D-2 Flow chart of Manual Powering Control submodule.

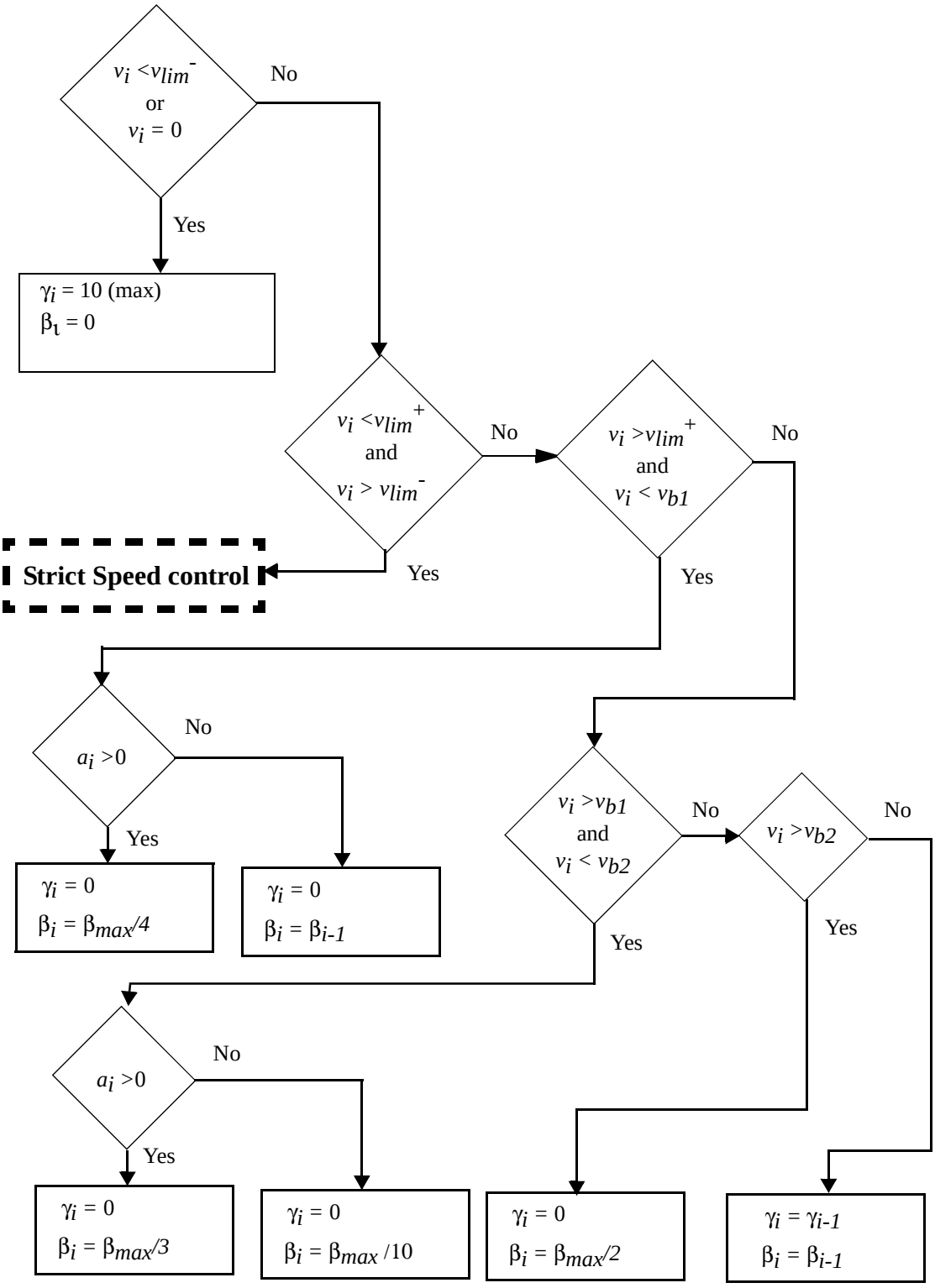

Figure D-3 Flow chart of driver of type MTD.

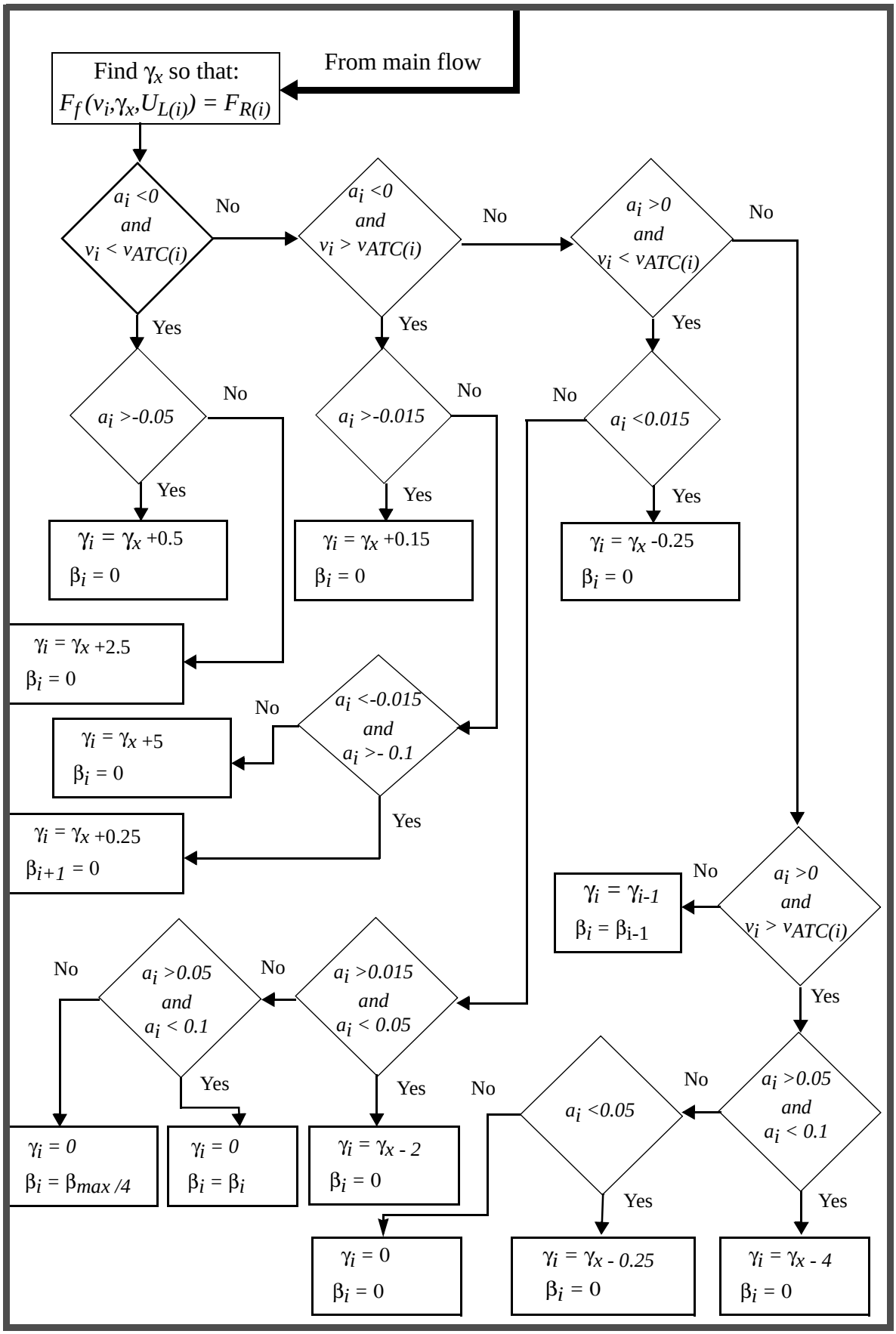

Figure D-4 Flow chart of Strict Speed Control Module

APPENDIX E

Description of trains tested

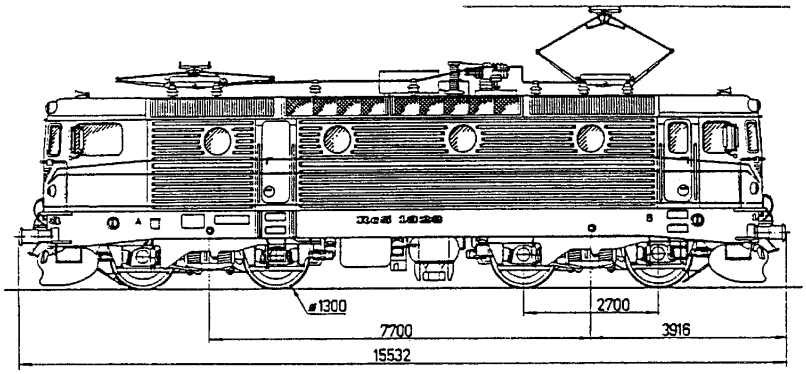

Fig. E - 1 Locomotive: SJ Rc. Length 15.5 m. Mass 79 tonnes.

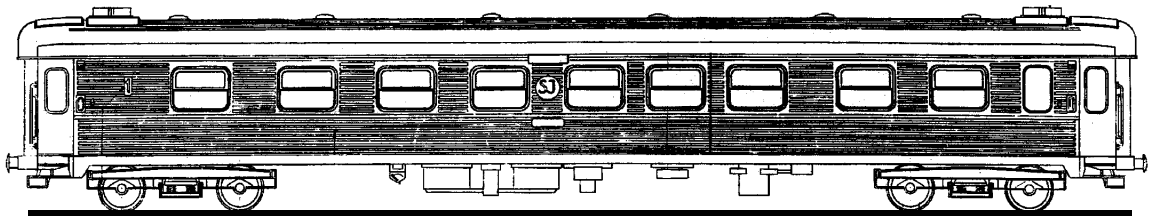

Fig. E - 2 Measuring car: passenger car SJ AB3RT. Length 24.1 m. Mass 45 tonnes.

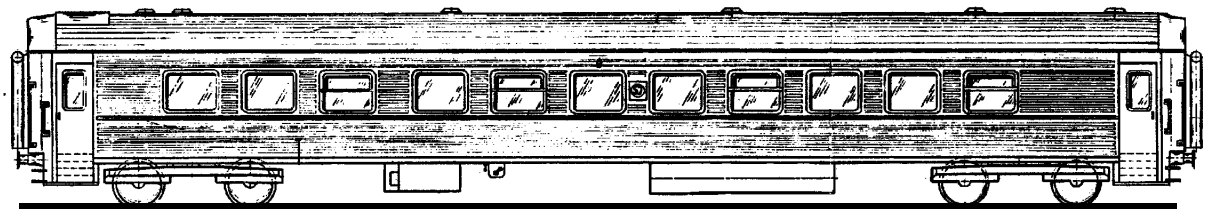

Fig. E - 3 Passenger car: SJ B7. Length 26.4 m. Mass 44 tonnes.

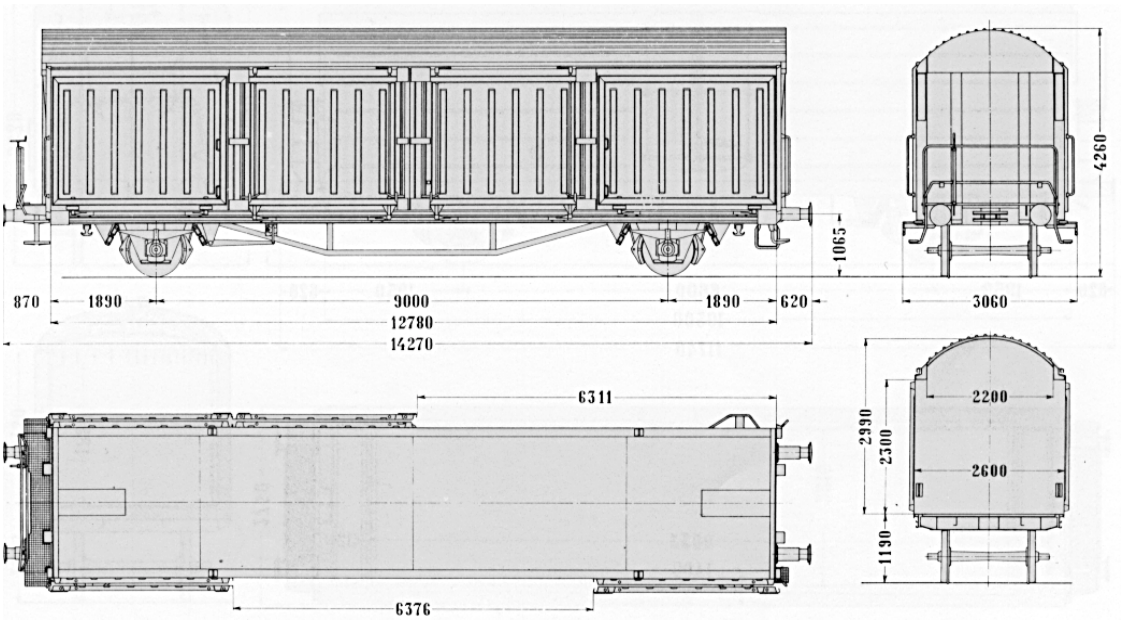

Fig. E - 4 Freight wagon: Hbis. Length 14.27 m. Mass 15.0 tonnes, (tare).

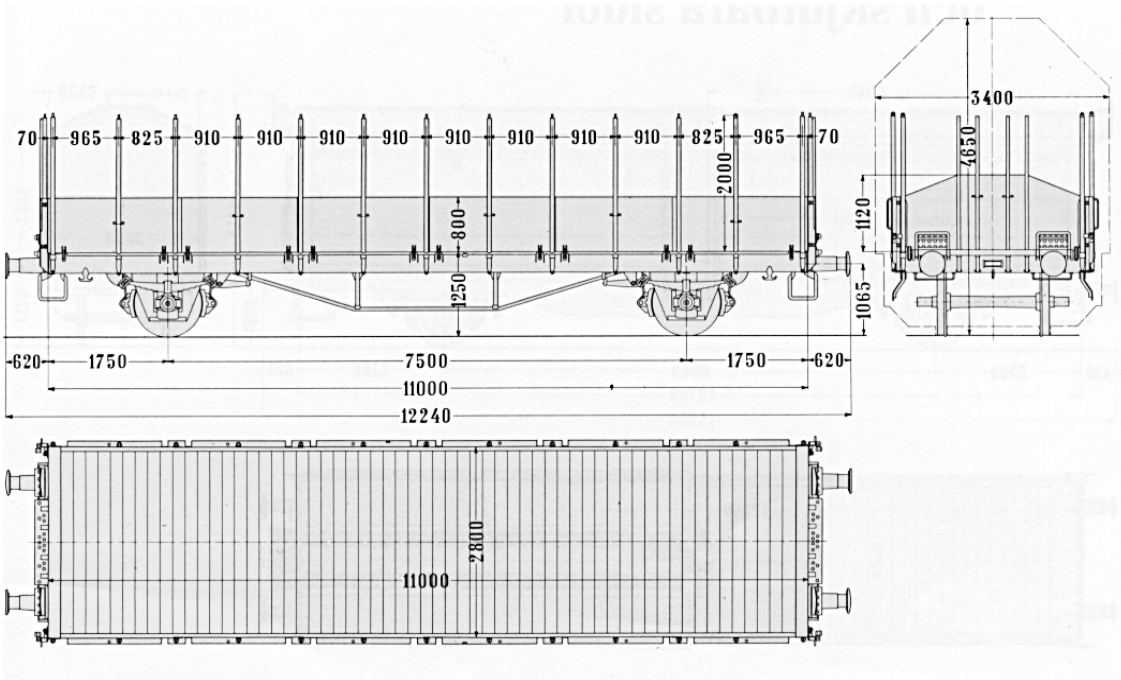

Fig. E - 5 Freight wagon: Oms. Length 12.24 m. Mass 11.5 tonnes, (tare).

Fig. E - 6 Alternated Hbis and Oms wagons, trains F1, F2 and F3.